HYPOLIMNETIC OXYGENATION:
COUPLING BUBBLE-PLUME AND RESERVOIR MODELS

Vickie L. Singleton

Dissertation submitted to the Faculty of
Virginia Polytechnic Institute and State University
in partial fulfillment of the requirements for the degree of

Doctor of Philosophy
in
Civil Engineering

Dr. John C. Little, Chair and Advisor
Dr. Panayiotis Diplas
Dr. Adil F. Godrej
Dr. Daniel F. McGinnis
Dr. Francisco J. Rueda

March 26, 2008
Blacksburg, Virginia

Keywords: bubble plume, hypolimnetic oxygenation, hypolimnetic aeration, hydrodynamic modeling, water quality modeling, CE-QUAL-W2, Si3D

Hypolimnetic Oxygenation: Coupling Bubble-Plume and Reservoir Models

Vickie L. Singleton

(ABSTRACT)

When properly designed, hypolimnetic aeration and oxygenation systems can replenish dissolved oxygen in water bodies while preserving stratification. A comprehensive literature review of design methods for the three primary devices was completed. Using fundamental principles, a discrete-bubble model was first developed to predict plume dynamics and gas transfer for a circular bubble-plume diffuser. This approach has subsequently been validated in a large vertical tank and applied successfully at full-scale to an airlift aerator as well as to both circular and linear bubble-plume diffusers. The unified suite of models, all based on simple discrete-bubble dynamics, represents the current state-of-the-art for designing systems to add oxygen to stratified lakes and reservoirs.

An existing linear bubble plume model was improved, and data collected from a full-scale diffuser installed in Spring Hollow Reservoir, Virginia (U.S.A.) were used to validate the model. The depth of maximum plume rise was simulated well for two of the three diffuser tests. Temperature predictions deviated from measured profiles near the maximum plume rise height, but predicted dissolved oxygen profiles compared very well to observations. Oxygen transfer within the hypolimnion was independent of all parameters except initial bubble radius. The results of this work suggest that plume dynamics and oxygen transfer can successfully be predicted for linear bubble plumes using the discrete-bubble approach.

To model the complex interaction between a bubble plume used for hypolimnetic oxygenation and the ambient water body, a model for a linear bubble plume was coupled to two reservoir models, CE-QUAL-W2 (W2) and Si3D. In simulations with a rectangular basin, predicted oxygen addition was directly proportional to the update frequency of the plume model. W2 calculated less oxygen input to the basin than Si3D and significantly less mixing within the hypolimnion. The coupled models were then applied to a simplified test of a full-scale linear

diffuser. Both the W2 and Si3D coupled models predicted bulk hypolimnetic DO concentrations well. Warming within the hypolimnion was overestimated by both models, but more so by W2. The lower vertical resolution of the reservoir grid in W2 caused the plume rise height to be over-predicted, enhancing erosion of the thermocline.

ACKNOWLEDGEMENTS

Obtaining my PhD has been quite a journey, and I have many people to thank. First of all, I would like to extend my deepest appreciation and gratitude to my advisor, Dr. John Little. It has been a great pleasure conducting research under him once more, and I consider him the best supervisor I have ever had. I can honestly say that if it were any other advisor at any other school, I probably would not have taken this academic path. So, thank you, John.

Next, I would like to recognize my committee members, both former and current, for their time and attention: Dr. Panos Diplas, Dr. Adil Godrej, Dr. Nancy Love, Dr. Daniel McGinnis, and Dr. Francisco Rueda. I give special thanks to Dan for being a much-needed friend and supportive colleague during my first semester back at Tech and beyond. I would also like to thank Francisco for his collaboration efforts and modeling expertise and assistance.

I would like to acknowledge the generous financial support provided by the U. S. National Science Foundation and Western Virginia Water Authority.

I also want to acknowledge the people that helped me collect data during the early years of my research. Thanks to the staff of Western Virginia Water Authority at Spring Hollow Reservoir (SHR) for use of their facilities and equipment. I would also like to thank Dr. Johny Wüest for allowing me to visit and conduct a field campaign while at EAWAG, a world-class research institute. Lastly, I am very grateful to Paul Gantzer for his tireless data collection on SHR in 2003 and 2004, which is a major part of this dissertation.

I would like to extend a warm thank you to Lee Bryant for being a wonderful friend and colleague. I thoroughly enjoyed all of our time together on campus and at EAWAG, and she never failed to make me smile.

I would also like to thank my parents, Marvin and Lan Burris, for always being proud of my accomplishments and teaching me the value of dedication and hard work. I am extremely thankful that my mom will be with me as I receive my diploma this spring.

Above all, I give many, many thanks to my little family, my husband Jay and my daughter Amelia. I thank you both for your unending patience and allowing me time to complete my work. Amelia, I hope that I will always be a good example to you of what women can achieve. And, Jay, I want to thank you from the bottom of my heart for your support, understanding, and countless sacrifices made on behalf of my research–for this, I am forever grateful. This PhD is as much yours as it is mine.

ATTRIBUTION

Several colleagues and coworkers aided in the writing and research behind three of the chapters of this dissertation. A brief description of their backgrounds and contributions are included here.

Prof. John Little- Ph.D. (Department of Civil and Environmental Engineering, University of California, Berkeley) is the primary Advisor and Committee Chair. Prof. Little provided continual guidance and feedback for modeling work, manuscript development and editing, and presentation preparation. Furthermore, he provided support during field data collection.

Chapter 2: Designing Hypolimnetic Aeration and Oxygenation Systems – A Review

Prof. John Little developed the original idea for the review and provided regular instruction on manuscript organization and content.

Chapter 3: Linear Bubble Plume Model for Hypolimnetic Oxygenation: Full-Scale Validation and Sensitivity Analysis

Paul Gantzer- Ph.D. (Department of Civil and Environmental Engineering, Virginia Tech) was a student in the author's research group and contributed to this chapter during his graduate studies by collecting numerous data sets during diffuser tests in Spring Hollow Reservoir, Virginia.

Prof. John Little provided general guidance on drafting the manuscript and edited the final document for this chapter.

Chapter 4: Coupled Bubble Plume/Reservoir Models for Hypolimnetic Oxygenation

Prof. Francisco Rueda- Ph.D. (Department of Civil and Environmental Engineering, University of California, Davis) is currently at Instituto del Agua y Dpto. Ingeniería Civil, Universidad de Granada in Spain. Prof. Rueda coupled the bubble-plume model with Si3D and provided extensive support for preparation of input files, application of the Si3D coupled model, and post-processing of model results.

Daniel McGinnis- Ph.D. (Department of Civil and Environmental Engineering, Virginia Tech) is currently a post-doctoral researcher at Surface Waters - Research and Management, Swiss Federal Institute for Environmental Science and Technology (Eawag). He was a former member of the author's research group, and his mentorship aided in coupling the bubble-plume model with CE-QUAL-W2 (W2). Dr. McGinnis also provided insightful comments and suggestions during the W2 model coupling and analysis.

Prof. John Little gave detailed direction for application of the coupled models and general guidance for analysis of model predictions. Prof. Little also provided helpful suggestions to improve the figures in this chapter.

Table of Contents

CHAPTER 1. LITERATURE REVIEW 1

EUTROPHICATION AND THE EFFECTS OF AQUATIC HYPOXIA 1
DESIGN OF HYPOLIMNETIC AERATION AND OXYGENATION 2
Hypolimnetic Aeration and Oxygenation Devices 2
Airlift Aerator 2
Speece Cone 3
Bubble-Plume Diffuser 3
Previous Studies 3
Airlift Aerator 5
Bubble-Plume Diffuser 6
LINEAR BUBBLE PLUME MODEL FOR HYPOLIMNETIC OXYGENATION 9
COUPLED BUBBLE-PLUME/RESERVOIR MODELS FOR HYPOLIMNETIC OXYGENATION 10
RESEARCH OBJECTIVES 11
REFERENCES 14

CHAPTER 2. DESIGNING HYPOLIMNETIC AERATION AND OXYGENATION SYSTEMS – A REVIEW 20

ABSTRACT 20
INTRODUCTION 21
HYPOLIMNETIC AERATION AND OXYGENATION DEVICES 22
Airlift Aerator 23
Speece Cone 23
Bubble-Plume Diffuser 23
DISCRETE BUBBLE MODEL 24
DESIGN STUDIES AND APPLICATION OF THE DISCRETE BUBBLE MODEL 27
Airlift Aerator 28
Speece Cone 29
Bubble-Plume Diffuser 30
FUTURE RESEARCH 35
ACKNOWLEDGEMENTS 37
SUPPORTING INFORMATION AVAILABLE 37
LITERATURE CITED 37
SUPPORTING INFORMATION: EARLY DESIGN STUDIES, NOMENCLATURE, TABLES, FIGURES, AND LITERATURE CITED 50
Early Design Studies 50
Airlift Aerator 50
Bubble-Plume Diffuser 52
Nomenclature 52
Tables and Figures 56
Literature Cited 71

CHAPTER 3. LINEAR BUBBLE PLUME MODEL FOR HYPOLIMNETIC OXYGENATION: FULL-SCALE VALIDATION AND SENSITIVITY ANALYSIS 76

ABSTRACT 76

INTRODUCTION 76
BUBBLE PLUMES IN STRATIFIED WATERBODIES 78
LINEAR BUBBLE PLUME MODEL 79
APPLICATION TO SPRING HOLLOW RESERVOIR, VA, U.S.A. 82
Field Data Collection *82*
Observations and Model Application *84*
Sensitivity Analysis *87*
COMPARISON OF LINEAR AND CIRCULAR BUBBLE PLUME MODELS 89
SUMMARY AND CONCLUSIONS 90
ACKNOWLEDGEMENTS 91
NOTATION 91
REFERENCES 94

CHAPTER 4. COUPLED BUBBLE PLUME/RESERVOIR MODELS FOR HYPOLIMNETIC OXYGENATION 108

ABSTRACT 108
KEYWORDS 108
INTRODUCTION 109
DESCRIPTION OF COUPLED MODELS 110
Linear Bubble Plume Model *111*
Reservoir Models *112*
CE-QUAL-W2 (W2) 112
Si3D 112
COUPLING BUBBLE PLUME AND RESERVOIR MODELS 113
W2 ..... *113*
Si3D *114*
APPLICATION OF COUPLED MODELS 115
Rectangular Basin *115*
Results and Discussion 116
Spring Hollow Reservoir, Virginia, U.S.A. *120*
Field Data Collection 120
Results and Discussion 121
CONCLUSIONS 124
ACKNOWLEDGEMENTS 125
NOTATION 125
REFERENCES 127

CHAPTER 5. DISSERTATION SUMMARY AND CONCLUSIONS 147

REFERENCES 148

List of Tables

TABLE 1. SUMMARY OF SELECTED HYPOLIMNETIC AERATION AND OXYGENATION INSTALLATIONS DOCUMENTED IN THE LITERATURE. BOTH EXPERIMENTAL AND PERMANENT UNITS ARE INCLUDED. 56
TABLE 2. CORRELATION EQUATIONS FOR HENRY'S CONSTANT, MASS TRANSFER COEFFICIENT, AND BUBBLE RISE VELOCITY [*WÜEST ET AL.*, 1992]. 61
TABLE 3. NON-LINEAR DIFFERENTIAL FLUX EQUATIONS OF THE AIRLIFT AERATOR [*BURRIS ET AL.*, 2002] AND SPEECE CONE [*MCGINNIS AND LITTLE*, 1998] MODELS. 62
TABLE 4. KEY VARIABLES AND WATER FLOW RATE EQUATIONS OF THE AIRLIFT AERATOR MODEL [*BURRIS ET AL.*, 2002; *LITTLE AND DEL VECCHIO*, 1996]. 63
TABLE 5. KEY VARIABLES OF THE SPEECE CONE MODEL [*MCGINNIS AND LITTLE*, 1998]. 64
TABLE 6. SPEECE CONE PERFORMANCE AT VARYING DEPTHS PREDICTED USING ASSUMED CONE DIMENSIONS AND OPERATIONAL PARAMETERS [*MCGINNIS AND LITTLE*, 1998]. 65
TABLE 7. KEY VARIABLES OF THE CIRCULAR [*WÜEST ET AL.*, 1992] AND LINEAR [*SINGLETON ET AL.*, 2005] BUBBLE-PLUME MODELS. 66
TABLE 8. NON-LINEAR DIFFERENTIAL FLUX EQUATIONS OF THE CIRCULAR [*WÜEST ET AL.*, 1992] AND LINEAR [*SINGLETON ET AL.*, 2005] BUBBLE-PLUME MODELS. 67
TABLE 9. KEY VARIABLES OF THE LINEAR BUBBLE PLUME MODEL (REVISED FROM MCGINNIS ET AL., 2001). 97
TABLE 10. NON-LINEAR DIFFERENTIAL FLUX EQUATIONS OF THE LINEAR BUBBLE PLUME MODEL (REVISED FROM MCGINNIS ET AL., 2001). 98
TABLE 11. CONDITIONS FOR LINEAR BUBBLE PLUME MODEL APPLICATION AND SENSITIVITY ANALYSIS FOR SPRING HOLLOW RESERVOIR, VA, U.S.A. RESERVOIR CONDITIONS ON TESTING DAYS ARE ALSO INCLUDED. 99
TABLE 12. CONDITIONS FOR COUPLED LINEAR BUBBLE PLUME/RESERVOIR MODEL APPLICATIONS FOR RECTANGULAR BASIN SIMULATION AND FULL-SCALE DIFFUSER TEST IN SPRING HOLLOW RESERVOIR (SHR), VA, U.S.A. DURING SEPTEMBER 28–OCTOBER 13, 1998. 131
TABLE 13. EFFECT OF PLUME UPDATE PERIOD AND DIFFUSER LENGTH ON OXYGEN INPUT TO RECTANGULAR BASIN PREDICTED BY CE-QUAL-W2 (W2) AND SI3D COUPLED MODELS... 132

List of Figures

FIGURE 1. PHOTOGRAPH OF FULL-LIFT AERATOR PRIOR TO INSTALLATION. (PHOTO FROM BOB KORTMANN OF ECOSYSTEM CONSULTING SERVICE, INC.) 43
FIGURE 2. PHOTOGRAPHS OF SPEECE CONE AND DIFFUSER PRIOR TO INSTALLATION AT CAMANCHE RESERVOIR, CALIFORNIA. (PHOTOS FROM ROD JUNG OF EAST BAY MUNICIPAL UTILITY DISTRICT.) 44
FIGURE 3. PHOTOGRAPHS OF LINEAR (TOP) AND CIRCULAR (BOTTOM) BUBBLE-PLUME DIFFUSERS. (PHOTO OF LINEAR DIFFUSER FROM MARK MOBLEY OF MOBLEY ENGINEERING, INC. PHOTO OF CIRCULAR DIFFUSER FROM SWISS FEDERAL INSTITUTE FOR AQUATIC SCIENCE AND TECHNOLOGY.) 45
FIGURE 4. OBSERVED AND PREDICTED DO CONCENTRATIONS BASED ON VALIDATION OF DISCRETE-BUBBLE MODEL DURING OXYGEN TRANSFER EXPERIMENTS IN A LARGE VERTICAL TANK [*MCGINNIS AND LITTLE*, 2002]. 46
FIGURE 5. OBSERVED AND MODEL DO PROFILES FOR AIRLIFT AERATOR IN LAKE PRINCE, VIRGINIA, USA FOR LOW (LEFT, 65 NM^3/H) AND HIGH (RIGHT, 227 NM^3/H) AIR FLOW RATES (— MODEL FIT, -·- MODEL PREDICTION, ● RISER DATA, ▲ DOWNCOMER 1 DATA, ■ DOWNCOMER 2 DATA). DATA WERE COLLECTED FROM AN AIRLIFT AERATOR EQUIPPED WITH TWO DOWNCOMERS [*BURRIS ET AL.*, 2002]. 47
FIGURE 6. TEMPERATURE (°C, TOP) AND DO (G/M^3, BOTTOM) CONTOURS IN LAKE HALLWIL, SWITZERLAND WITH CIRCULAR BUBBLE-PLUME MODEL PREDICTIONS FOR PLUME WIDTH AND DEPTH OF MAXIMUM RISE OVERLAID. FOR CLARITY, THE TEMPERATURE AND DO CONTOURS WERE SCALED TO SHOW ONLY VALUES FROM 5.5–8 °C AND 0–5 G/M^3, RESPECTIVELY [*MCGINNIS ET AL.*, 2004]. 48
FIGURE 7. MEASURED AND PREDICTED IN-PLUME CONSTITUENT PROFILES FOR LINEAR BUBBLE-PLUME MODEL EVALUATION USING DATA FROM SPRING HOLLOW RESERVOIR, VIRGINIA, USA [*SINGLETON ET AL.*, 2005]. 49
FIGURE 8. AVERAGED MEASURED IN-PLUME TEMPERATURE AND DO PROFILE AND CIRCULAR BUBBLE-PLUME MODEL PREDICTIONS FOR LAKE HALLWIL, SWITZERLAND [*MCGINNIS ET AL.*, 2004]. 68
FIGURE 9. MEASURED PLUME TEMPERATURE (TOP) AND DO (BOTTOM) CONTOURS WITH LINEAR BUBBLE-PLUME MODEL PREDICTIONS FOR DIFFUSER OPERATION WITH PURE OXYGEN ON 23 OCTOBER 2004 IN SPRING HOLLOW RESERVOIR, VIRGINIA, USA [*SINGLETON ET AL.*, 2005]. 69
FIGURE 10. MEASURED TEMPERATURE (TOP) AND DISSOLVED OXYGEN (BOTTOM) PROFILES WITH COUPLED BUBBLE PLUME-RESERVOIR MODEL PREDICTIONS FOR LINEAR DIFFUSER OPERATION IN SPRING HOLLOW RESERVOIR, VIRGINIA, USA DURING 1997 [*MCGINNIS ET AL.*, 2001]..... 70
FIGURE 11. EFFECT OF INITIAL FROUDE NUMBER (Fr_O) ON PREDICTIONS OF PLUME WATER VELOCITY AND PLUME WIDTH USING LINEAR BUBBLE PLUME MODEL. 100
FIGURE 12. PHOTOGRAPH AND SCHEMATIC OF LINEAR BUBBLE PLUME DIFFUSER IN SPRING HOLLOW RESERVOIR, VA, U.S.A. (COURTESY OF MARK MOBLEY, MOBLEY ENGINEERING, INC.). 101
FIGURE 13. BATHYMETRIC MAP OF SPRING HOLLOW RESERVOIR, VA, U.S.A. SHOWING LOCATIONS OF LINEAR BUBBLE PLUME DIFFUSER AND LATERAL CTD TRANSECTS. 102
FIGURE 14. MEASURED PLUME TEMPERATURE (°C) (LEFT) AND DO (G/M^3) (RIGHT) CONTOURS WITH LINEAR BUBBLE PLUME MODEL PREDICTIONS FOR DIFFUSER OPERATION WITH AIR (2 JULY 2003) AND PURE OXYGEN (17 AUGUST 2003 AND 23 OCTOBER 2004) IN SPRING HOLLOW RESERVOIR, VA, U.S.A. CONTOURS WERE INTERPOLATED FROM CTD PROFILES

COLLECTED AT LOCATIONS INDICATED BY SMALL BLACK SQUARES ALONG THE BOTTOM OF EACH PLOT. 103
FIGURE 15. INPUT BOUNDARY CONDITIONS FOR LINEAR BUBBLE PLUME MODEL EVALUATION AND SENSITIVITY ANALYSIS. DATA COLLECTED FROM SPRING HOLLOW RESERVOIR, VA, U.S.A. DURING DIFFUSER OPERATION WITH COMPRESSED AIR [2 JULY 2003 (×)] AND PURE OXYGEN [17 AUGUST 2003 (●) AND 23 OCTOBER 2004 (○)]. 104
FIGURE 16. IN-PLUME PROFILES PREDICTED BY LINEAR BUBBLE PLUME MODEL, REPRESENTED AS SOLID LINES (A–C) AND AS SOLID LINES AND SYMBOLS (D–F). INPUT DATA COLLECTED FROM SPRING HOLLOW RESERVOIR, VA, U.S.A. DURING DIFFUSER OPERATION WITH COMPRESSED AIR [2 JULY 2003 (×)] AND PURE OXYGEN [17 AUGUST 2003 (●) AND 23 OCTOBER 2004 (○)]. MEASURED AVERAGE IN-PLUME TEMPERATURE, DO, AND PLUME WATER DENSITY REPRESENTED AS SYMBOLS (A–C). 105
FIGURE 17. EFFECT OF LINEAR BUBBLE PLUME MODEL PARAMETERS ON DEPTH OF MAXIMUM PLUME RISE (DMPR). STANDARD VALUES FOR EACH PARAMETER ARE INDICATED BY THE VERTICAL DASHED LINES. INPUT DATA COLLECTED FROM SPRING HOLLOW RESERVOIR, VA, U.S.A. DURING DIFFUSER OPERATION WITH COMPRESSED AIR [2 JULY 2003 (×)] AND PURE OXYGEN [17 AUGUST 2003 (●) AND 23 OCTOBER 2004 (○)]. 106
FIGURE 18. EFFECT OF INITIAL BUBBLE RADIUS ON OXYGEN TRANSFER EFFICIENCY PREDICTED BY LINEAR BUBBLE PLUME MODEL. INPUT DATA COLLECTED FROM SPRING HOLLOW RESERVOIR, VA, U.S.A. DURING DIFFUSER OPERATION WITH COMPRESSED AIR (2 JULY 2003) AND PURE OXYGEN (17 AUGUST 2003 AND 23 OCTOBER 2004). 107
FIGURE 19. TWO-DIMENSIONAL GRID OF SPRING HOLLOW RESERVOIR, VIRGINIA, U.S.A. IN CE-QUAL-W2. COLUMNS WITH GREY CELLS INDICATE LOCATION OF LINEAR DIFFUSER ALONG BOTTOM OF RESERVOIR. LIGHT AND DARK GREY CELLS REPRESENT PLUME ENTRAINMENT AND DETRAINMENT ZONES, RESPECTIVELY. 133
FIGURE 20. SCHEMATIC OF COUPLING OF LINEAR BUBBLE PLUME MODEL WITH SI3D, SHOWING ENTRAINMENT AND DETRAINMENT CELLS. 134
FIGURE 21. TEMPERATURE AND DO PROFILES PREDICTED BY COUPLED BUBBLE PLUME/W2 MODEL FOR RECTANGULAR BASIN SIMULATION WITH 60 M (TOP) AND 360 M (BOTTOM) DIFFUSER AND 1 HOUR PLUME UPDATE PERIOD. PROFILES ARE FROM CENTER OF BASIN. 135
FIGURE 22. TEMPERATURE AND DO PROFILES PREDICTED BY COUPLED BUBBLE PLUME/SI3D MODEL FOR RECTANGULAR BASIN SIMULATION WITH 60 M (TOP) AND 360 M (BOTTOM) DIFFUSER AND 1 HOUR PLUME UPDATE PERIOD. PROFILES ARE FROM CENTER OF BASIN..... 136
FIGURE 23. LONGITUDINAL VIEW OF HORIZONTAL (TOP ROW) AND VERTICAL (BOTTOM ROW) VELOCITY INDUCED BY LINEAR BUBBLE PLUME OPERATION IN RECTANGULAR BASIN SIMULATION, AS PREDICTED BY COUPLED BUBBLE PLUME/W2 MODEL. GRAPHS ON RIGHT AND LEFT CORRESPOND TO 60 AND 360 M DIFFUSER, RESPECTIVELY, AND ARE FROM DAY 2.25. THE VELOCITY CONTOURS AND VECTORS FOR THE 360 M DIFFUSER ARE SHOWN AT HALF THE SCALE AS FOR THE 60 M DIFFUSER. 137
FIGURE 24. SECTIONAL VIEW OF LONGITUDINAL AND VERTICAL VELOCITY INDUCED BY LINEAR BUBBLE PLUME OPERATION IN RECTANGULAR BASIN SIMULATION, AS PREDICTED BY COUPLED BUBBLE PLUME/SI3D MODEL FOR 60 M (TOP) AND 360 M (BOTTOM) DIFFUSER FOR DAY 2.25. 138
FIGURE 25. PLANAR VIEW OF LONGITUDINAL AND LATERAL VELOCITY INDUCED BY LINEAR BUBBLE PLUME OPERATION IN RECTANGULAR BASIN SIMULATION, AS PREDICTED BY COUPLED BUBBLE PLUME/SI3D MODEL FOR 60 M (LEFT) AND 360 M (RIGHT) DIFFUSER FOR DAY 2.25.

Graphs represent 23 m (top) and 45 m (bottom) depths for 60 m diffuser and 28 m (top) and 45 m (bottom) depths for 360 m diffuser. For all plots, the diffuser is oriented vertically along the north-south axis of the basin. 139
Figure 26. Bathymetric map of Spring Hollow Reservoir, VA, U.S.A. showing location of linear bubble plume diffuser in 1998. 140
Figure 27. Observed temperature and DO profiles in Spring Hollow Reservoir, Virginia, U.S.A. in Fall 1998. Profiles from September 28 were used as initial boundary conditions for the coupled models. 141
Figure 28. Three-dimensional grid of Spring Hollow Reservoir, Virginia, U.S.A in Si3D. 142
Figure 29. Hypolimnetic profiles predicted by coupled bubble plume/W2 model, represented as solid lines. Input data collected from Spring Hollow Reservoir, VA, U.S.A. during diffuser operation in 1998. Observed temperature and DO represented as symbols. 143
Figure 30. Hypolimnetic profiles predicted by coupled bubble plume/Si3D model, represented as solid lines. Input data collected from Spring Hollow Reservoir, VA, U.S.A. during diffuser operation in 1998. Observed temperature and DO represented as symbols. 144
Figure 31. Longitudinal view of (a) temperature, (b) DO, (c) horizontal velocity, and (d) vertical velocity predicted by coupled bubble plume/W2 model for Spring Hollow Reservoir, VA, U.S.A. during diffuser operation on October 5, 1998. Temperature and DO scaled to show gradients caused by plume operation. 145
Figure 32. Two-dimensional view of longitudinal and vertical velocity field with temperature (top) and DO (bottom) contours predicted by coupled bubble plume/Si3D model for Spring Hollow Reservoir, VA, U.S.A. during diffuser operation on October 5, 1998. Temperature and DO scaled to show gradients caused by plume operation. 146

CHAPTER 1. LITERATURE REVIEW

Eutrophication and the Effects of Aquatic Hypoxia

One of the most urgent water quality problems in the world today, especially in densely populated regions, is hypoxia resulting from cultural eutrophication and organic pollutants [*Goldberg*, 1995]. A number of coastal ecosystems have reported a consistent decline in dissolved oxygen (DO) concentrations over time, with a strong correlation between human activities and decreasing oxygen levels [*Diaz*, 2001]. The projected population increase, particularly near water bodies, will exacerbate organic and nutrient loading into aquatic ecosystems. Concurrently, the accumulation of greenhouses gasses in the atmosphere will lead to increased air temperatures, which will enhance naturally occurring thermoclines and haloclines and extend the stratification period of many water bodies. The combined effect of these factors will likely result in the propagation of hypoxic waters [*Pollock and Dubé*, 2007].

The negative consequences of hypoxia in aquatic ecosystems have been extensively reported in the literature. Of particular interest in freshwater lakes and reservoirs that stratify is hypoxia or anoxia within the bottom-most layer or hypolimnion. Anoxia within lake sediments can increase the rate of soluble phosphorus release [*Bostrom et al.*, 1988], and this internal nutrient loading can trigger the growth of nuisance algal blooms [*French and Petticrew*, 2007]. The effects of low DO levels on fish have been studied for decades and include mass mortalities, ecological disruption, physiological stress, and modification of complex behaviors such as schooling, swimming, and reproduction [*Pollock and Dubé*, 2007]. Hypolimnetic anoxia, when combined with elevated concentrations of toxic compounds, can eliminate the use of cold, summertime waters for salmonid habitats [*Beutel et al.*, 2001]. Hypoxia has also been shown to be an endocrine disrupter in fish, impairing reproduction [*Wu et al.*, 2003]. Methylation of inorganic mercury by microorganisms to a soluble and more bioavailable form is enhanced under anoxic conditions [*Mailman et al.*, 2006]. Additionally, anoxic water has been shown to greatly increase the release of major greenhouse gasses from lake sediments [*Liikanen et al.*, 2002]. Oxygen depletion within the hypolimnion may also lead to increases in reduced species such as hydrogen sulfide and ammonia, and the release of soluble iron and manganese from the sediments. Hydrogen sulfide, iron, and manganese in raw water used for potable purposes typically requires additional treatment [*Cooke and Carlson*, 1989], and elevated ammonia concentrations can be toxic to aquatic organisms. The removal of reduced compounds from raw

drinking water creates an increased oxidant demand at the treatment plant, resulting in higher operating costs. Chlorine can also react with certain organics in raw water to produce disinfection-by-products such as trihalomethanes, which are suspected carcinogens and therefore strictly regulated in finished water [*Tate and Arnold*, 1990].

Design of Hypolimnetic Aeration and Oxygenation

Because of increasingly rigorous regulatory and customer-driven standards for finished drinking water, lake and reservoir managers are recognizing the importance of protecting source water quality. One of the methods typically employed to combat anoxia in the hypolimnion and subsequently lower the dosage of chlorine or other oxidants applied at the treatment plant is hypolimnetic aeration/oxygenation. Hypolimnetic aeration and oxygenation involve adding DO to the hypolimnion through the use of compressed air or pure oxygen, respectively, without disturbing the density gradient associated with stratification [*Kortmann et al.*, 1994].

Hypolimnetic Aeration and Oxygenation Devices

The primary types of hypolimnetic aeration and oxygenation systems currently in use include airlift aerators, Speece Cones, and bubble plume diffusers [*McGinnis and Little*, 2002]. Most documented installations use one of these three primary devices. Also, most reported models and studies regarding system design are related to these methods of oxygenation. These specific hypolimnetic oxygenation devices are thus the focus of this section and Chapter 2 of this dissertation.

Airlift Aerator

Full-lift hypolimnetic aerators typically consist of 1) a vertical riser tube, 2) a diffuser inside the bottom of the riser tube, 3) an air-water separation chamber at the top of the riser, and 4) one or two return pipes, called downcomers [*McQueen and Lean*, 1986]. Compressed air is delivered to the aerator and bubbles freely from the diffuser. This creates a positively-buoyant gas-water mixture that ascends the riser. At the top of the riser, some of the bubbles are released to the atmosphere, although some may be entrained in the water that enters the downcomers. The oxygenated water flows through the downcomers and is returned to the hypolimnion [*Burris et al.*, 2002].

Speece Cone

The Speece Cone, developed by Dr. Richard Speece, was originally known as a downflow bubble contact system [*Speece et al.*, 1973; *Thomas et al.*, 1994]. The system consists of a source of oxygen gas, a conical bubble contact chamber, a submersible pump, and a diffuser that disperses highly oxygenated water into the hypolimnion. Ambient water and oxygen gas bubbles are introduced at the top of the cone. As water flows down the cone, the velocity decreases because the cross-sectional area of the cone increases. The system is designed so that the downward velocity of the water is sufficient to overcome the rise velocity of the bubbles at all levels. The applied water flow rate and slope of the cone walls control the water velocity and, therefore, the time available for gas transfer [*McGinnis and Little*, 1998].

Bubble-Plume Diffuser

Bubble-plume diffusers generally have a linear or circular geometry and inject either air or oxygen at a relatively low gas flow rate [*McGinnis and Little*, 2002]. These systems are most suitable for deep lakes where the bulk of the bubbles dissolves in the hypolimnion and the momentum generated by the plume is low enough to prevent significant erosion of the thermocline [*Wüest et al.*, 1992]. Gas bubbles are injected into the water column through a porous diffuser creating a gas/water mixture that rises and gains momentum due to a positive buoyancy flux. The buoyant mixture entrains water at the boundaries, which increases the water flow rate and cross-sectional area, but decreases the momentum. The plume rises against the vertical density gradient until the depth of maximum plume rise (DMPR) is reached, which is where the plume momentum is zero. The plume water at this depth is negatively buoyant and is expected to fall back to an equilibrium depth (ED) where the plume density equals the ambient density [*McGinnis et al.*, 2004]. Upon reaching the ED, the plume water disperses horizontally into the far-field [*McGinnis et al.*, 2004].

Previous Studies

Numerous studies have been conducted documenting the physical, chemical, and biological effects of hypolimnetic aeration and oxygenation on lakes and reservoirs. These studies have been reviewed by *Fast and Lorenzen* [1976], *Taggart and McQueen* [1981], *Pastorok et al.* [1981; 1982], *McQueen and Lean* [1986], and, more recently, *Beutel and Horne* [1999]. In their extensive review of literature on the effects of hypolimnetic aeration on water

quality, lake biota, and stratification, *McQueen and Lean* [1986] summarized the results of the studies: (1) well designed aeration systems have maintained stratification and have not increased hypolimnetic water temperature significantly; (2) hypolimnetic oxygen levels increased, (3) iron, manganese, hydrogen sulfide, and methane levels decreased; (4) zooplankton populations were generally unaffected; (5) chlorophyll levels were usually not altered; and (6) depth distributions of cold water fish populations increased. The effects of hypolimnetic aeration on phosphorus levels have been more variable. *McQueen et al.* [1986] attribute this to pH levels and iron availability for phosphorus sedimentation. The published effects of aeration on nitrogen levels have not been consistent either; ammonium and total nitrogen decreased in some studies, but increased in others. *McQueen and Lean* [1986] concluded that this is also related to pH levels. It has been reported that gaseous nitrogen concentrations were elevated to super-saturation levels during hypolimnetic oxygenation with compressed air, and there has been some concern expressed over this causing gas bubble disease in fish [*Fast et al.*, 1975b]. However, there have been no reported adverse effects of hypolimnetic aeration on fish populations [*McQueen and Lean*, 1986].

Beutel and Horne [1999] conducted a comprehensive literature review on the effects of hypolimnetic oxygenation and reported the following after evaluation of several detailed case studies: (1) unlike some hypolimnetic aeration systems, oxygenation projects maintained stratification and only caused minor increases in hypolimnetic temperature, (2) average hypolimnetic dissolved oxygen concentrations were maintained at greater than 4 mg L^{-1}, (3) induced oxygen demand reported for oxygenated lakes and reservoirs was lower than values reported for aerated waterbodies, and (4) oxygenation decreased hypolimnetic concentrations of dissolved phosphorus, ammonia, manganese, and hydrogen sulfide by 50-100%.

A survey of the literature on hypolimnetic aeration effects published since the review of *McQueen and Lean* [1986] generally supports the findings of that paper [*Ashley*, 1988; *Gachter and Wehrli*, 1998; *Gemza*, 1995; *Gibbons et al.*, 1994; *Jaeger*, 1990; *Nordin et al.*, 1995; *Soltero et al.*, 1994]. Similarly, a survey of the effects of hypolimnetic oxygenation reported since the review of *Beutel and Horne* [1999] confirms the conclusions of that work [*Jung et al.*, 1999; *Søndergaard et al.*, 2000].

While the vast majority of studies regarding hypolimnetic aerators and oxygenators have focused on their effects, relatively little work has been undertaken to examine the parameters that

impact system performance. A review of these early design studies of full-lift aerators and bubble plume diffusers is presented in the following subsections. Because the Speece Cone has not been as widely used as other oxygenation devices, no early design literature was available.

Airlift Aerator

One of the earliest attempts to design airlift aerators, developed by *Lorenzen and Fast* [1977], consists of determining approximate specifications for the compressor. The design air flow rate is based on the hypolimnetic oxygen depletion rate and the induced water flow rate through the aeration device. The authors assumed that water reaching the top of the aerator is saturated with oxygen. The water flow rate needed is found using the hypolimnetic depletion rate and volume and the change in the DO concentration. The air flow rate required to induce this water flow rate is a function of the aerator dimensions. The authors assumed that the theoretical head available in the full-lift aerator results from the difference in density between the air-water mixture in the riser and the ambient lake water. It was also assumed that half of the theoretical head is used to convey water to the surface and that the remainder is dissipated as water exits the aerator through the downcomer.

The method of *Taggart and McQueen* [1982] involves determining the dimensions of the riser and downcomer when compressor capacity is known. The authors presented a detailed, empirically-based approach for establishing full-lift aerator specifications including diffuser depth, air flow rate, water flow rate, and riser and downcomer cross-sectional areas. Water flow rate is calculated with an empirical equation that was developed using a proportionality relationship from the literature and a regression of data collected from 20 published experiments. To determine the riser cross-sectional area, the authors assumed that the maximum induced water velocity is a function of the median estimated bubble rise velocity.

Another empirical full-lift aerator design model was proposed by *Ashley* [1985]. In addition to aerator sizing, Ashley also discussed other practical design aspects including air supply, rated and actual air flow, and performance specifications. The model was derived from the work of *Lorenzen and Fast* [1977] and *Taggart and McQueen* [1982] as well as experience with a full-scale system. Ashley developed a step-wise procedure for sizing compressors and full-lift aerators. The model assumes that the induced water flow rate will completely satisfy the oxygen consumption in the hypolimnion measured during spring stratification. The model also

requires an estimate of the increase in the DO concentration produced by the aerator. Determination of the DO increase is an important variable, and *Ashley* [1985] suggested that this parameter may be difficult to predict.

Little [1995] developed a model to predict oxygen transfer in a full-lift hypolimnetic aerator. Cocurrent flow of water and gas, variation of the saturated DO concentration as a function of depth, and depletion of gaseous oxygen are accounted for in the model. Input parameters include aerator dimensions, volumetric air flow rate, diffuser depth, and ambient water conditions. To calculate water flow rate, an empirical correlation that is a function of superficial gas velocity and riser length was developed. The correlation was derived from the same data set used by *Taggart and McQueen* [1982], except dependence on riser diameter was eliminated. Mass balance equations were used to determine the amount of oxygen transferred from the bubbles to the water. Literature correlations, originally developed for bubble columns and airlift reactors, were used to estimate the mass transfer coefficient and gas holdup in the riser. The model assumes that gas-phase holdup is small, that water is in plug flow, and that nitrogen transfer may be neglected.

Bubble-Plume Diffuser

Because bubble plumes are encountered in a variety of natural and man-made systems, numerous studies have been conducted on plume dynamics. Less work has been performed on bubble plumes in stratified environments [*Asaeda and Imberger*, 1993; *Lemckert and Imberger*, 1993; *McDougall*, 1978; *Schladow*, 1993; *Socolofksy and Adams*, 2003], and even fewer investigations on bubble plumes incorporating gas transfer [*Sahoo and Luketina*, 2003; *Speece and Murfee*, 1973; *Speece and Rayyan*, 1973; *Tsang*, 1990]. Bubble plumes intended for hypolimnetic oxygenation must be capable of increasing dissolved oxygen concentrations, and most lakes and reservoirs have vertical density and concentration gradients. Therefore, only design methods that account for gas transfer and stratification were reviewed. Also, because this work focuses on oxygenation methods that preserve stratification, destratification models [*Asaeda and Imberger*, 1993; *Davis*, 1980; *Sahoo and Luketina*, 2003; *Schladow*, 1993] were not reviewed.

A model was developed by *Rayyan and Speece* [1977] to describe the hydrodynamics of circular bubble plumes in stratified environments. The model accounts for non-linear

stratification and oxygen transfer. The model predicts maximum plume rise height, centerline velocity and nominal half-width, and density and temperature differences between the plume and the ambient water column. Conservation principles were applied to a circular plume to derive equations for water mass flux, oxygen flow, momentum flux, buoyancy flux, and heat flux. These equations are functions of characteristic plume width, entrainment coefficient, water and bubble rise velocities, gas concentration, bubble and water spreading coefficients, and local plume and ambient water densities and temperatures. The entrainment coefficient was set equal to 0.04 for low flow rates in the laboratory and 0.055 for higher flow rates in the field. The water and bubble spreading coefficients were 1.25 and 0.2, respectively. Bubble size varies along the height of the circular plume and is a function of oxygen transfer and the local hydrostatic pressure. It was assumed that the velocity and density profiles are similar at all heights above the diffuser, and normally distributed. The Boussinesq assumption was invoked.

Hypolimnetic oxygenation using bubble plumes released from areal sources was modeled by *Tsang* [1990]. The author described bubble plume dynamics as consisting of two primary mechanisms: hydrodynamics (macroscopic) and gas/bubble dynamics (microscopic). Tsang applied fundamental principles to relate the various parameters that govern bubble plume dynamics and gas transfer, which resulted in three equations. The conservation of mass and energy were used to obtain equations for average water velocity across the plume $W(z)$ and volumetric gas flux. The gas flux equation accounts for bubble radius variations with depth due to changing hydrostatic pressure and gas transfer. For the third equation, formulas describing the absorption of gas across bubble walls and isothermal expansion of gas bubbles were combined. The three equations can be solved simultaneously to determine the three unknowns: the entrainment coefficient α, average water velocity $W(z)$, and bubble radius $R_b(z)$. The following assumptions were made by *Tsang* [1990] during his theoretical analysis of bubble plumes. The areal diffuser source is considered to be circular, and a top-hat distribution for vertical velocity is assumed. The plume expansion angle, number flux of bubbles, and bubble rise velocity are assumed to be constant. The potential and kinetic energy fluxes of the gas phase are negligible compared to those for the liquid phase. It is also assumed that the ambient dissolved gas concentration is constant during bubble ascent. Lastly, it is unclear whether the model accounts for stratified ambient conditions.

Early literature on design of airlift aerators and bubble plumes for hypolimnetic oxygenation provides useful insight and field observations of factors affecting device performance. However, each of the models has deficiencies that can result in incorrect sizing of oxygenation devices and/or gas supply facilities. *Lorenzen and Fast* [1977] provided practical guidance and information about the major variables that affect the performance of airlift aerators. However, their aerator sizing method makes a number of critical assumptions that are unverified. *Taggart and McQueen's* [1982] model presents a simple, straightforward approach for the hydrodynamic design of airlift aerators. However, the model lacks key elements, namely prediction of oxygen transfer. Also, the effect of gas flux on induced water velocity was not considered. The authors did account for gas flow when developing a correlation to estimate induced water flow rate as a function of volumetric air flow and riser depth. *Ashley* [1985] presented a detailed, step-wise method to size airlift aerators and provided helpful information on engineering aspects such as compressors, power supply, oxygen transfer, and oxygenation capacity. The model was field tested by *Ashley et al.* [1987], but the aeration system was unable to satisfy hypolimnetic oxygen demand because the induced water velocity and oxygen input were overestimated during design. The model proposed by *Little* [1995] was the first attempt at using a fundamental approach to predict oxygen transfer in airlift aerators, but the model relies on empirical equations to determine critical variables. Also, nitrogen transfer can be significant for deep installations and will affect bubble volume and bubble-size dependent properties like the rise velocity and mass transfer coefficient. The bubble-plume model of *Rayyan and Speece* [1977] is based on fundamental principles and captures many of key hydrodynamic features of plumes. However, the model does not account for nitrogen transfer, ambient salinity gradients, or the effect of changing bubble size on rise velocity and the mass transfer coefficient. While hydrodynamic predictions from the model have been verified with laboratory and field testing, oxygen transfer estimates have not been validated. Similarly, the bubble-plume model of *Tsang* [1990] has not been validated with data. Also, the effect of changing bubble size on rise velocity is not considered. Lastly, it is unclear whether Tsang's model accounts for ambient concentration gradients.

In each oxygenation device, gas bubbles in contact with water facilitate interfacial transfer of oxygen, nitrogen and other soluble gases. Using fundamental principles, a discrete-bubble model was first developed to predict plume dynamics and gas transfer for a circular

bubble plume diffuser. The discrete-bubble approach has subsequently been validated using oxygen transfer tests in a large tank and applied successfully at full-scale to an airlift aerator as well as to both circular and linear bubble plume diffusers. The discrete-bubble approach has also been extended to the Speece Cone, but the model has not yet been validated due to a lack of suitable data.

Linear Bubble Plume Model for Hypolimnetic Oxygenation

As stated previously, bubble plume diffusers are one of the primary types of hypolimnetic oxygenation devices. Two areal diffuser geometries are typically installed, circular and linear. A bubble plume model to predict oxygen transfer from linear diffusers was presented by *McGinnis et al.* [2001], based on the model for a circular diffuser developed earlier by *Wüest et al.* [1992]. While a number of models for point-source or circular bubble plumes have been proposed [*Asaeda and Imberger*, 1993; *Brevik and Killie*, 1996; *Brevik and Kluge*, 1999; *Cederwall and Ditmars*, 1970; *Ditmars and Cederwall*, 1974; *Fanneløp and Sjøen*, 1980; *Johansen*, 2000; *Kobus*, 1968; *McDougall*, 1978; *Milgram*, 1983; *Rayyan and Speece*, 1977; *Sahoo and Luketina*, 2003; *Schladow*, 1992; *Speece and Rayyan*, 1973; *Tsang*, 1990; *Wüest et al.*, 1992; *Zheng et al.*, 2002] less work has been conducted on linear (also referred to as two-dimensional or planar) bubble plumes. *Kobus* [1968] developed one of the first detailed analytical models for linear bubble plumes, but the model calculates the transport rate of buoyancy empirically using experimental data as a function of air discharge rate and bubble size [*Ditmars and Cederwall*, 1974]. *Cederwall and Ditmars* [1970] and *Ditmars and Cederwall* [1974] presented a model similar to that of *Kobus* [1968], but included bubble slip velocity. *Brevik* [1977] proposed a phenomenological theory for two-dimensional bubble plumes comparable to that of *Cederwall and Ditmars* [1970], except that a kinetic energy equation was used to predict entrainment as opposed to assuming that entrainment is proportional to the vertical plume velocity. *Wilkinson* [1979] proposed that full-scale linear plumes could be characterized by a Weber number. *Laureshen and Rowe* [1987] presented a model for two-dimensional bubble plumes that assumed constant bubble slip velocity. Plume spreading, entrainment, and momentum amplification were assumed to be functions of the plume Weber number and empirical constants. *Fanneløp et al.* [1991] developed a model for linear plumes in shallow water and studied the resulting surface currents and recirculation cells. Other

researchers that have studied linear bubble plumes include *Brevik and Kluge* [1999], who expanded a previous phenomenological theory to account for the influence of vertical turbulence.

Although much insight into plume dynamics was gained, none of the previous models for linear or two-dimensional bubble plumes accounted for ambient stratification or gas transfer. The first linear bubble plume model to include gas transfer was presented by *McGinnis et al.* [2001], who converted the circular bubble plume model of *Wüest et al.* [1992] to linear geometry. The incorporation of gas transfer is critical because the rapid dissolution rate of oxygen, and nitrogen when compressed air is used, strongly influences the buoyancy of the plume [*Wüest et al.*, 1992]. Gas transfer is especially important in deep water bodies and for weak plumes because of the increased contact time allows greater gas exchange. Lastly, the prediction of oxygen addition from hypolimnetic oxygenation systems is facilitated. Despite the usefulness of the linear bubble plume model, it has not yet been validated at full-scale and over a range of operating conditions.

Coupled Bubble-Plume/Reservoir Models for Hypolimnetic Oxygenation

While bubble plumes are successful at adding oxygen, the added energy may induce large-scale hypolimnetic mixing. An unconfined bubble plume is in intimate contact with the ambient water column and is strongly influenced by the local density profile. Plume-induced mixing changes the thermal structure of the reservoir, and plume performance depends strongly on the vertical density gradient, establishing a feedback loop that continually changes plume behavior [*McGinnis et al.*, 2004]. Mixing may partially erode the thermocline and subsequently lead to warming of the hypolimnion and even premature destratification of the reservoir. Higher hypolimnetic temperatures and plume-induced mixing may also be responsible for increased sediment oxygen uptake (SOU). A number of studies have reported that small increases in water velocity above lake sediments can significantly increase SOU [*Arega and Lee*, 2005; *Beutel*, 2003; *Hondzo*, 1998; *Josiam and Stefan*, 1999; *Lorke et al.*, 2003; *Mackenthun and Stefan*, 1998]. Because the sediment is the largest sink of oxygen in most lakes and reservoirs, the effect of plume-induced mixing must be included to avoid serious under-sizing of oxygenation systems. The specific plume-induced mixing mechanisms should be identified and incorporated in a coupled bubble-plume/reservoir model for successful design and operation.

A number of models for predicting plume dynamics and/or oxygen transfer from bubble-plumes have been developed [*Singleton and Little*, 2006], but less research has focused on modeling the interaction between bubble-plumes and ambient water bodies. Most of the coupled bubble-plume/reservoir models proposed in the literature involve whole-lake artificial circulation or destratification systems and, consequently, do not account for oxygen transfer from the bubbles [*Johnson et al.*, 2000; *Schladow*, 1993; *Zic and Stefan*, 1994]. Similar to *Schladow* [1993], *Lindenschmidt and Hamblin* [1997] coupled the one-dimensional hydrodynamic model DYRESM with stirrer and bubbler modules to simulate mixing induced by Limnox hypolimnetic aerators, an enclosed type of aeration device. To analyze the effectiveness of bubble-plume destratification on reducing algal blooms, *Imteaz and Asaeda* [2000] coupled DYRESM with a bubble plume model and an ecological model that tracks factors related to phytoplankton growth. *Bravo et al.* [2007] used a comprehensive and commercially available hydrodynamic model, FLUENT, and constructed a two-fluid, dispersed turbulence model to simulate bubble plume dynamics. Despite their performance and applicability, none of these coupled models included mass transfer between the bubbles and water, which is critical to predicting the performance and evaluating the effectiveness of hypolimnetic oxygenation systems.

Research Objectives

The overall goal of this research is to model the induced large-scale mixing and oxygen addition by linear bubble plumes used for hypolimnetic oxygenation. To accomplish this, a linear bubble plume model was coupled to two different reservoir models, CE-QUAL-W2 (W2) and Si3D, and the predictions were compared against field observations. As a prelude to the model coupling, an existing linear bubble-plume model was improved and validated with data collected from a full-scale linear diffuser installed in Spring Hollow Reservoir (SHR), Virginia, U.S.A. The stand-alone performance of the bubble-plume model was evaluated prior to coupling with the reservoir models to ensure representative plume model results.

One of the motivations for developing the coupled bubble-plume/reservoirs models is that they may become valuable predictive tools for design and optimization of hypolimnetic oxygenation systems. As a corollary to the overall research goal as well as addressing a deficiency in the literature, an extensive review of models for sizing and designing hypolimnetic aeration/oxygenation devices was conducted. In addition to models for bubble plumes diffusers,

those for airlift aerators and Speece Cones were reviewed. The current state-of-the-art for designing each hypolimnetic oxygenation device was presented. The resulting suite of models, which includes the recently validated linear bubble plume model, can be coupled with either W2 and/or Si3D to predict the performance of a range of hypolimnetic oxygenation devices. This comprehensive coupled model could be then used to compare the effects of different oxygenation scenarios in order to implement the most suitable one.

In support of the overall research goal of modeling plume-induced mixing and oxygen addition from hypolimnetic oxygenators, the specific research objectives are to:

1. Review the literature to develop a historical perspective of hypolimnetic oxygenation devices and sizing/design methods and to determine the current state-of-the-art with respect to design models ;
2. Improve and validate the linear bubble-plume model using data collected from a full-scale system at SHR under a range of operating conditions;
3. Formally integrate the linear bubble plume model into W2 and Si3D via coupling to model the effects of diffuser operation on reservoir temperature and DO concentrations.

A chapter is dedicated to each research objective, starting with Chapter 2. The chapters are in manuscript format, primarily in the style of Water Resources Research. The manuscripts in Chapters 2 and 3 have already been published in Environmental Science & Technology [*Singleton and Little*, 2006] and Water Resources Research [*Singleton et al.*, 2007], respectively. A summary of each chapter is as follows.

In Chapter 2, the various types of hypolimnetic oxygenation devices are briefly discussed, select installations are summarized, and a suite of published design methods that have been validated using data collected from full-scale field installations is reviewed in detail. The unified suite of models, all based on simple discrete-bubble dynamics, represents the current state-of-the-art for designing systems to add oxygen to stratified lakes and reservoirs. Despite the large number of hypolimnetic oxygenation investigations, relatively few have examined the parameters that impact system performance, and there is no comprehensive review of published hypolimnetic oxygenation design methods.

In Chapter 3, an improved linear bubble plume model is presented, observations and model predictions are compared, and results of a sensitivity analysis are discussed. The motivation for this work includes verification of model performance prior to use for design and

investigation of critical model parameters through sensitivity analysis. Also, the accuracy of predictions for depth of maximum plume rise (DMPR), induced water flow rate, and oxygen addition should be assessed prior to coupling with lake and reservoir models such as CE-QUAL-W2 and Si3D.

Chapter 4 presents the coupling of a linear bubble plume model that includes gas transfer with two different reservoir models, CE-QUAL-W2 (W2) Version 3.2 and Si3D. The coupled models are used to predict plume dynamics, induced mixing, and oxygen addition from a linear diffuser used for hypolimnetic oxygenation. W2 is a two-dimensional (2D), laterally averaged hydrodynamic and water quality model, and Si3D is a three-dimensional (3D) hydrodynamic model. In this chapter, the components of the coupled models and the coupling procedures are described, results from simulations using a rectangular basin are discussed, and field data from a full-scale system are compared to model predictions.

References

Arega, F., and J. H. W. Lee (2005), Diffusional mass transfer at sediment-water interface of cylindrical sediment oxygen demand chamber, *J. Environ. Engineer.*, *131*(5), 755-766.

Asaeda, T., and J. Imberger (1993), Structure of bubble plumes in linearly stratified environments, *J. Fluid Mech.*, *249*, 35-57.

Ashley, K. I. (1985), Hypolimnetic aeration: Practical design and application, *Water Res.*, *19*(6), 735-740.

Ashley, K. I., et al. (1987), Hypolimnetic aeration: Field test of the empirical sizing method, *Water Res.*, *21*(2), 223-227.

Ashley, K. I. (1988), Hypolimnetic aeration research in British Columbia, *Verh. Internat. Verein. Limnol.*, *23*(1), 215-219.

Beutel, M. W., and A. J. Horne (1999), A review of the effects of hypolimnetic oxygenation on lake and reservoir water quality, *Lake Reservoir Manage.*, *15*(4), 285-297.

Beutel, M. W., et al. (2001), Limnological effects of anthropogenic dessication in a large, saline lake, Walker Lake, Nevada, *Hydrobiol.*, *446*, 91-105.

Beutel, M. W. (2003), Hypolimnetic anoxia and sediment oxygen demand in California drinking water reservoirs, *Lake Reservoir Manage.*, *19*(3), 208-221.

Bostrom, B., et al. (1988), Exchange of phosphorus across the sediment and water interface, *Hydrobiol.*, *170*, 229-244.

Bravo, H. R., et al. (2007), Development of a commercial-code based two-fluid model for bubble plumes, *Environ. Modelling & Software*, *22*, 536-547.

Brevik, I. (1977), Two-dimensional air-bubble plume, *J. Waterway, Port, Coastal, and Ocean Div., Proc. American Soc. of Civil Engineers*, *103*(WW1), 101-115.

Brevik, I., and R. Killie (1996), Phenomenological description of the axisymmetric air-bubble plume, *Internat. J. Multiphase Flow*, *22*(3), 535-549.

Brevik, I., and R. Kluge (1999), On the role of turbulence in the phenomenological theory of plane and axisymmetric air-bubble plumes *Internat. J. Multiphase Flow*, *25*, 87-108.

Burris, V. L., et al. (2002), Predicting oxygen transfer and water flow rate in airlift aerators, *Water Res.*, *36*(18), 4605-4615.

Cederwall, K., and J. D. Ditmars (1970), Analysis of Air-Bubble Plumes, W. M. Keck Laboratory of Hydraulics and Water Resources, Division of Engineering and Applied Science, California Institute of Technology, Pasadena, CA.

Cooke, G. D., and R. E. Carlson (1989), *Reservoir Management for Water Quality and THM Precursor Control*, 387 pp., American Water Works Association Research Foundation, Denver, CO.

Davis, J. M. (1980), Destratification of reservoirs - A design approach for perforated-pipe compressed-air systems, *Water Services*, *84*, 497-505.

Diaz, R. J. (2001), Overview of hypoxia around the world, *J. Environ. Qual.*, *30*(2), 275-281.

Ditmars, J. D., and K. Cederwall (1974), Analysis of air-bubble plumes, paper presented at 14th Coastal Engineering Conference, Am. Soc. Civ. Engineers, Copenhagen, Denmark, 24-28 June.

Fanneløp, T. K., and K. Sjøen (1980), Hydrodynamics of underwater blowouts, *Norweg. Maritime Res.*, *4*, 17-33.

Fanneløp, T. K., et al. (1991), Surface current and recirculating cells generated by bubble curtains and jets, *J. Fluid Mech.*, *229*, 629-657.

Fast, A. W., et al. (1975), Hypolimnetic oxygenation using liquid oxygen, *Water Resour. Res.*, *11*(2), 294-299.

Fast, A. W., and M. W. Lorenzen (1976), Synoptic survey of hypolimnetic aeration, *Journal of the Environmental Engineering Division, American Society of Civil Engineers*, *102*(EE6), 1161-1173.

French, T. D., and E. L. Petticrew (2007), Chlorophyll a seasonality in four shallow eutrophic lakes (northern British Columbia, Canada) and the crirtical roles of internal phosphorus loading and temperature, *Hydrobiol.*, *575*(1), 285-299.

Gachter, R., and B. Wehrli (1998), Ten years of artificial mixing and oxygenation: No effect on the internal phosphorus loading of two eutrophic lakes, *Environ. Sci. Technol.*, *32*(23), 3659-3665.

Gemza, A. (1995), Some practical aspects of whole lake mixing and hypolimnetic oxygenation: Ecological impacts of aeration on lakes and reservoirs in southern Ontario, *Lake Reservoir Manage.*, *11*(2), 141-142.

Gibbons, H. L., et al. (1994), Worlds largest attempt at hypolimnetic aeration, *Lake Reservoir Manage.*, *9*(2), 76.

Goldberg, E. D. (1995), Emerging problems in the coastal zone for the twenty-first century, *Mar. Pollut. Bull.*, *31*, 152-158.

Hondzo, M. (1998), Dissolved oxygen transfer at the sediment-water interface in a turbulent flow, *Water Resour. Res.*, *34*(12), 3525-3533.

Imteaz, M. A., and T. Asaeda (2000), Artificial mixing of lake water by bubble plume and effects of bubbling operations on algal bloom, *Water Res.*, *34*(6), 1919-1929.

Jaeger, D. (1990), TIBEAN: A new hypolimnetic water aeration plant, *Internat. Vereinigung fuer Theoret. und Angewandte Limnol.*, *24*(1), 184-187.

Johansen, O. (2000), DeepBlow - a Lagrangian plume model for deep water blowouts, *Spill Sci. & Tech. Bull.*, *6*(2), 103-111.

Johnson, G. P., et al. (2000), Methodology, Data Collection, and Data Analysis for Determination of Water-Mixing Patterns Induced by Aerators and Mixers, 48 pp, U.S. Geological Survey.

Josiam, R. M., and H. G. Stefan (1999), Effect of flow velocity on sediment oxygen demand: comparison of theory and experiments, *J. Am. Water Resour. Assoc.*, *35*, 433-439.

Jung, R., et al. (1999), Improving water quality through lake oxygenation at Camanche Reservoir, paper presented at North American Lake Management Society Annual Symposium, Reno, NV, December 1.

Kobus, H. E. (1968), Analysis of the flow induced by air-bubble systems, paper presented at 11th Coastal Engineering Conference, Am. Soc. Civ. Engineers, London, England.

Kortmann, R. W., et al. (1994), Aeration of stratified lakes: Theory and practice, *Lake Reservoir Manage.*, *8*(2), 99-120.

Laureshen, C. J., and R. D. Rowe (1987), Modeling of plane bubble plumes, paper presented at 24th National Heat Transfer Conference and Exhibition, Am. Soc. Mech. Engineers, Pittsburgh, PA, 9-12 Aug.

Lemckert, C. J., and J. Imberger (1993), Energetic bubble plumes in arbitrary stratification, *J. Hydraul. Engr.*, *119*(6), 680-703.

Liikanen, A., et al. (2002), Gas dynamics in eutrophic lake sediments affected by oxygen, nitrate, and sulfate, *J. Environ. Qual.*, *31*, 338-349.

Lindenschmidt, K. E., and P. F. Hamblin (1997), Hypolimnetic aeration in Lake Tegel, Berlin, *Water Res.*, *31*(7), 1619-1628.

Little, J. C. (1995), Hypolimnetic aerators: Predicting oxygen transfer and hydrodynamics, *Water Res.*, *29*(11), 2475-2482.

Lorenzen, M. W., and A. W. Fast (1977), A Guide to Aeration/Circulation Techniques for Lake Management, 125 pp, U.S. Environmental Protection Agency Ecol. Res. Serv.

Mackenthun, A. A., and H. G. Stefan (1998), Effect of flow velocity on sediment oxygen demand: Experiments, *J. Environ. Engineer.*, *124*(3), 222-230.

Mailman, M., et al. (2006), Strategies to lower methyl mercury concentrations in hydroelectric reservoirs and lakes: A review, *Sci. Tot. Envr.*, *368*, 224-235.

McDougall, T. J. (1978), Bubble plumes in stratified environments, *J. Fluid Mech.*, *85*, 655-672.

McGinnis, D. F., and J. C. Little (1998), Bubble dynamics and oxygen transfer in a Speece Cone, *Water Sci. Technol.*, *37*, 285-292.

McGinnis, D. F., et al. (2001), Hypolimnetic oxygenation: Coupling bubble-plume and reservoir models, paper presented at Asian Waterqual 2001: First IWA Asia-Pacific Regional Conference, Intl. Wat. Assoc., Fukuoka, Japan, 12-15 Sept.

McGinnis, D. F., and J. C. Little (2002), Predicting diffused-bubble oxygen transfer rate using the discrete-bubble model, *Water Res.*, *36*(18), 4627-4635.

McGinnis, D. F., et al. (2004), Interaction between a bubble plume and the near-field in a stratified lake, *Water Resour. Res.*, *40*(10, W10206).

McQueen, D. J., and D. R. S. Lean (1986), Hypolimnetic aeration: An overview, *Water Pollution Research Journal of Canada*, *21*(2), 205-217.

McQueen, D. J., et al. (1986), Effects of hypolimnetic aeration on iron-phosphorus interactions, *Water Res.*, *20*(9), 1129-1135.

Milgram, J. H. (1983), Mean flow in round bubble plumes, *J. Fluid Mech.*, *133*, 345-376.

Nordin, R., et al. (1995), Hypolimnetic aeration of St Mary Lake, British Columbia, Canada, *Lake Reservoir Manage.*, *11*(2), 176.

Pastorok, R. A., et al. (1981), Evaluation of Aeration/Circulation as a Lake Restoration Technique, Report, U. S. Environ. Protect. Agency, Off. Res. & Devel., Corvalis, OR.

Pastorok, R. A., et al. (1982), Environmental Aspects of Artificial Aeration and Oxygenation of Reservoirs: A review of Theory, Techniques, and Experiences, Report, 192 pp, U.S. Army Engineering Waterways Experiment Station, Vicksburg, MS.

Pollock, L. M. J., and M. G. Dubé (2007), The effects of hypoxia on fishes: from ecological relevance to physiological effects, *Environ. Rev.*, *15*, 1-14.

Rayyan, F., and R. E. Speece (1977), Hydrodynamics of bubble plumes and oxygen absorption in stratified impoundments, *Prog. Water Technol.*, *9*, 129-142.

Sahoo, G. B., and D. Luketina (2003), Modeling of bubble plume design and oxygen transfer for reservoir restoration, *Water Res.*, *37*(2), 393-401.

Schladow, S. G. (1992), Bubble plume dynamics in a stratified medium and the implications for water quality amelioration in lakes, *Water Resour. Res.*, *28*, 313-321.

Schladow, S. G. (1993), Lake destratification by bubble-plume systems: Design methodology, *J. Hydraul. Engr.*, *119*(3), 350-368.

Singleton, V. L., and J. C. Little (2006), Designing hypolimnetic aeration and oxygenation systems - A review, *Environ. Sci. Technol.*, *40*, 7512-7520.

Singleton, V. L., et al. (2007), Linear bubble plume model for hypolimnetic oxygenation – Full-scale validation and sensitivity analysis, *Water Resour. Res.*, *43*, W02405.

Socolofsky, S. A., and E. E. Adams (2003), Liquid volume fluxes in stratified multiphase plumes, *J. Hydraul. Engr.*, *129*(11), 905-914.

Soltero, R. A., et al. (1994), Partial and full lift hypolimnetic aeration of Medical Lake, WA to improve water quality, *Water Res.*, *28*(11), 2297-2308.

Søndergaard, M., et al. (2000), Lake restoration in Denmark, *Lakes & Reservoirs: Research and Management*, *5*(3), 151-159.

Speece, R. E., and G. Murfee (1973), Hypolimnetic Aeration with Commercial Oxygen - Volume 2: Bubble Plume Gas Transfer, US Environmental Protection Agency, Washington, DC.

Speece, R. E., and F. Rayyan (1973), Hypolimnetic Aeration with Commercial Oxygen - Volume I: Dynamics of Bubble Plume, US Environmental Protection Agency, Washington, DC.

Speece, R. E., et al. (1973), Alternative considerations in the oxygenation of reservoir discharges and rivers, in *Applications of Commercial Oxygen to Water and Wastewater Systems*,

edited by R. E. Speece and J. F. Malina, pp. 342-361, Center for Research in Water Resources, Austin, TX.

Taggart, C. T., and D. J. McQueen (1981), Hypolimnetic aeration of a small eutrophic kettle lake: Physical and chemical changes, *Archiv fur Hydrobiologie*, *91*(2), 150-180.

Taggart, C. T., and D. J. McQueen (1982), A model for the design of hypolimnetic aerators, *Water Res.*, *16*, 949-956.

Tate, C. H., and K. F. Arnold (1990), Health and aesthetic aspects of water quality, in *Water Quality and Treatment*, edited by F. W. Pontius, pp. 63-154, McGraw-Hill, Inc., New York.

Thomas, J. A., et al. (1994), Short term changes in Newman Lake following hypolimnetic aeration with the Speece Cone, *Lake Reservoir Manage.*, *9*(1), 111-113.

Tsang, G. (1990), Theoretical investigation of oxygenating bubble plumes, paper presented at Second International Symposium on Gas Transfer at Water Surfaces, Am. Soc. Civ. Engineers, Minneapolis, MN, 11-14 Sept.

Wilkinson, D. L. (1979), Two-dimensional bubble plumes, *J. Hydraulics Div., Proc. Am. Soc. of Civil Engineers*, *105*(HY2), 139-154.

Wu, R. S. S., et al. (2003), Aquatic hypoxia is an endocrine disruptor and impairs fish reproduction, *Environ. Sci. Technol.*, *37*(6), 1137-1141.

Wüest, A., et al. (1992), Bubble plume modeling for lake restoration, *Water Resour. Res.*, *28*, 3235-3250.

Zheng, L., et al. (2002), A model for simulating deepwater oil and gas blowouts–Part I: theory and model formulation *Journal of Hydraulic Research*, *41*, 339-351.

Zic, K., and H. G. Stefan (1994), Destratification Induced by Bubble Plumes, 39 pp, U.S. Army Corps of Engineers, Waterways Experiment Station.

CHAPTER 2. DESIGNING HYPOLIMNETIC AERATION AND OXYGENATION SYSTEMS – A REVIEW

VICKIE L. SINGLETON AND JOHN C. LITTLE*
Department of Civil and Environmental Engineering, Virginia Polytechnic Institute and State University, Blacksburg, Virginia 24061, U.S.A.
* Corresponding author phone: (540) 231 8737; fax: (540) 231 7916; e-mail: jcl@vt.edu

Published in 2006 in Environmental Science and Technology, Volume 40, 7512-7450

Abstract

When properly designed, hypolimnetic aeration and oxygenation systems can replenish dissolved oxygen in water bodies while preserving stratification. The three primary devices are airlift aerators, Speece Cones, and bubble-plume diffusers. Early design procedures for airlift aerators were empirical, while most bubble-plume models did not account for stratification or gas transfer. In each device, gas bubbles in contact with water facilitate interfacial transfer of oxygen, nitrogen and other soluble gases. Using fundamental principles, a discrete-bubble model was first developed to predict plume dynamics and gas transfer for a circular bubble-plume diffuser. The discrete-bubble approach has subsequently been validated using oxygen transfer tests in a large vertical tank and applied successfully at full-scale to an airlift aerator as well as to both circular and linear bubble-plume diffusers. The performance of each of the four completely different full-scale systems (on a scale of 10 m or more) was predicted based on the behavior of individual bubbles (on a scale of about 1 mm). The combined results suggest that the models can be used with some confidence to predict system performance based on applied air or oxygen flow rate, initial bubble size, and, in the case of bubble plume diffusers, near-field boundary conditions. The discrete-bubble approach has also been extended to the Speece Cone, but the model has not yet been validated due to a lack of suitable data. The unified suite of models, all based on simple discrete-bubble dynamics, represents the current state-of-the-art for designing systems to add oxygen to stratified lakes and reservoirs.

Introduction

Low dissolved oxygen concentrations in the hypolimnia of lakes or reservoirs can negatively affect releases downstream of hydropower reservoirs, the drinking-water treatment process, and cold-water fisheries [*Little and McGinnis*, 2001]. In the U.S., releases from hydropower reservoirs typically must comply with state water quality criteria for minimum dissolved oxygen (DO) concentrations [*Peterson et al.*, 2003]. Oxygen depletion can lead to increases in hydrogen sulfide, ammonia, and phosphorus and can also cause reduced iron and manganese in the sediments to solubilize. If entrained into the productive surface zone, phosphorus may stimulate algal growth and ultimately fuel additional oxygen demand. Hydrogen sulfide and reduced iron and manganese cause problems associated with taste, odor, and color if hypolimnetic water is treated for potable use [*Cooke and Carlson*, 1989]. The presence of reduced compounds also results in increased oxidant demand at the water treatment plant, leading to increased drinking water treatment costs. The increased use of oxidants such as chlorine may also contribute to the formation of disinfection by-products. Winter fishkills in ice-covered lakes with anoxic hypolimnia are also a serious concern [*Mackenthun and Stefan*, 1998]. Finally, hypoxia has been shown to be an endocrine disrupter in fish, which impairs fish reproduction [*Wu et al.*, 2003].

Hypolimnetic aeration and oxygenation are commonly used to add dissolved oxygen to water bodies while preserving stratification (Supporting Information, Table 1). Numerous studies have been conducted documenting the physical, chemical, and biological effects of hypolimnetic aeration and oxygenation in lakes and reservoirs. These studies have been reviewed by *Fast and Lorenzen* [1976], *Taggart and McQueen* [1981], *Pastorok et al.* [1981], *Pastorok et al.* [1982], *McQueen and Lean* [1986], and *Beutel and Horne* [1999]. Despite the large number of hypolimnetic aeration and oxygenation investigations, relatively few have examined the parameters that impact system performance, and there is no comprehensive review of published hypolimnetic aeration and oxygenation design methods. In this paper, the various types of aeration and oxygenation devices are briefly discussed, select installations are summarized, and a suite of published design methods that have been validated using data collected from full-scale field installations is reviewed in detail. A unifying feature of these recently published works is the use of a simple discrete-bubble model to predict oxygen transfer in the various hypolimnetic aeration and oxygenation systems. The performance of each of the

four completely different full-scale systems (on a scale of 10 m or more) is predicted based on the behavior of individual bubbles (on a scale of about 1 mm).

Hypolimnetic Aeration and Oxygenation Devices

Mercier and Perret [1949] developed one of the earliest aeration systems, which utilized mechanical agitation of water pumped from the hypolimnion into a splash basin on the surface of a lake. Another type of aeration method is layer aeration, which redistributes available dissolved oxygen obtained from algal photosynthesis and contact with the atmosphere [*Kortmann*, 1994; *Kortmann et al.*, 1994]. Airlift devices have also been used for hypolimnetic aeration. Partial-lift systems operate by injecting compressed air near the bottom of the hypolimnion. The air-water mixture travels up a vertical tube to a given depth in the lake from which the remaining gas bubbles are vented to the atmosphere through a pipe to the surface. The oxygenated water is returned to the hypolimnion. Full-lift systems are similar except the air-water mixture rises to the surface before residual gas bubbles are released. Regarding hypolimnetic oxygenation, one technique involves withdrawing water to the shore, injecting it with pure oxygen gas under high pressure, and then returning it to the hypolimnion. This is known as side-stream pumping and is one of the earliest reported oxygenation systems [*Beutel and Horne*, 1999; *Fast*, 1979]. Another side-stream method entails mixing air or pure oxygen into withdrawn water, pumping or passing the bubble-water mixture down a deep U-tube to enhance gas transfer, and returning oxygenated water that is discharged at the top of the tube [*Bruijn and Tuinzaad*, 1958; *Speece and Adams*, 1968]. In submerged contact systems, oxygen is injected into an enclosed chamber usually located in the hypolimnion, and water is either pumped or entrained into the device [*Beutel and Horne*, 1999]. Oxygen transfer occurs within the chamber, and oxygenated water is discharged to the hypolimnion. A Speece Cone employs this principle [*Speece et al.*, 1973]. Finally, either compressed air or pure oxygen gas can be introduced into the hypolimnion through diffusers to form a rising, unconfined bubble-plume. While the devices described represent the majority of hypolimnetic aeration and oxygenation systems, it should be noted that this selection is not all-inclusive.

The primary types of hypolimnetic aeration and oxygenation systems currently in use include airlift aerators, Speece Cones, and bubble-plume diffusers [*McGinnis and Little*, 2002]. Most documented installations use one of these three primary devices (Supporting Information,

Table 1). Also, most reported models and studies regarding system design are related to these methods of aeration and oxygenation. These specific hypolimnetic aeration and oxygenation devices are thus the focus of this paper.

Airlift Aerator

Full-lift hypolimnetic aerators typically consist of 1) a vertical riser tube, 2) a diffuser inside the bottom of the riser tube, 3) an air-water separation chamber at the top of the riser, and 4) one or two return pipes, called downcomers (Figure 1) [McQueen and Lean, 1986]. Compressed air is delivered to the aerator and bubbles freely from the diffuser. This creates a positively-buoyant gas-water mixture that ascends the riser. At the top of the riser, some of the bubbles are released to the atmosphere, although some may be entrained in the water that enters the downcomers. The oxygenated water descends the downcomers and is returned to the hypolimnion [Burris et al., 2002].

Speece Cone

The Speece Cone, developed by Dr. Richard Speece, was originally known as a submerged downflow bubble contactor [*Speece et al.*, 1971; *Speece et al.*, 1973]. The system consists of a source of oxygen gas, a conical bubble contact chamber, a submersible pump, and a diffuser that disperses highly oxygenated water into the hypolimnion (Figure 2). Ambient water and oxygen gas bubbles are introduced at the top of the cone. As water flows down the cone, the velocity decreases because the cross-sectional area of the cone increases. The system is designed so that the downward velocity of the water at the top of the cone is sufficient to overcome the rise velocity of the bubbles. At the bottom of the cone, the water velocity is designed to be less than the bubble rise velocity. The sloping cone walls help the bubbles remain within the cone as the water flows through [*Speece et al.*, 1971]. The applied water flow rate and slope of the walls control the water velocity and, therefore, the time available for gas transfer [*McGinnis and Little*, 1998].

Bubble-Plume Diffuser

Bubble-plume diffusers are generally linear or circular (Figure 3) and inject either air or oxygen at a relatively low gas flow rate [*McGinnis and Little*, 2002]. Circular plumes are also referred to as round plumes, and linear bubble plumes are often identified as line bubble plumes

or bubble curtains in the literature. These systems are most suitable for deep lakes where the bulk of the bubbles dissolves in the hypolimnion and the momentum generated by the plume is low enough to prevent significant erosion of the thermocline [*Wüest et al.*, 1992]. Gas bubbles are injected into the water column through a porous diffuser creating a gas/water mixture that rises and gains momentum due to a positive buoyancy flux. The buoyant mixture entrains water at the boundaries, which increases the water flow rate and cross-sectional area, but decreases the momentum. The plume rises against the vertical density gradient until the depth of maximum plume rise (DMPR) is reached, which is where the plume momentum is zero. The plume water at this depth is negatively buoyant and is expected to fall back to an equilibrium depth (ED) where the plume density equals the ambient density [*McGinnis et al.*, 2004]. Upon reaching the ED, the plume water intrudes horizontally into the far-field [*McGinnis et al.*, 2004].

Discrete Bubble Model

A significant unifying advance in hypolimnetic aeration and oxygenation system design is the use of the discrete-bubble model for predicting oxygen transfer. In each of the three primary devices, interfacial gas transfer is accomplished through individual bubbles in contact with water. Bubble size is an important parameter because it is directly related to the interfacial surface area, bubble-rise velocity [*Clift et al.*, 1978; *Haberman and Morton*, 1954], and the mass-transfer coefficient [*Clift et al.*, 1978; *Motarjemi and Jameson*, 1978]. In addition, bubble size may vary significantly as the bubbles pass through the system or ascend the water column. For these reasons, *Wüest et al.* [1992] developed a discrete-bubble model for a circular bubble-plume that accounts for volumetric changes due to gas transfer as well as changing hydrostatic pressure and water temperature. The method has subsequently been applied to diffused-bubble aeration in a large vertical tank [*McGinnis and Little*, 2002], an airlift aerator [*Burris and Little*, 1998; *Burris et al.*, 2002], a Speece Cone [*McGinnis and Little*, 1998], and a linear bubble-plume diffuser [*Little and McGinnis*, 2001; *Singleton et al.*, 2005].

The discrete-bubble model previously developed by *Wüest et al.* [1992] was verified by *McGinnis and Little* [2002] for individual bubbles rising in plug flow through a well-mixed volume of water. The molar flow rate or flux of gaseous species transferred per unit height under steady-state conditions is:

$$\frac{dF_{G_i}}{dz} = -K_L \left(H_i P_i - C_i \right) \frac{4\pi r^2 N}{v + v_b} \tag{1}$$

where F_{Gi} is the gas flux, z is the vertical coordinate, K_L is the mass transfer coefficient, H_i is Henry's constant, P_i is gas partial pressure at a given depth, C_i is the bulk aqueous concentration, r is the bubble radius, v is the water velocity, and v_b is the bubble rise velocity. N is the number flux of bubbles introduced by the diffuser per unit time and is equivalent to Q_{gas}/V_o, where Q_{gas} is the actual volumetric gas flow rate through the diffuser and V_o is the initial volume of a bubble formed at the diffuser. Gas-phase mass-transfer resistance may be neglected for transfer of oxygen and nitrogen, and Henry's constants are provided by *Wüest et al.* [1992] as a function of temperature (Supporting Information, Table 2). Because the bulk aqueous concentration changes very slowly, pseudo-steady state conditions may be assumed. Consequently, Equation 1 can be integrated to obtain the change in the molar flow rate of undissolved gas during the bubble contact period. The results can then be used to predict the evolving aqueous concentration in the well-mixed volume of water with respect to time.

In Equation 1, the bubble radius r is a function of hydrostatic pressure and the mass of oxygen and nitrogen within the bubble at a given depth. These parameters change as the bubble rises, resulting in a change in the partial pressure of oxygen and nitrogen within the bubble. *Wüest et al.* [1992] developed correlations for K_L and v_b (Supporting Information, Table 2) based on published experimental data for bubble-rise velocity [*Haberman and Morton*, 1954] and the mass-transfer coefficient [*Motarjemi and Jameson*, 1978]. These correlations are functions of bubble radius, so the mass transfer coefficient and rise velocity may be adjusted as the bubble changes in size. In addition to the correlations by *Wüest et al.* [1992], other equations for H, K_L, and v_b are available in the literature. *Clift et al.* [1978] and *Leifer and Patro* [2002] presented detailed parameterizations for K_L and v_b, and *Weiss* [1970] developed relationships for H or solubility as a function of temperature and salinity. Also, *Vasconcelos et al.* [2003] and *Alves et al.* [2005] reported that bubble contamination can affect mass transfer and bubble rise velocity.

The initial dissolved oxygen concentration, water temperature, and depth at the diffuser are known. The initial dissolved nitrogen concentration is assumed to be at equilibrium with the atmosphere. If the initial bubble diameter formed by the diffuser is also known, then the initial gaseous molar flow rate of oxygen or nitrogen (M_{oi}) can be calculated by:

$$M_{o_i} = \frac{Y_{o_i} P_{std} Q_{std}}{R T_{std}} \tag{2}$$

where Y_{oi} is initial mole fraction of the gas, P_{std} is standard pressure, Q_{std} is gas flow rate at standard conditions (0 ^{o}C and 1 bar), R is the ideal gas constant, and T_{std} is standard temperature. For deep diffusers subject to relatively high pressures, the Van der Waals equation of state can be used to more accurately calculate the initial gaseous flow rates [*Wüest et al.*, 1992].

In the differential gas flux equation of the discrete-bubble model (Equation 1), the quantity $v + v_b$ represents the net bubble velocity due to the water velocity v and the bubble rise velocity v_b. The rise velocity is a function of bubble radius [*Clift et al.*, 1978; *Leifer and Patro*, 2002; *Wüest et al.*, 1992] and varies as the bubbles rise because of decompression and gas transfer. For the Speece Cone, v can be easily calculated because water flow rate and the cone dimensions are typically known. In the case of the airlift aerator, water flow rate is constant through the device but is not generally known and must be calculated using the gas flow rate, gas holdup, and aerator dimensions. For the bubble plume, v varies along the plume rise height due to entrainment and must be modeled by separate dynamic equations of motion. Thus, the discrete-bubble model is generally solved as a coupled system of equations for hydrodynamics and gas transfer when applied to bubble plumes.

The discrete-bubble model was validated by *McGinnis and Little* [2002] using oxygen transfer data collected in a large vertical tank and the initial bubble-size distribution and applied air flow rate. In addition to the previously listed assumptions, bubble size distribution and the rate of bubble formation were assumed constant, bubble coalescence and mass transfer of gases other than nitrogen and oxygen were neglected, and mass transfer at the water surface was assumed to be small. Also, it was assumed that the water velocity induced by the rising bubbles v (Equation 1) was negligible. Therefore, the net bubble velocity was equal to the bubble rise velocity.

The oxygen transfer tests were conducted in a 14-m high by 2-m diameter tank equipped with a porous hose diffuser supplied with air flow rates of 0.43, 0.68, and 2.88 Nm^3/h (normal conditions of 1 bar and 0 ^{o}C). Another set of experiments was conducted at four air flow rates and two water depths to determine the effects of gas flow rate and hydrostatic pressure on initial

bubble size. The released bubbles formed a weak plume within the tank during testing, but the induced vertical velocity could not be measured. Bubble size distributions were measured from digitized photos of the bubble swarms in the tank immediately above the diffuser. McGinnis and Little found that the differences between bubble sizes formed at the two different depths was negligible. To simplify model application, a representative Sauter-mean diameter (diameter of a sphere having the same volume-to-surface ratio as the distribution of bubbles) [*Chisti*, 1989; *Orsat et al.*, 1993] was calculated. A correlation equation was developed to relate bubble size to actual volumetric gas flow rate at the diffuser. The range of bubble diameters included the region of greatest variation in rise velocity and mass-transfer coefficient. The calculated bubble sizes and measured air flow rates were used in the discrete-bubble model to predict the DO profiles over time (Figure 4). The observed and predicted DO curves are comparable, with root mean square errors of 0.65, 0.60 and 1.31 for the 0.43, 0.68 and 2.88 Nm^3/h tests, respectively. Although the model is biased towards higher than observed DO concentrations, all of the test data were predicted to within 15 percent.

McGinnis and Little [2002] investigated several assumptions of the discrete-bubble model. The responses of the three oxygen probes at different depths within the tank for each test were essentially equivalent, confirming that the water was well-mixed. To check the validity of using the Sauter-mean diameter as opposed to the full bubble size distribution, the model was modified to include a range of bubble sizes, and similar oxygen transfer rates were obtained. The correlation equation for bubble-rise velocity was also examined, but using theoretically-derived rise velocities made virtually no difference to the model results. The model was modified to include an induced vertical water velocity of 0.04 m s^{-1}, but the modification did not change the predicted oxygen concentrations appreciably.

Design Studies and Application of the Discrete Bubble Model

In this section, hypolimnetic aeration and oxygenation design studies are reviewed for each of the primary devices. For each type of aerator or oxygenator, a brief overview of early models and design studies is provided, and the major contributions and shortcomings of these models are emphasized. Then, models that utilize the discrete-bubble approach and related validation studies are reviewed in greater detail.

Airlift Aerator

Of the three primary devices, airlift aerators were probably installed most frequently during the early years of hypolimnetic aeration and oxygenation (Supporting Information, Table 1). Consequently, a number of researchers have conducted design studies of airlift aerators, including *Lorenzen and Fast* [1977], *Taggart and McQueen* [1982], *Ashley* [1985], and *Little* [1995]. Because these early design methods and models do not employ the discrete bubble approach, details have been included in the Supporting Information. In general, the early studies of airlift aerators provided useful information on aerator design and operation but are primarily empirically based and make a number of key assumptions that have not been confirmed (Supporting Information).

Burris and Little [1998] developed a fundamental approach to predict oxygen transfer in airlift aerators, patterned after the discrete-bubble approach of *Wüest et al.* [1992]. The first fundamental model for predicting water flow rate in airlift aerators, which is based on an energy balance, was developed by *Little and Del Vecchio* [1996]. *Burris et al.* [2002] extended and validated these oxygen transfer and water flow rate models using experimental data collected from a full-scale aerator in Lake Prince, Virginia. Dissolved oxygen profiles, water flow rates, and gas holdups were measured over a wide range of applied air flow rates (65 Nm^3/h–227 Nm^3/h).

The oxygen transfer model focuses on individual bubbles and accounts for changes in bubble size due to decreasing hydrostatic pressure as well as mass transfer of oxygen and nitrogen. Assuming steady-state, and based on the discrete-bubble model (Supporting Information, Table 2), a set of four equations was obtained by applying a differential mass balance on each phase (dissolved and gaseous) and each molecular species of interest (oxygen and nitrogen) (Supporting Information, Tables 3 and 4).

The primary equations for the water flow rate model for the full-lift aerator come from literature on airlift bioreactors. The model is based on a steady-state macroscopic energy balance over the entire aerator (Supporting Information, Table 4). The rate of energy input due to gas flow is equal to the rate of energy dissipation due to fluid flow [*Lee et al.*, 1986]. The energy balance includes terms for energy input due to isothermal gas expansion [*Chisti*, 1989], energy dissipation due to bubble wakes in the riser [*Lee et al.*, 1986], energy loss due to riser and downcomer wall friction [*Chisti*, 1989; *Merchuk and Stein*, 1981], energy loss due to local flow

disturbances, and energy loss due to fluid turn-around at the top of the riser [*Chisti*, 1989] (Supporting Information, Table 4).

By varying a single parameter (the initial bubble size), the oxygen transfer model was applied to predict DO concentrations (Figure 5) and gas holdups in the riser over the range of air flow rates tested. The model provided a close fit to the experimental DO profiles, and nearly all the gas holdup values were predicted within 20 percent of the observed. The calculated bubble sizes agreed well with the Sauter-mean diameters measured during replicated laboratory experiments. To test the validity of assuming a uniform initial bubble size, an analysis was performed using a bubble size distribution. The predicted oxygen concentrations did not differ significantly from those obtained using the Sauter-mean bubble diameter, similar to the results obtained by *McGinnis and Little* [2002] when applying the discrete-bubble model to experiments conducted in a large, well-mixed tank. The model was extended to account for oxygen transfer in the air-water separator and to predict, *a priori*, the DO profiles in the downcomers (Figure 5). Oxygen transfer in the separator and downcomers is due to contact with the atmosphere and bubble carry-over from the riser, respectively. As shown in Figure 5, the model output compares very well with the experimental data.

In the *Burris et al.* [2002] study, the only unknown with respect to the water flow rate model was K_t, the loss coefficient for the top section of the aerator. An empirical relationship was obtained for K_t as a function of superficial water velocity, with a root mean square value of 0.92. Excluding data at the lowest air flow rate, the range of calculated values for K_t (3 to 8) is close to a literature value of 5.5 proposed for hydrodynamically similar external airlift bioreactors. Additionally, the authors reported that frictional loss terms for the top section and local flow disturbances are relatively important in the overall energy balance, suggesting that attention should be given to these features during aerator design.

Speece Cone

The downflow bubble contactor, or Speece Cone, was originally proposed by *Speece* [1969] in 1969. Two years later, *Speece et al.* [1971] described the device in greater detail and conducted bench- and pilot-scale experiments to measure oxygen transfer performance. Even though the concept of using a submerged contact chamber for downflow bubble aeration/oxygenation has been available for over thirty years, only a few Speece Cone

installations have been reported in the literature (Supporting Information, Table 1). Currently, the only published model that predicts oxygen transfer in a Speece Cone was developed by *McGinnis and Little* [1998]. However, an earlier gas transfer model for U-tube aeration was developed by *Speece and Orosco* [1970] in 1970, and U-tubes have some features that are similar to Speece Cones.

The Speece Cone model of *McGinnis and Little* [1998] is based on the discrete-bubble approach, and oxygen transfer efficiency is calculated as a function of initial bubble size, gas and water flow rates, depth of operation, and cone dimensions. It is assumed that the bubbles are spherical and of uniform initial size, no bubble coalescence or breakup occurs, water and gas are in plug flow, and the system is at steady-state. Mass balances for dissolved and gaseous oxygen and nitrogen result in a system of equations that incorporate gas transfer between phases, change in gas partial pressure and water velocity with depth, influence of gas holdup, and changing radius of the cone (Supporting Information, Tables 3 and 5), again based on the discrete-bubble approach (Supporting Information, Table 2).

Experimental data for a Speece Cone were not available for model validation, so *McGinnis and Little* [1998] performed a preliminary analysis using assumed cone dimensions and operational parameters. A high oxygen transfer capacity was predicted, due to the relatively long bubble contact time calculated for the baseline conditions. The performance of the Speece Cone was also estimated as a function of depth (Supporting Information, Table 6) by adjusting the standard gas flow rate to provide an equivalent volumetric gas flow rate (20.5 L s^{-1}) at the cone inlet for each depth. This resulted in increasing gas mass flow rates as the cone depth was increased. The predicted oxygen transfer efficiencies were all between 92 and 93 percent. Model results revealed sensitivity to initial bubble size. If too large a bubble is produced, the bubbles do not dissolve rapidly enough, and cone performance may be impaired. For the baseline conditions, the most rapid increase in DO was predicted to occur mid-depth in the cone, where the bubble velocity relative to the cone was lowest.

Bubble-Plume Diffuser

Because bubble-plumes are encountered in a variety of natural and man-made systems, numerous studies have been conducted on plume dynamics [*Asaeda and Imberger*, 1993; *Borchers et al.*, 1999; *Brevik and Killie*, 1996; *Brevik and Kluge*, 1999; *Cederwall and Ditmars*,

1970; *Ditmars and Cederwall*, 1974; *Fanneløp and Sjøen*, 1980; *Fanneløp et al.*, 1991; *Kobus*, 1968; *Laureshen and Rowe*, 1987; *McDougall*, 1978; *Milgram*, 1983; *Schladow*, 1992; *Speece and Rayyan*, 1973; *Wilkinson*, 1979]. Less work has been performed on bubble-plumes in stratified environments [*Asaeda and Imberger*, 1993; *Lemckert and Imberger*, 1993; *McDougall*, 1978; *Schladow*, 1993; *Socolofksy and Adams*, 2003], and even fewer investigations on bubble-plumes incorporating gas transfer [*McGinnis et al.*, 2006; *Sahoo and Luketina*, 2003; *Speece and Murfee*, 1973; *Speece and Rayyan*, 1973; *Tsang*, 1990]. Bubble-plumes intended for hypolimnetic aeration or oxygenation must be capable of increasing dissolved oxygen concentrations, and lakes and reservoirs commonly have vertical density and concentration gradients. Therefore, only hypolimnetic aeration and oxygenation design methods that account for gas transfer and stratification were reviewed. Also, because this work focuses on aeration and oxygenation methods that preserve stratification, destratification models [*Asaeda and Imberger*, 1993; *Davis*, 1980; *Sahoo and Luketina*, 2003; *Schladow*, 1993] were not reviewed. One of the earliest models to predict oxygen transfer and hydrodynamics of bubble-plumes in stratified hypolimnia was introduced by *Rayyan and Speece* [1977] and is similar to the discrete-bubble approach. However, there are several significant differences from the bubble-plume model of *Wüest et al.* [1992], so details of the *Rayyan and Speece* [1977] work have been provided in the Supporting Information.

Plume hydrodynamics are strongly influenced by initial bubble size and gas flow rate. A model that uses the discrete-bubble approach to predict hydrodynamics and constituent concentrations in circular bubble-plumes was developed by *Wüest et al.* [1992]. The plume model theory is based on horizontally integrated equations of the conservation of mass, momentum, heat, salinity and gas species [*McDougall*, 1978]. Entrainment is also considered, and the entrainment velocity is assumed proportional to the local plume velocity and plume circumference [*McDougall*, 1978]. The plume model includes the effects of density stratification due to vertical temperature and salinity gradients. A key contribution of the *Wüest et al.* [1992] model was the use of a variable buoyancy flux to account for changing bubble size not only due to decompression and thermal expansion, but also gas dissolution and stripping. Although previous studies neglected gas exchange, it is particularly important in deep systems or for weak plumes where gas transfer can be significant.

Table 7 (Supporting Information) lists the key variables of the plume model. Based on eight flux equations (Supporting Information, Table 8) that are solved simultaneously, the model predicts water flow rate, water entrainment, gas transfer, plume temperature, constituent concentrations (oxygen, nitrogen and salinity), DMPR, and ED for the given boundary conditions of diffuser depth and diameter, applied gas flow rate, initial bubble size, and boundary profiles (temperature, DO, and salinity). The initial plume water velocity (v_o) is determined based on an initial densimetric Froude number (Fr_o) of 1.6, or:

$$Fr_o = \frac{v_o}{\left[2\lambda bg\left(\rho_a - \rho_p\right)/\rho_p\right]^{1/2}} \tag{3}$$

where λ is the spreading ratio of bubbles to fluid flow, b is plume radius for velocity and dissolved species, g is gravitational acceleration, ρ_a is ambient water density, and ρ_p is plume bubble-water mixture density. The equations of the circular bubble plume model are valid above the zone of flow establishment. Therefore, the Froude number is used to calculate an initial plume water velocity to solve the equations, even though the actual water velocity is zero.

McGinnis et al. [2004] conducted a detailed analysis of the plume-lake interaction in Lake Hallwil, Switzerland by collecting high spatial-resolution temperature, salinity, and DO profiles and used the results for a full-scale evaluation of the *Wüest et al.* [1992] circular bubble-plume model. During testing, the circular diffuser was supplied with compressed air at 30 Nm^3/h. In contrast to model assumptions, the bubble core was not observed to spread at the same rate as the plume. This will result in a higher localized buoyancy flux, which will cause higher inner core water velocities and a greater local rise height. Additionally, multiple detrainment, plume wandering, and cross-flow due to seiching was observed, which may have altered the plume entrainment coefficient and the boundary conditions. The entrainment coefficient is considered to be constant in the circular bubble model, but *McGinnis et al.* [2004] suggested that entrainment likely varies along the plume rise height because of differing levels of turbulence at the plume boundaries as the plume water velocity changes, variations in the ambient density gradient, and mixing where the plume stops rising. Entrainment occurred from the near-field, which was where detrained water accumulated over tens of meters from the plume, as opposed to the far-field as previously thought. In Lake Hallwil, the seiche-enhanced near-field was mixed

much more than the ambient, or far-field, environment. This resulted in a greater plume rise height because there was a lower density gradient to overcome. Because entrainment was mostly from the near-field, plume temperature and constituent concentrations depended strongly on that region, which was created by the plume itself. Therefore, plume properties and model predictions were strongly dependent on the evolving near-field boundary conditions. Currently, near-field boundary conditions cannot be predicted for bubble plume design and must either be measured or assumed. (Prediction of the plume-affected near-field is discussed further in the Future Research section.)

Using the near-field boundary profiles, the circular plume model predicted both the plume width and depth of maximum plume rise very well (Figure 6). Figure 8 in the Supporting Information shows the averaged measured in-plume temperature and DO profiles and the model predictions. The predicted temperature profile compares well but diverges towards the top of the plume to approximately 0.3 °C less than the measured temperature. This may be a result of somewhat inaccurate boundary profiles. The plume may have entrained and detrained water at different rates and with different properties depending on the direction and magnitude of the horizontal seiche current and the interaction with varying ambient density gradients along the plume rise height. Also, the average plume temperature and DO are based on a two-dimensional transect and may have been laterally heterogeneous. The plume boundaries were not well defined due to inhomogeneity caused by seiching and detrainment. The variation in DO around the plume was also substantial (Figure 6 and Supporting Information, Figure 8), and selection of improper DO boundary conditions may have resulted in the slight underprediction of the DO profile [*McGinnis et al.*, 2004].

Using data collected from a full-scale linear diffuser installed in Spring Hollow Reservoir (SHR), Virginia, USA, *Singleton et al.* [2007] validated the performance of the linear bubble-plume model developed earlier by *McGinnis et al.* [2001]. The model equations were derived using the discrete-bubble approach of *Wüest et al.* [1992], who developed a model for circular bubble plumes. The linear bubble-plume model is nearly identical to the circular plume model except for the geometry of the plume (Supporting Information, Tables 7 and 9). *Singleton et al.* [2005] refined the linear plume model by more accurately characterizing the plume geometry at the ends of the linear diffuser and by using a correlation equation to calculate initial bubble size, while *Singleton et al.* [2007] corrected λ and the entrainment coefficient α for top-hat profiles

and derived relationships to determine v_o as a function of Fr_o. The values of α and λ used were 0.11 and 0.93, respectively, as reported by *Fanneløp et al.* [1991] for linear bubble plumes and adjusted for top-hat profiles [*Fanneløp and Sjøen*, 1980]. Similar to the circular bubble-plume model, v_o was determined based on Fr_o equal to 2.0, or:

$$Fr_o = \frac{v_o}{\left[\lambda W g\left(\rho_a - \rho_p\right)/\rho_p\right]^{1/2}} \tag{4}$$

where W is the linear plume width for velocity and dissolved species.

To fully evaluate the linear bubble-plume model, high spatial-resolution temperature, salinity, and DO profiles were collected during diffuser operation in SHR using compressed air at 38 Nm^3/h during July 2003 and pure oxygen at 13 and 40 Nm^3/h during August 2003 and October 2004, respectively. Measured contour plots of temperature and DO were compared to model predictions for plume width and the depth of maximum plume rise. For July 2003 and October 2004 (Supporting Information, Figure 9), the DMPR is simulated well by the model. However, the plume rise height was underestimated for August 2003, when the gas flow rate was comparatively low. The under-prediction may have been due to an overestimated value for α. The linear bubble-plume model assumes that α is constant, but *Milgram* [1983] concluded that α for round or circular bubble plumes is directly proportional to the plume gas fraction. Predicted vertical profiles of temperature and DO within the plumes were also compared to average measured values for the three diffuser test conditions (Figure 7). The temperature predictions for July 2003 and October 2004 (Supporting Information, Figure 9) deviated from the measured profiles where the plumes reach the top of the hypolimnion, or where the rate of plume spreading was greatest. The model underpredicted the final plume temperature by approximately 0.3 and 0.2 °C for July 2003 and October 2004, respectively. Proposed reasons for the temperature differences include variable entrainment as the plume width increases and inaccuracy in selected boundary conditions. The entrainment coefficient for circular bubble plumes has been found to also increase with values of a characteristic length that is a function of the 4/5 power of the plume radius [*Milgram*, 1983]. The model simulated the plume DO profiles well for all three diffuser tests (Figure 7) and characterized the initial increase in DO immediately above the diffuser quite accurately for July and August 2003.

Future Research

When properly designed, hypolimnetic aeration and oxygenation systems can replenish dissolved oxygen in water bodies while preserving stratification. The discrete-bubble model, first employed by *Wüest et al.* [1992] to predict gas transfer in a circular bubble-plume, has been independently validated by *McGinnis and Little* [2002] using data collected during oxygen transfer tests in a large vertical tank. The discrete-bubble approach has subsequently been applied to an airlift aerator [*Burris et al.*, 2002], a Speece Cone [*McGinnis and Little*, 1998], a circular bubble-plume diffuser [*McGinnis et al.*, 2004; *Wüest et al.*, 1992] and a linear bubble-plume diffuser [*Little and McGinnis*, 2001; *McGinnis et al.*, 2001; *Singleton et al.*, 2005; *Singleton and Little*, 2005]. With the exception of the Speece Cone, for which few data exist, all the models employing the discrete-bubble approach have been successfully validated at full scale. The discrete bubble-model, which describes gas transfer based on bubble properties on a millimeter scale, has been successfully applied to predict oxygen transfer from devices with dimensions that are typically on the scale of ten meters or more. These combined results suggest that the suite of models can be used with some confidence when designing systems to add oxygen to stratified lakes and reservoirs. The models of *Burris et al.* [2002], *McGinnis and Little* [1998], *Wüest et al.* [1992], and *Singleton et al.* [2005] therefore represent the current state-of-the-art for predicting oxygen transfer in airlift aerators, Speece Cones, circular bubble-plume diffusers, and linear bubble-plume diffusers, respectively, based on the applied air or oxygen flow rate and the initial bubble-size formed at the diffuser. Despite these encouraging results, there are several aspects that need further investigation. Because a frictional loss coefficient was empirically fit to experimental data, the general applicability of the energy-balance model for airlift aerators should be further verified. The airlift model should also be extended to other full- and partial-lift aerator designs. The Speece Cone model should be verified against field data for a range of applied gas flow rates. Also, a method should be developed to predict the effect of plume operation on near-field boundary conditions, short circuiting of plume detrainment, and plume fallback beyond the equilibrium depth [*McGinnis et al.*, 2004].

Operation of hypolimnetic aeration and oxygenation devices usually alters the DO concentration profiles and thermal structure of a waterbody. Oxygen transfer efficiency is a

function of the surrounding water column properties, establishing a feedback loop that continually changes system performance. This effect is most pronounced during operation of bubble-plume diffusers because plume performance depends strongly on the vertical density gradient. The plume-lake interaction should be accounted for in the design and operation of bubble-plume diffusers, as well as the other aeration and oxygenation devices. To this end, *McGinnis et al.* [2001] performed a preliminary coupling of the linear bubble-plume model with a reservoir model, CE-QUAL-W2 (W2). The coupled model was tested using data collected from Spring Hollow Reservoir, Virginia. W2 is a two-dimensional, laterally averaged, hydrodynamic and water quality model developed by the U.S. Army Corps of Engineers [*Cole and Wells*, 2003]. The coupled model predicted mixing and warming induced by plume operation quite accurately (Supporting Information, Figure 10). In addition, the evolution of hypolimnetic DO was predicted well (Supporting Information, Figure 10), although the model incorporates a zero- or first-order estimate of sediment oxygen demand (with respect to particulate organic matter) that has not been conclusively verified. As currently represented, the coupled model underpredicts the rate of oxygen addition because additional oxygen transfer after plume detrainment is not calculated. Based on the promising *McGinnis et al.* [2001] results, the coupled model is being developed to predict plume dynamics and plume-induced mixing. A natural extension of this work is to incorporate the other hypolimnetic aeration and oxygenation devices, such as the airlift aerator and Speece Cone.

Another alternative to predicting the effect of plume operation on the near-field was presented by *Asaeda and Imberger* [1993]. These researchers developed a partial double-plume model, in which the upward momentum is contained within an inner plume and the detraining water forms an outer annular plume that flows downward. The annular downdraught is assumed to descend to the neutral buoyancy depth and flow out horizontally as an intrusion. Above the intrusion depth, the ascending inner plume entrains water from the descending outer plume. Although the plume model of *Asaeda and Imberger* [1993] is intended for destratification systems and therefore does not consider gas transfer, the model provides valuable insight into the hydrodynamics of plume interaction with the near-field.

Acknowledgements

Financial support was provided by the National Science Foundation (Grant No. BES 0202034). The authors would like to thank three anonymous reviewers for their constructive comments that significantly improved the manuscript. Also, this work would not have been possible without the valuable contributions of Daniel McGinnis throughout the past ten years.

Supporting Information Available

Details regarding early design studies, hypolimnetic aeration and oxygenation installations documented in the literature, additional figures, and equations for models utilizing the discrete bubble approach. This material is available free of charge via the Internet at http://pubs.acs.org.

Literature Cited

Alves, S. S., et al. (2005), Effect of bubble contamination on rise velocity and mass transfer, *Chemical Engineering Science*, *60*, 1-9.

Asaeda, T., and J. Imberger (1993), Structure of bubble plumes in linearly stratified environments, *J. Fluid Mech.*, *249*, 35-57.

Ashley, K. I. (1985), Hypolimnetic aeration: Practical design and application, *Water Res.*, *19*(6), 735-740.

Beutel, M. W., and A. J. Horne (1999), A review of the effects of hypolimnetic oxygenation on lake and reservoir water quality, *Lake Reservoir Manage.*, *15*(4), 285-297.

Borchers, O., et al. (1999), Applicability of standard k-epsilon turbulence model to the dynamic simulation of bubble columns. Part II: Comparsion of detailed experiments and flow simulations, *Chemical Engineering Science*, *54*, 5927-5935.

Brevik, I., and R. Killie (1996), Phenomenological description of the axisymmetric air-bubble plume, *Internat. J. Multiphase Flow*, *22*(3), 535-549.

Brevik, I., and R. Kluge (1999), On the role of turbulence in the phenomenological theory of plane and axisymmetric air-bubble plumes *Internat. J. Multiphase Flow*, *25*, 87-108.

Bruijn, J., and H. Tuinzaad (1958), The relationships between depth of U-tubes and the aeration process, *Journal of the American Water Works Association*, *7*, 879.

Burris, V. L., and J. C. Little (1998), Bubble dynamics and oxygen transfer in a hypolimnetic aerator, *Water Sci. Technol.*, *37*(2), 293-300.

Burris, V. L., et al. (2002), Predicting oxygen transfer and water flow rate in airlift aerators, *Water Res.*, *36*(18), 4605-4615.

Cederwall, K., and J. D. Ditmars (1970), Analysis of Air-Bubble Plumes, W. M. Keck Laboratory of Hydraulics and Water Resources, Division of Engineering and Applied Science, California Institute of Technology, Pasadena, CA.

Chisti, M. Y. (1989), *Airlift Bioreactors*, 345 pp., Elsevier Science Publishing, New York, New York.

Clift, R., et al. (1978), *Bubble, Drops, and Particles*, 380 pp., New York, NY.

Cole, T. M., and S. A. Wells (2003), CE-QUAL-W2: A Two-Dimensional, Laterally Averaged, Hydrodynamic and Water Quality Model, Version 3.2, U.S. Army Engineering and Research Development Center, Vicksburg, MS.

Cooke, G. D., and R. E. Carlson (1989), *Reservoir Management for Water Quality and THM Precursor Control*, 387 pp., American Water Works Association Research Foundation, Denver, CO.

Davis, J. M. (1980), Destratification of reservoirs - A design approach for perforated-pipe compressed-air systems, *Water Services*, *84*, 497-505.

Ditmars, J. D., and K. Cederwall (1974), Analysis of air-bubble plumes, paper presented at 14th Coastal Engineering Conference, Am. Soc. Civ. Engineers, Copenhagen, Denmark, 24-28 June.

Fanneløp, T. K., and K. Sjøen (1980), Hydrodynamics of underwater blowouts, *Norweg. Maritime Res.*, *4*, 17-33.

Fanneløp, T. K., et al. (1991), Surface current and recirculating cells generated by bubble curtains and jets, *J. Fluid Mech.*, *229*, 629-657.

Fast, A. W., and M. W. Lorenzen (1976), Synoptic survey of hypolimnetic aeration, *Journal of the Environmental Engineering Division, American Society of Civil Engineers*, *102*(EE6), 1161-1173.

Fast, A. W. (1979), Artificial aeration as a lake restoration technique, paper presented at Lake Restoration, U.S. Environmental Protection Agency, Minneapolis, MN.

Haberman, W. L., and R. K. Morton (1954), An experimental study of bubbles moving in liquids, *Proc. Am. Soc. Civ. Eng.*, *80*, 379-427.

Kobus, H. E. (1968), Analysis of the flow induced by air-bubble systems, paper presented at 11th Coastal Engineering Conference, Am. Soc. Civ. Engineers, London, England.

Kortmann, R. W. (1994), Oligotrophication of Lake Shenipsit by layer aeration, *Lake Reservoir Manage.*, *9*(1), 94-97.

Kortmann, R. W., et al. (1994), Aeration of stratified lakes: Theory and practice, *Lake Reservoir Manage.*, *8*(2), 99-120.

Laureshen, C. J., and R. D. Rowe (1987), Modeling of plane bubble plumes, paper presented at 24th National Heat Transfer Conference and Exhibition, Am. Soc. Mech. Engineers, Pittsburgh, PA, 9-12 Aug.

Lee, C. H., et al. (1986), Liquid circulation in airlift fermentors, in *Biotechnology Processes: Scale-Up and Mixing*, edited by C. S. Ho and J. Y. Oldshue, pp. 50-59, American Institute of Chemical Engineers, New York, NY.

Leifer, I., and R. K. Patro (2002), The bubble mechanism for methane transport from the shallow sea bed to the surface: A review and sensitivity study, *Continental Shelf Research*, *22*, 2409-2428.

Lemckert, C. J., and J. Imberger (1993), Energetic bubble plumes in arbitrary stratification, *J. Hydraul. Engr.*, *119*(6), 680-703.

Little, J. C. (1995), Hypolimnetic aerators: Predicting oxygen transfer and hydrodynamics, *Water Res.*, *29*(11), 2475-2482.

Little, J. C., and D. C. Del Vecchio (1996), Predicting water flow rate in hypolimnetic aerators, paper presented at International Association on Water Quality, Biennial Conference, Singapore.

Little, J. C., and D. F. McGinnis (2001), Hypolimnetic oxygenation: Predicting performance using a discrete-bubble model, *Water Science & Technology: Water Supply*, *1*(4), 185-191.

Lorenzen, M. W., and A. W. Fast (1977), A Guide to Aeration/Circulation Techniques for Lake Management, 125 pp, U.S. Environmental Protection Agency Ecol. Res. Serv.

Mackenthun, A. A., and H. G. Stefan (1998), Effect of flow velocity on sediment oxygen demand: Experiments, *J. Environ. Engineer.*, *124*(3), 222-230.

McDougall, T. J. (1978), Bubble plumes in stratified environments, *J. Fluid Mech.*, *85*, 655-672.

McGinnis, D. F., and J. C. Little (1998), Bubble dynamics and oxygen transfer in a Speece Cone, *Water Sci. Technol.*, *37*, 285-292.

McGinnis, D. F., et al. (2001), Hypolimnetic oxygenation: Coupling bubble-plume and reservoir models, paper presented at Asian Waterqual 2001: First IWA Asia-Pacific Regional Conference, Intl. Wat. Assoc., Fukuoka, Japan, 12-15 Sept.

McGinnis, D. F., and J. C. Little (2002), Predicting diffused-bubble oxygen transfer rate using the discrete-bubble model, *Water Res.*, *36*(18), 4627-4635.

McGinnis, D. F., et al. (2004), Interaction between a bubble plume and the near-field in a stratified lake, *Water Resour. Res.*, *40*(10, W10206).

McGinnis, D. F., et al. (2006), Fate of rising methane bubbles in stratified waters: How much methane reaches the atmosphere?, *Journal of Geophysical Research*, *111*(C09007).

McQueen, D. J., and D. R. S. Lean (1986), Hypolimnetic aeration: An overview, *Water Pollution Research Journal of Canada*, *21*(2), 205-217.

Merchuk, J. C., and Y. Stein (1981), Local hold-up and liquid velocity in airlift reactors, *AICHE Journal*, *27*, 377-388.

Mercier, P., and J. Perret (1949), Aeration of Lake Bret, Monastbull, Schwiez, *Ver. Gas. Wasser-Fachm*, *29*, 25.

Milgram, J. H. (1983), Mean flow in round bubble plumes, *J. Fluid Mech.*, *133*, 345-376.

Motarjemi, M., and G. J. Jameson (1978), Mass transfer from very small bubbles - The optimum bubble size for aeration, *Chemical Engineering Science*, *33*, 1415-1423.

Orsat, V., et al. (1993), Air diffusers characterization using a digitized image analysis system, *Applied Engineering in Agriculture*, *9*(1), 115-121.

Pastorok, R. A., et al. (1981), Evaluation of Aeration/Circulation as a Lake Restoration Technique, Report, U. S. Environ. Protect. Agency, Off. Res. & Devel., Corvalis, OR.

Pastorok, R. A., et al. (1982), Environmental Aspects of Artificial Aeration and Oxygenation of Reservoirs: A review of Theory, Techniques, and Experiences, Report, 192 pp, U.S. Army Engineering Waterways Experiment Station, Vicksburg, MS.

Peterson, M. J., et al. (2003), Regulatory Approaches for Addressing Dissolved Oxygen Concerns at Hydropower Facilities, 38 pp, U.S. Department of Energy, Office of Energy Efficiency and Renewable Energy, Wind and Hydropower Technologies Idaho Falls, ID.

Rayyan, F., and R. E. Speece (1977), Hydrodynamics of bubble plumes and oxygen absorption in stratified impoundments, *Prog. Water Technol.*, *9*, 129-142.

Sahoo, G. B., and D. Luketina (2003), Modeling of bubble plume design and oxygen transfer for reservoir restoration, *Water Res.*, *37*(2), 393-401.

Schladow, S. G. (1992), Bubble plume dynamics in a stratified medium and the implications for water quality amelioration in lakes, *Water Resour. Res.*, *28*, 313-321.

Schladow, S. G. (1993), Lake destratification by bubble-plume systems: Design methodology, *J. Hydraul. Engr.*, *119*(3), 350-368.

Singleton, V. L., et al. (2005), Linear bubble plume model for hypolimnetic oxygenation: Full-scale validation and sensitivity analysis, *Accepted for publication in Water Resources Research*.

Singleton, V. L., and J. C. Little (2005), Linear bubble plume model for hypolimnetic oxygenation: Full-scale evaluation and sensitivity analysis, paper presented at 9th Workshop on Physical Processes in Natural Waters, Lancaster Univ., Lancaster, England, 4-6 Sept.

Socolofsky, S. A., and E. E. Adams (2003), Liquid volume fluxes in stratified multiphase plumes, *J. Hydraul. Engr.*, *129*(11), 905-914.

Speece, R. E., and J. L. Adams (1968), U-tube oxygenation operating characteristics, paper presented at Proceedings of the Industrial Waste Conference, May.

Speece, R. E. (1969), The use of pure oxygen in river and impoundment aeration, paper presented at 24th Industrial Waste Conference, Purdue University, Lafayette, IN, 6-8 May.

Speece, R. E., and R. Orosco (1970), Design of U-tube aeration systems, *Journal of the Sanitary Engineering Division, Proceedings of the American Society of Civil Engineers*, *96*, 715-725, 7348.

Speece, R. E., et al. (1971), Downflow bubble contact aeration, *Journal of the Sanitary Engineering Division, Proceedings of the American Society of Civil Engineers*, *SA 4*, 433-441.

Speece, R. E., and G. Murfee (1973), Hypolimnetic Aeration with Commercial Oxygen - Volume 2: Bubble Plume Gas Transfer, US Environmental Protection Agency, Washington, DC.

Speece, R. E., and F. Rayyan (1973), Hypolimnetic Aeration with Commercial Oxygen - Volume I: Dynamics of Bubble Plume, US Environmental Protection Agency, Washington, DC.

Speece, R. E., et al. (1973), Alternative considerations in the oxygenation of reservoir discharges and rivers, in *Applications of Commercial Oxygen to Water and Wastewater Systems*, edited by R. E. Speece and J. F. Malina, pp. 342-361, Center for Research in Water Resources, Austin, TX.

Taggart, C. T., and D. J. McQueen (1981), Hypolimnetic aeration of a small eutrophic kettle lake: Physical and chemical changes, *Archiv fur Hydrobiologie*, *91*(2), 150-180.

Taggart, C. T., and D. J. McQueen (1982), A model for the design of hypolimnetic aerators, *Water Res.*, *16*, 949-956.

Tsang, G. (1990), Theoretical investigation of oxygenating bubble plumes, paper presented at Second International Symposium on Gas Transfer at Water Surfaces, Am. Soc. Civ. Engineers, Minneapolis, MN, 11-14 Sept.

Vasconcelos, J. M. T., et al. (2003), Effect of contaminants on mass transfer coefficients in bubble column and airlift contactors, *Chemical Engineering Science*, *58*, 1431-1440.

Weiss, R. F. (1970), The solubility of nitrogen, oxygen and argon in water and seawater, *Deep-Sea Research*, *17*, 721-735.

Wilkinson, D. L. (1979), Two-dimensional bubble plumes, *J. Hydraulics Div., Proc. Am. Soc. of Civil Engineers*, *105*(HY2), 139-154.

Wu, R. S. S., et al. (2003), Aquatic hypoxia is an endocrine disruptor and impairs fish reproduction, *Environ. Sci. Technol.*, *37*(6), 1137-1141.

Wüest, A., et al. (1992), Bubble plume modeling for lake restoration, *Water Resour. Res.*, *28*, 3235-3250.

Figure 1. Photograph of full-lift aerator prior to installation. (Photo from Bob Kortmann of Ecosystem Consulting Service, Inc., used with permission.)

Figure 2. Photographs of Speece Cone and diffuser prior to installation at Camanche Reservoir, California. (Photos from Rod Jung of East Bay Municipal Utility District., used with permission.)

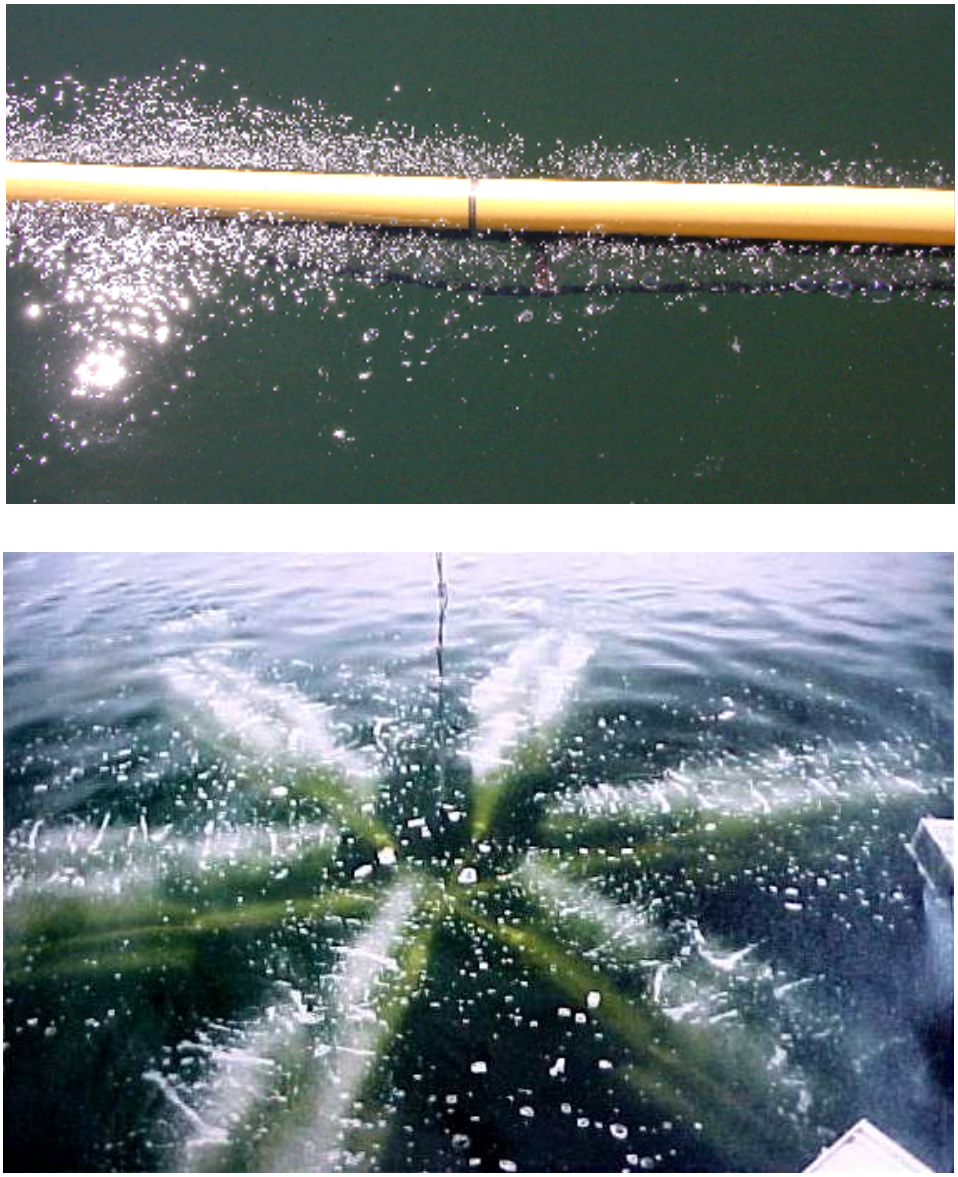

Figure 3. Photographs of linear (top) and circular (bottom) bubble-plume diffusers. (Photo of linear diffuser from Mark Mobley of Mobley Engineering, Inc. Photo of circular diffuser from Swiss Federal Institute for Aquatic Science and Technology. Both photos used with permission.)

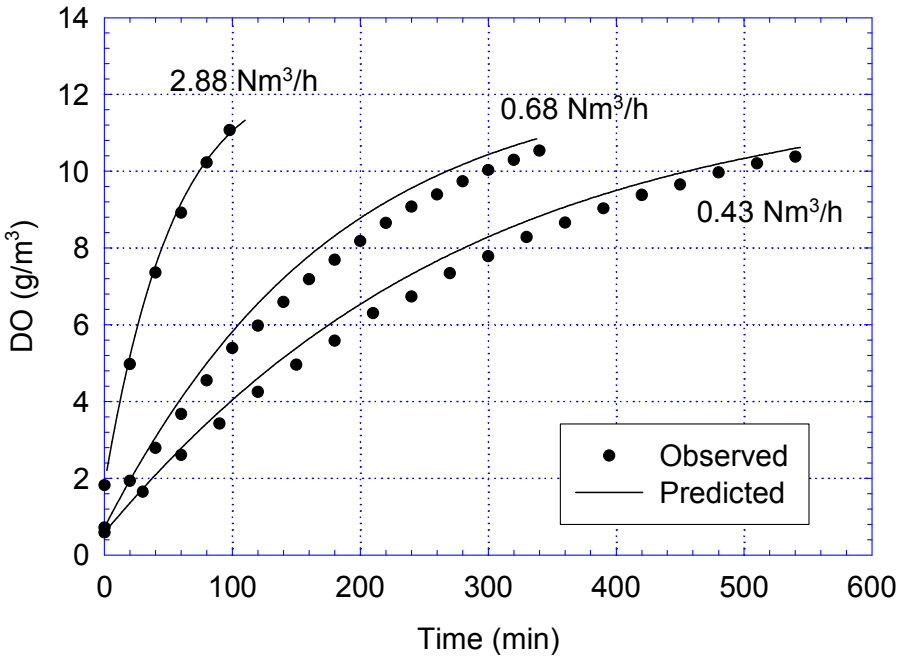

Figure 4. Observed and predicted DO concentrations based on validation of discrete-bubble model during oxygen transfer experiments in a large vertical tank [*McGinnis and Little*, 2002].

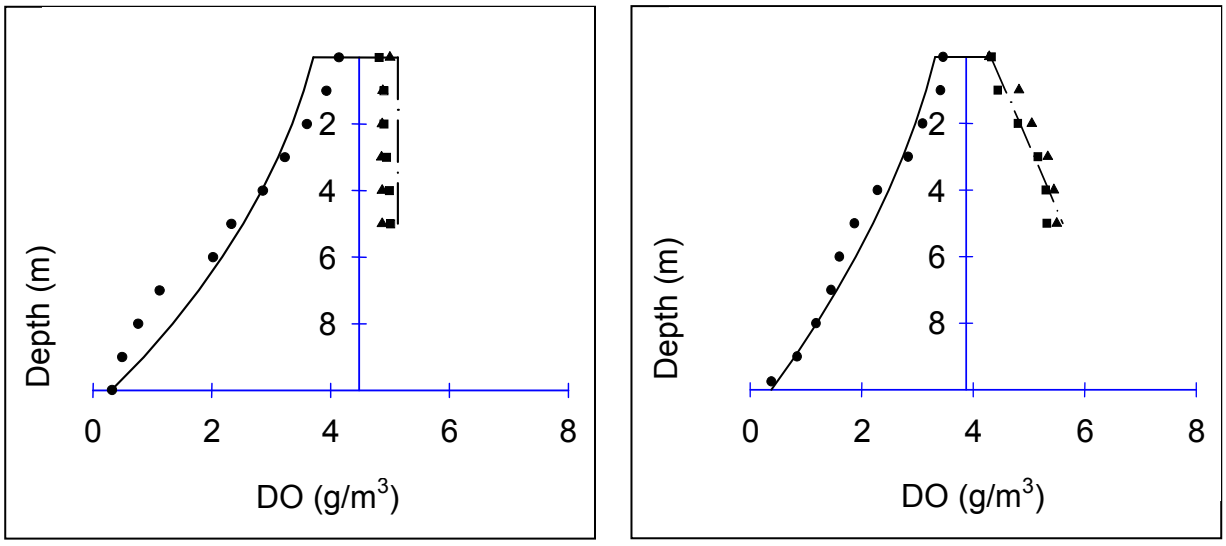

Figure 5. Observed and model DO profiles for airlift aerator in Lake Prince, Virginia, USA for low (left, 65 Nm^3/h) and high (right, 227 Nm^3/h) air flow rates (— model fit, -·- model prediction, ● riser data, ▲ downcomer 1 data, ■ downcomer 2 data). Data were collected from an airlift aerator equipped with two downcomers [*Burris et al.*, 2002].

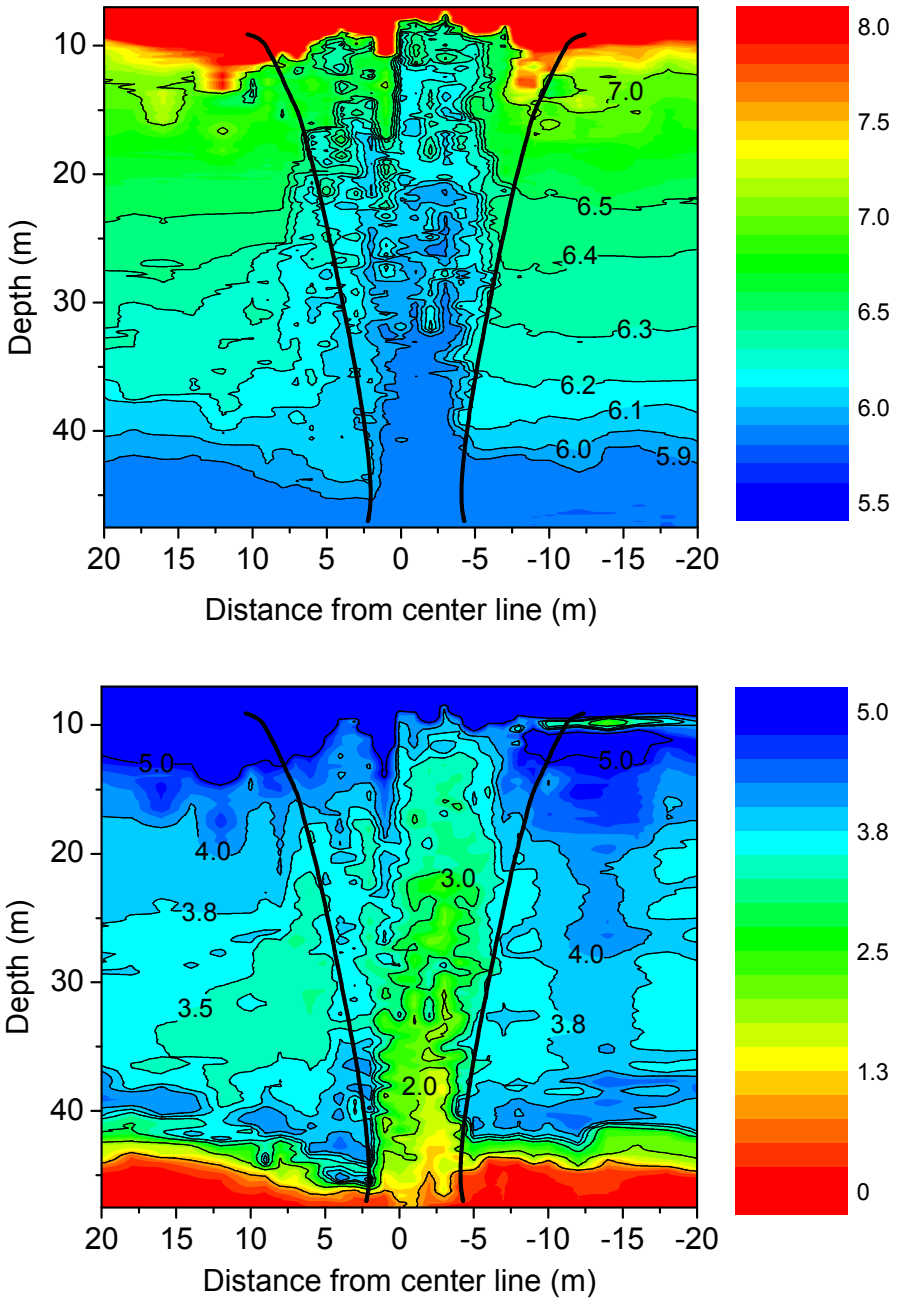

Figure 6. Temperature (°C, top) and DO (g/m^3, bottom) contours in Lake Hallwil, Switzerland with circular bubble-plume model predictions for plume width and depth of maximum rise overlaid. For clarity, the temperature and DO contours were scaled to show only values from 5.5–8 °C and 0–5 g/m^3, respectively [*McGinnis et al.*, 2004].

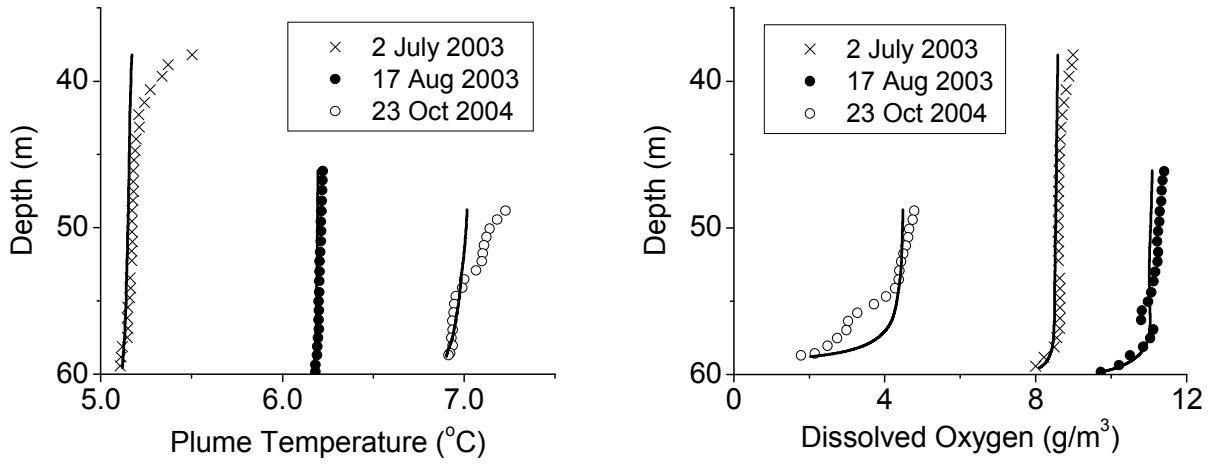

Figure 7. Measured and predicted in-plume constituent profiles for linear bubble-plume model evaluation using data from Spring Hollow Reservoir, Virginia, USA [*Singleton et al.*, 2005].

Supporting Information: Early Design Studies, Nomenclature, Tables, Figures, and Literature Cited

Early Design Studies

Airlift Aerator

One of the first attempts to design airlift aerators was developed by *Lorenzen and Fast* [1977]. The primary objective was to size a compressor by determining the design air flow rate. The air flow rate is calculated using the hypolimnetic oxygen depletion rate and the induced water flow rate through the aerator. Based on general observations of full-lift aerators, the authors assumed that water reaching the top of the device is saturated with oxygen. The air flow rate required to induce this water flow rate is a function of the aerator dimensions. The available theoretical head results from the difference in density between the air-water mixture in the riser and the ambient lake water. It was also assumed that half of the theoretical head is used to convey water to the surface and that the remainder is dissipated in the downcomer. *Lorenzen and Fast* [1977] provided practical guidance and information regarding the major variables that affect the performance of airlift aerators. However, the aerator sizing method presented makes a number of critical assumptions that are unverified.

The design method of *Taggart and McQueen* [1982] involves determining the dimensions of the riser and downcomer when compressor capacity is known. The authors presented an empirically-based approach for establishing full-lift aerator specifications including diffuser depth, air flow rate, water flow rate, and riser and downcomer cross-sectional areas. Water flow rate is calculated using a correlation that was developed from a regression of data collected from 20 published experiments. To determine the optimum riser cross-sectional area, the authors assumed that the maximum induced water velocity is a function of the median estimated bubble rise velocity. The method of *Taggart and McQueen* [1982] represents a simple, straightforward approach for the hydrodynamic design of airlift aerators. While the model did provide additional insight into aerator sizing, it lacks key elements. Oxygen transfer cannot be predicted by the model and the authors did not consider the effect of gas flux on induced water velocity. However, *Taggart and McQueen* [1982] did account for gas flow when developing a correlation to calculate induced water flow rate as a function of volumetric air flow rate and riser depth.

Another empirical airlift aerator model was proposed by *Ashley* [1985]. In addition to aerator sizing, Ashley also discussed other practical design features including air supply, rated and actual air flow, and performance specifications. The model was derived from the work of *Lorenzen and Fast* [1977] and *Taggart and McQueen* [1982] as well as experience with a full-scale system. The model assumes that the induced water flow rate will completely satisfy the oxygen consumption in the hypolimnion measured during spring stratification. The model also requires an estimate of the increase in the DO concentration produced by the aerator. Determination of the DO increase is an important variable, and *Ashley* [1985] suggested that this parameter may be difficult to predict. *Ashley* [1985] presented a detailed, step-wise method for sizing an airlift aerator and provided useful information related to engineering aspects such as compressors, power supply, oxygen transfer efficiency, and oxygenation capacity. The model of *Ashley* [1985] was field tested by *Ashley and co-workers* [1987] (Supporting Information, Table 1), but the aeration system was unable to satisfy the hypolimnetic oxygen demand because the induced water velocity and oxygen input were overestimated during design.

Little [1995] developed a model to predict oxygen transfer in a full-lift hypolimnetic aerator by applying mass balance equations. Input parameters include aerator dimensions, volumetric air flow rate, diffuser depth, and ambient water conditions. To calculate water flow rate, an empirical correlation that is a function of superficial gas velocity (volumetric gas flow rate/entire riser cross-sectional area) and riser length was developed. The correlation was derived from the same data set used by *Taggart and McQueen* [1982], except dependence on riser diameter was eliminated. Literature correlations, originally developed for bubble columns and airlift reactors, were used to estimate the mass transfer coefficient and gas holdup (volume fraction of gas in the bubble-water mixture) in the riser. The model assumes that gas holdup is small, water is in plug flow, and nitrogen transfer is negligible. The model proposed by *Little* [1995] was the first attempt to develop a fundamental approach for predicting oxygen transfer in full-lift aerators, but the model relies on empirical correlations to calculate important variables. Also, nitrogen transfer can be significant for relatively deep systems and will subsequently affect bubble volume and bubble-size dependent properties including the rise velocity and mass transfer coefficient [*Clift et al.*, 1978; *Leifer and Patro*, 2002; *Wüest et al.*, 1992].

Bubble-Plume Diffuser

Rayyan and Speece [1977] developed one of the earliest models to predict oxygen transfer and hydrodynamics of bubble-plumes in stratified environments. The model derivation extended the round or circular bubble-plume equations of *Cederwall and Ditmars* [1970] to incorporate gas transfer and non-linear stratification. The model calculates maximum plume rise height, centerline velocity and nominal half-width, and density and temperature differences between the plume and the ambient water column. Conservation principles were applied to a circular plume to derive relationships for water, oxygen, momentum, buoyancy, and heat fluxes. Entrainment of ambient water is proportional to the plume centerline velocity [*Morton et al.*, 1956], and the entrainment coefficient was set equal to 0.04 for low flow rates in the laboratory and 0.055 for higher flow rates in the field. The water and bubble spreading coefficients were 1.25 and 0.2, respectively. Bubble size varies along the plume height and is a function of oxygen transfer and local hydrostatic pressure. The model of *Rayyan and Speece* [1977] represents a significant advance in bubble-plume modeling because both oxygen transfer and stratification are considered. Although the model employs elements of the discrete-bubble approach, there are several key differences. The bubble rise velocity and mass transfer coefficients are not functions of bubble radius. Also, the transfer of gases other than oxygen is neglected. As mentioned previously, gaseous nitrogen exchange can significantly affect bubble size and related properties. The effect of salinity gradients on plume dynamics was not considered as in the *Wüest et al.* [1992] model. Hydrodynamic predictions from the model were verified during both laboratory and field testing (Supporting Information, Table 1). However, the oxygen transfer portion of the model has not been validated with experimental data.

Nomenclature

A_d: downcomer cross-sectional area, m^2

A_e: exit cross-sectional area, m^2

A_r: riser cross-sectional area, m^2

b: circular plume radius for velocity and dissolved species, m

C: aqueous-phase concentration, mol/m^3

C_a: aqueous-phase concentration of ambient water, mol/m^3

C_f: Fanning friction factor, dimensionless

D_d: downcomer diameter, m

D_r: riser diameter, m

E: plume entrainment, m^2/s

E_E: Energy loss due to local flow disturbances, J/s

E_F: Energy loss due to wall friction, J/s

E_I: Energy input due to isothermal gas expansion, J/s

E_T: Energy loss due to friction at the top of aerator, J/s

E_W: Energy dissipation due to bubble wakes, J/s

F_D: dissolved gas flux, mol/s

F_G: gas flux, mol/s

F_S: plume dissolved solids flux, kg/s

F_T: plume temperature flux, °C m^3/s

g: gravitational constant, m/s^2

H: Henry's constant, $mol/m^3/bar$

h_D: aerated liquid height, m

h_L: unaerated liquid height. M

K_{en}: entrance loss coefficient, dimensionless

K_{ex}: exit loss coefficient, dimensionless

K_L: liquid-side mass transfer coefficient, m/s

K_t: top section loss coefficient, dimensionless

L: linear plume length, m

L_d: length of downcomer, m

M: plume momentum flux, m^4/s^2

N: number flux of bubbles, 1/s

P: partial pressure, bar

P_{atm}: atmospheric pressure, Pa

P_{tot}: total pressure, bar

Q: plume water volume flux, m^3/s

Q_G: volumetric gas flow rate at atmospheric pressure, m^3/s

Q_{gas}: actual volumetric gas flow rate at Speece Cone inlet, m^3/s

Q_w: volumetric water flow rate, m^3/s

R: ideal gas constant, m^3 bar/mol/K, or radius of Speece Cone, m

R_1: radius of top of Speece Cone, m

R_2: radius of bottom of Speece Cone, m

r: bubble radius, m

S: salinity of plume water, kg/kg

S_a: salinity of ambient water, kg/kg

T: temperature, °C or K

T_a: temperature of ambient water, °C

T_p: temperature of plume water, °C

U_G: average superficial gas velocity, m/s

U_{Ld}: superficial water velocity in downcomer, m/s

U_{Le}: superficial water velocity in exit, m/s

U_{Lr}: superficial water velocity in riser, m/s

V_{Lr}: actual water velocity in riser, m/s

v: actual water velocity, m/s

v_b: bubble rise velocity, m/s

W: linear plume width, m

y: gaseous-phase concentration, mol/m^3

z: depth, m (defined as positive downwards for Speece Cone)

ΔC_{O2}: change in dissolved oxygen concentration, g/m^3

α: entrainment coefficient, dimensionless

ε: gas holdup, dimensionless

λ: plume radius or spreading ratio, dimensionless

ρ: average density of air/water mixture in airlift aerator, kg/m^3

ρ_L: water density, kg/m^3

ρ_a: ambient water density, kg/m^3

ρ_p: plume bubble-water mixture density, kg/m^3

ρ_w: density of plume water, kg/m^3

Subscripts

a: ambient

i: individual chemical species (oxygen or nitrogen)

r: riser

O: oxygen

N: nitrogen

Tables and Figures

Table 1. Summary of selected hypolimnetic aeration and oxygenation installations documented in the literature. Both experimental and permanent units are included.

Waterbody	Maximum Depth (m)	Volume (10^6 m^3)	Oxygenator Type	Year Installed	Oxygen Addition (kg/d)	References
Wahnbach Reservoir, Germany	45	42	full-lift aerator	1966	1560	[*Bernhardt*, 1967; *Bernhardt and Wilhelms*, 1975]
Mirror Lake, Wisconsin	13	0.40	full-lift aerator	1972	111	[*Wirth et al.*, 1975]
Silver Lake, Wisconsin	12		full-lift aerator	1972	85	[*Wirth et al.*, 1975]
Larson Lake, Wisconsin	12	0.19	full-lift aerator	1973	26	[*Wirth et al.*, 1975]
Lake Waccabuc, New York	13	4.1	partial-lift aerator	1973	350	[*Fast et al.*, 1975a]
Ottoville Quarry, Ohio	18	0.063	side stream pumping	1973	14	[*Fast et al.*, 1975b]
Spruce Knob Lake, West Virginia	6		full-lift aerator	1974	49	[*Hess*, 1975]
Clark Hill Reservoir, Georgia		3,096	bubble-plume diffuser	1975	54,400	[*Rayyan and Speece*, 1977]
Lake Ghirla, Italy	14	2.0	submerged pumping oxygenation system[a]	1976	0.13	[*Beutel and Horne*,

Waterbody	Maximum Depth (m)	Volume (10^6 m^3)	Oxygenator Type	Year Installed	Oxygen Addition (kg/d)	References
						1999; *Bianucci and Bianucci*, 1979]
Lake Nantua, France	42		side stream oxygen injection	1976	200-250	[*Barroin*, 1994]
Black Lake, British Columbia	9	0.18	full-lift aerator	1978		[*Ashley and Hall*, 1990]
Tory Lake, Ontario	10	0.055	full-lift aerator	1978		[*Taggart and McQueen*, 1981; *Taggart*, 1984]
Lake Särkinen, Finland	17	2.5	Mixox aerator	1980		[*Lappalainen*, 1994]
Lake St. George, Ontario	16		full-lift aerator	1980		[*McQueen and Lean*, 1983; *McQueen et al.*, 1986]
Lake Tegal, Germany	16	24.6	Limnox partial-lift aerator	1980	4500	[*Lindenschmidt and Hamblin*, 1997]
WeBlinger See, Germany	12	1.0	Limno full-lift aerator	1981	120	[*Steinberg and Arzet*, 1984]

Waterbody	Maximum Depth (m)	Volume (10^6 m^3)	Oxygenator Type	Year Installed	Oxygen Addition (kg/d)	References
Lake Baldegg, Switzerland	66	176	bubble-plume diffuser	1982	3000-4500	[*Gachter and Wehrli*, 1998; *Wüest et al.*, 1992]
Lake Pyhäjärvi, Finland	42		Mixox aerator	1983	1300	[*Lappalainen*, 1994]
Lake Sempach, Switzerland	87	662	bubble-plume diffuser	1984	3000	[*Gachter and Wehrli*, 1998]
Lake Hald, Denmark	31	44	bubble-plume diffuser		575	[*Søndergaard et al.*, 2000]
Richard B. Russell, Georgia	47	1,270	bubble-plume diffuser	1985	200,000	[*Beutel and Horne*, 1999; *Mauldin et al.*, 1988]
Glen Lake, British Columbia	13		full-lift aerator	1986	40	[*Ashley et al.*, 1987]
Lake Hallwil, Switzerland	47	285	bubble-plume diffuser	1986	1.3-7.1	[*McGinnis et al.*, 2004]
Lake Kallvesi, Finland	38		Mixox aerator	1986		[*Matinvesi*, 1996]
Medical Lake, Washington	18	6.2	LIMNO partial-lift aerator	1986	225	[*Soltero et al.*, 1994]
St. Mary Lake, British Columbia	9.1 (mean)		full-lift aerator	1986	311 512 (after retrofit)	[*Ashley*, 1988; 2000]
Lake Shenipsit, Connecticut	21	12.3	layer aeration	1987		[*Kortmann*, 1994;

Waterbody	Maximum Depth (m)	Volume (10^6 m^3)	Oxygenator Type	Year Installed	Oxygen Addition (kg/d)	References
						Kortmann et al., 1994]
Lake Muggesfelde, Germany	21	21	TIBEAN full-lift aerator	1987	500	[*Jaeger*, 1990]
Amisk Lake, Alberta	34 (north basin)	25 (north basin)	bubble-plume diffuser	1988	750-1000	[*Prepas and Burke*, 1997; *Prepas et al.*, 1997]
Lake Huruslahti, Finland	26		Mixox aerator	1990		[*Matinvesi*, 1996]
Lake Krupunder, Germany	10.5	0.28	TIBEAN full-lift aerator	1990	80	[*Jaeger*, 1994]
Medical Lake, Washington	18	6.2	full-lift aerator	1990	500	[*Soltero et al.*, 1994]
Lake Prince, Virginia	10	13.9	full-lift aerator	1991	4100	[*Burris and Little*, 1998; *Burris et al.*, 2002]
Newman Lake, Washington	10	28.6	Speece Cone	1992	2000	[*Moore et al.*, 1996; *Thomas et al.*, 1994]
Camanche Reservoir, California	41	545	Speece Cone	1993	9,000	[*Jung et al.*, 1999]
Douglas Dam, Tennessee	38	1700	bubble-plume diffuser	1993	100,000	[*Mobley and Brock*, 1995]
Lake Western Branch, Virginia	11	24.4	full-lift aerator	1993	6600	[*Burris and Little*, 1998; *Burris et al.*, 2002]

Waterbody	Maximum Depth (m)	Volume (10^6 m^3)	Oxygenator Type	Year Installed	Oxygen Addition (kg/d)	References
Lake Stevens, Washington	44		full-lift aerator	1994	2900	[*Gibbons et al.*, 1994]
Tombigbee River, Alabama	11	n/a	U-tube		23,600	[*Speece*, 1996]
Heart Lake, Ontario	10.9	0.78	full-lift oxygenator	1995	140-200	[*Gemza*, 1997]
Whittaker Lake, Ontario	11	0.39	full-lift oxygenator	1995	140-200	[*Gemza*, 1997]
Spring Hollow Reservoir, Virginia	55	7.2	bubble-plume diffuser	1998	250	[*Little and McGinnis*, 2001; *Little*, 2005]
Upper San Leandro Reservoir, California		51	bubble-plume diffuser	2002	9,000	[*Jung et al.*, 2003; *Little*, 2005]

[a]as classified by Beutel and Horne (1999)

Table 2. Correlation equations for Henry's constant, mass transfer coefficient, and bubble rise velocity [*Wüest et al.*, 1992].

Equation	Range
$H_O = 2.125 - 5.021 \times 10^{-2}T + 5.77 \times 10^{-4}T^2$ $H_N = 1.042 - 2.450 \times 10^{-2}T + 3.171 \times 10^{-4}T^2$	(T in Celsius)
$K_L = 0.6r$	$r < 6.67 \times 10^{-4}$ m
$K_L = 4 \times 10^{-4}$	$r \geq 6.67 \times 10^{-4}$ m
$v_b = 4474r^{1.357}$	$r < 7 \times 10^{-4}$ m
$v_b = 0.23$	$7 \times 10^{-4} \leq r < 5.1 \times 10^{-3}$ m
$v_b = 4.202r^{0.547}$	$r \geq 5.1 \times 10^{-3}$ m

Table 3. Non-linear differential flux equations of the airlift aerator [*Burris et al.*, 2002] and Speece Cone [*McGinnis and Little*, 1998] models.

Dissolved gas flux (oxygen and nitrogen)	$\frac{dF_{D_i}}{dz} = K_L \left(H_i P_i - C_i \right) \frac{4\pi r^2 N}{\left(v + v_b \right)\left(1 - \varepsilon \right)}$
Gas flux (oxygen and nitrogen)	$\frac{dF_{G_i}}{dz} = -K_L \left(H_i P_i - C_i \right) \frac{4\pi r^2 N}{v + v_b}$

Table 4. Key variables and water flow rate equations of the airlift aerator model [*Burris et al.*, 2002; *Little and Del Vecchio*, 1996].

Dissolved gas flux (oxygen and nitrogen)	$F_{D_i} = A_r(1-\varepsilon)vC_i$
Gas flux (oxygen and nitrogen)	$F_{G_i} = A_r(v+v_b)y_i$
Bubble radius	$r = \left[\frac{3\varepsilon A_r(v+v_b)}{4\pi N}\right]^{\frac{1}{3}}$
Energy balance for water flow rate	$E_I = E_W + E_F + E_E + E_T$
Energy input due to isothermal gas expansion	$E_I = Q_G P_{atm} \ln\left(1+\frac{\rho g h_D}{P_{atm}}\right)$
Energy dissipation due to bubble wakes	$E_W = \rho_L g h_L A_r \varepsilon_r v_b$
Energy loss due to wall friction	$E_F = 2C_f\rho_L U_{Lr}(U_{Lr}+U_G)\frac{h_D}{D_r}(U_{Lr}A_r) + 2C_f\rho_L\frac{L_d}{D_d}\left(U_{Ld}^3 A_d\right)$
Energy loss due to local flow disturbances	$E_E = \frac{1}{2}\rho_L\left[V_{Lr}^3 K_{en} A_r(1-\varepsilon_r) + U_{Le}^3 K_{ex} A_e\right]$
Energy loss due to friction at the top of aerator	$E_T = \frac{1}{2}\rho_L V_{Lr}^3 K_t A_r(1-\varepsilon_r)$

Table 5. Key variables of the Speece Cone model [*McGinnis and Little*, 1998].

Molar dissolved gas flow rate	$F_{D_i} = \pi R^2 v C_i$
Molar gas flow rate	$F_{G_i} = \pi R^2 (v + v_b) y_i$
Cone radius	$R = \frac{R_2 - R_1}{h} z + R_1$
Actual water velocity	$v = \frac{Q_w}{\pi} \left(\frac{R_2 - R_1}{h} z + R_1 \right)^{-2} \left(\frac{1}{1 - \varepsilon} \right)$

Table 6. Speece Cone performance at varying depths predicted using assumed cone dimensions and operational parameters [*McGinnis and Little*, 1998].

Depth (m)	Q_{gas} (L/s)	ΔC_{O2} (g/m)	Total Oxygen Transfer (kg O_2/day)	Bubble Residence Time (s)
0	20.5	17	2200	107
10	40.4	33	4300	75
20	60.3	50	6400	69
30	80.2	66	8600	66
40	100.1	83	10700	64
50	120	101	12800	62

Table 7. Key variables of the circular [*Wüest et al.*, 1992] and linear [*Singleton et al.*, 2005] bubble-plume models.

Variable	Circular Bubble Plume	Linear Bubble Plume
Entrainment	$E = 2\alpha\pi bv$	$E = 2(L + W)\alpha v$
Plume water volume flux	$Q = \pi b^2 v$	$Q = LWv$
Momentum flux	$M = \pi b^2 v^2$	$M = LWv^2$
Temperature flux	$F_T = QT_p$	$F_T = QT_p$
Dissolved solids flux	$F_s = QS\rho_w$	$F_s = QS\rho_w$
Dissolved O_2 and N_2 fluxes	$F_{D_i} = QC_i$	$F_{D_i} = QC_i$
Gaseous O_2 and N_2 fluxes	$F_{G_i} = \pi b^2 \lambda^2 \left(v + v_b\right) y_i$	$F_{G_i} = \lambda W\left[L - \left(W - \lambda W\right)\right]\left(v + v_b\right) y_i$

Table 8. Non-linear differential flux equations of the circular [*Wüest et al.*, 1992] and linear [*Singleton et al.*, 2005] bubble-plume models.

Water volume flux	$\frac{dQ}{dz} = E$
Momentum flux (circular bubble plume)	$\frac{dM}{dz} = \frac{\rho_a - \rho_p}{\rho_p} g\pi b^2 \lambda^2 + \frac{\rho_a - \rho_w}{\rho_p} g\pi b^2 (1-\lambda^2)$
Momentum flux (linear bubble plume)	$\frac{dM}{dz} = \frac{\rho_a - \rho_w}{\rho_p} gLW + \frac{\rho_w - \rho_p}{\rho_p} g\lambda W\left[L - W(1-\lambda)\right]$
Temperature flux	$\frac{dF_T}{dz} = ET_a$
Salinity flux	$\frac{dF_s}{dz} = E\rho_a S_a$
Dissolved gas flux (oxygen and nitrogen)	$\frac{dF_{Di}}{dz} = EC_{ai} + K_L(H_i P_i - C_i)\frac{4\pi r^2 N}{v + v_b}$
Gas flux (oxygen and nitrogen)	$\frac{dF_{Gi}}{dz} = -K_L(H_i P_i - C_i)\frac{4\pi r^2 N}{v + v_b}$

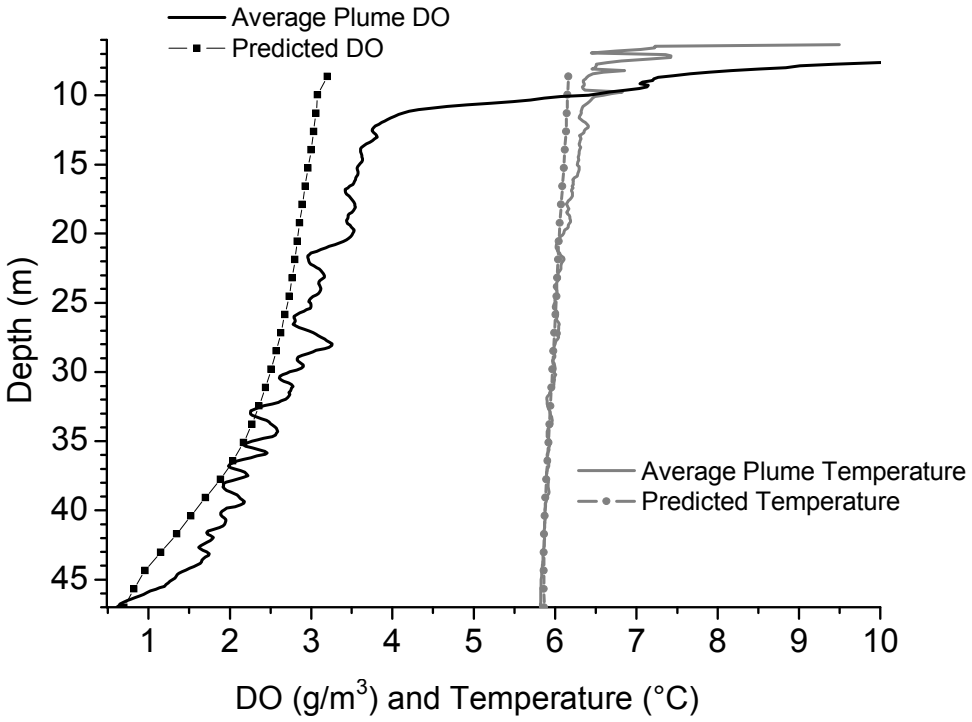

Figure 8. Averaged measured in-plume temperature and DO profile and circular bubble-plume model predictions for Lake Hallwil, Switzerland [*McGinnis et al.*, 2004].

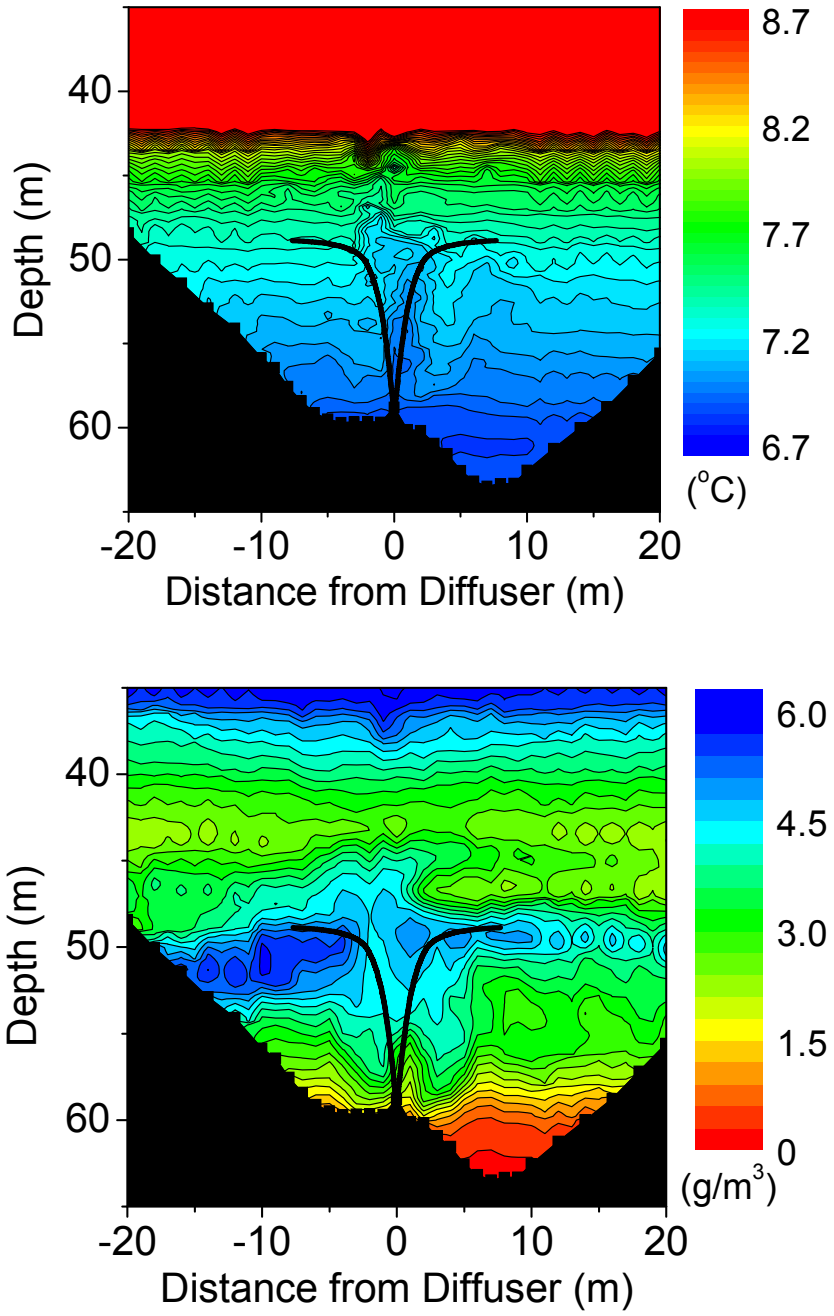

Figure 9. Measured plume temperature (top) and DO (bottom) contours with linear bubble-plume model predictions for diffuser operation with pure oxygen on 23 October 2004 in Spring Hollow Reservoir, Virginia, USA [*Singleton et al.*, 2005].

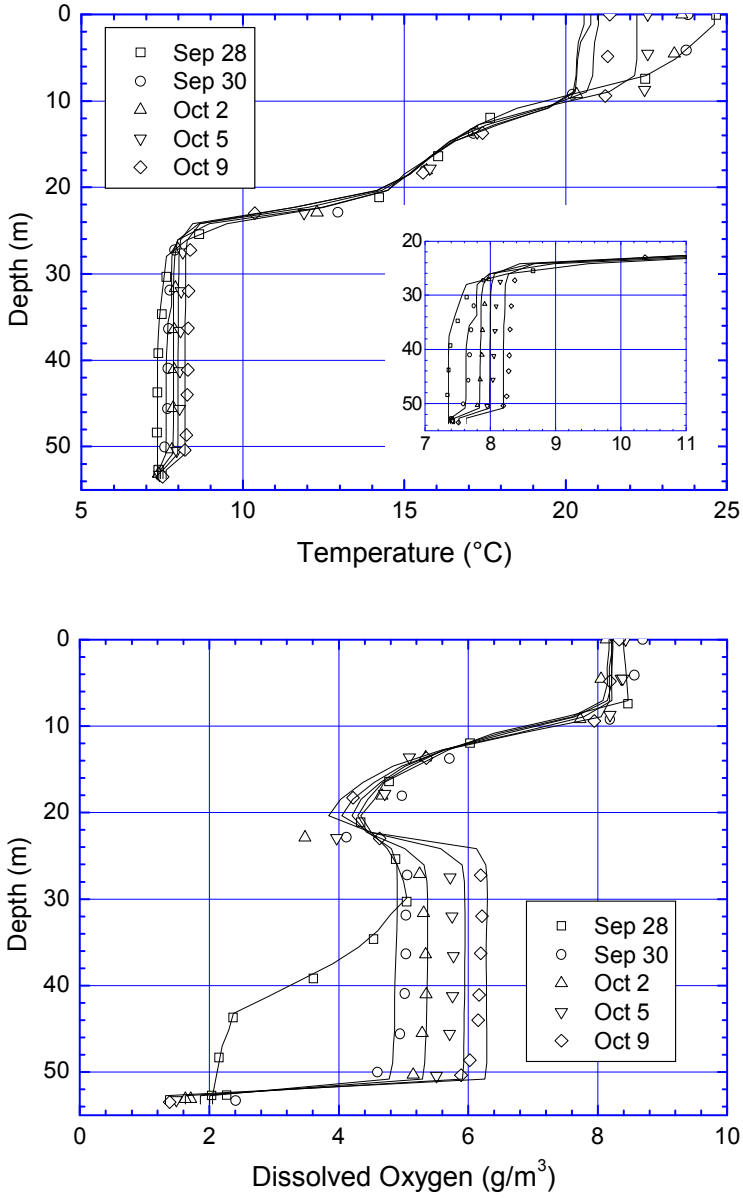

Figure 10. Measured temperature (top) and dissolved oxygen (bottom) profiles with coupled bubble plume-reservoir model predictions for linear diffuser operation in Spring Hollow Reservoir, Virginia, USA during 1997 [*McGinnis et al.*, 2001].

Literature Cited

Ashley, K. I. (1985), Hypolimnetic aeration: Practical design and application, *Water Res.*, *19*(6), 735-740.

Ashley, K. I., et al. (1987), Hypolimnetic aeration: Field test of the empirical sizing method, *Water Res.*, *21*(2), 223-227.

Ashley, K. I. (1988), Hypolimnetic aeration research in British Columbia, *Verh. Internat. Verein. Limnol.*, *23*(1), 215-219.

Ashley, K. I., and K. J. Hall (1990), Factors influencing oxygen transfer in hypolimnetic aeration systems, *Internat. Vereinigung fuer Theoret. und Angewandte Limnol.*, *24*(1), 179-183.

Ashley, K. I. (2000), Recent advances in hypolimnetic aeration design, *Verh. Internat. Verein. Limnol.*, *27*, 2256-2260.

Barroin, G. (1994), The sewage diversion and hypolimnetic oxygenation projects: Techniques and effectiveness, *Arch. Hydrobiol. Beih.*, *41*, 17-31.

Bernhardt, H. (1967), Aeration of Wahnbach Reservoir without changing the temperature profile, *Journal of the American Water Works Association*, *59*, 943-964.

Bernhardt, H., and A. Wilhelms (1975), Hypolimnetic aeration as a means of controlling redox processes on the bottom of a eutrophic reservoir, *Verh. Internat. Verein. Limnol.*, *19*, 1957-1959.

Beutel, M. W., and A. J. Horne (1999), A review of the effects of hypolimnetic oxygenation on lake and reservoir water quality, *Lake Reservoir Manage.*, *15*(4), 285-297.

Bianucci, G., and E. R. Bianucci (1979), Oxygenation of a polluted lake in northern Italy, *Effluent and Water Treatment J.*, *19*(3), 117-127.

Burris, V. L., and J. C. Little (1998), Bubble dynamics and oxygen transfer in a hypolimnetic aerator, *Water Sci. Technol.*, *37*(2), 293-300.

Burris, V. L., et al. (2002), Predicting oxygen transfer and water flow rate in airlift aerators, *Water Res.*, *36*(18), 4605-4615.

Cederwall, K., and J. D. Ditmars (1970), Analysis of Air-Bubble Plumes, W. M. Keck Laboratory of Hydraulics and Water Resources, Division of Engineering and Applied Science, California Institute of Technology, Pasadena, CA.

Clift, R., et al. (1978), *Bubble, Drops, and Particles*, 380 pp., New York, NY.

Fast, A. W., et al. (1975a), A submerged hypolimnion aerator, *Water Resour. Res.*, *11*(2), 287-293.

Fast, A. W., et al. (1975b), Hypolimnetic oxygenation using liquid oxygen, *Water Resour. Res.*, *11*(2), 294-299.

Gachter, R., and B. Wehrli (1998), Ten years of artificial mixing and oxygenation: No effect on the internal phosphorus loading of two eutrophic lakes, *Environ. Sci. Technol.*, *32*(23), 3659-3665.

Gemza, A. F. (1997), Water quality improvements during hypolimnetic oxygenation in two Ontario lakes, *Water Qual. Res. J. Can.*, *32*(2), 365-390.

Gibbons, H. L., et al. (1994), Worlds largest attempt at hypolimnetic aeration, *Lake Reservoir Manage.*, *9*(2), 76.

Hess, L. (1975), The effect of the 1st year of artificial hypolimnion aeration on oxygen, temperature, and the depth distribution of rainbow trout Salmo gairdneri in Spruce Knob Lake, West Virginia, U.S.A., paper presented at Proceedings of the West Virginia Academy of Science.

Jaeger, D. (1990), TIBEAN: A new hypolimnetic water aeration plant, *Internat. Vereinigung fuer Theoret. und Angewandte Limnol.*, *24*(1), 184-187.

Jaeger, D. (1994), Effects of hypolimnetic water aeration and iron-phosphate precipitation on the trophic level of Lake Krupunder, *Hydrobiol.*, *275/276*, 433-444.

Jung, R., et al. (1999), Improving water quality through lake oxygenation at Camanche Reservoir, paper presented at North American Lake Management Society Annual Symposium, Reno, NV, December 1.

Jung, R., et al. (2003), Hypolimnetic oxygenation operating experience in a eutrophic reservoir and its effect on water treatment, paper presented at Water Quality Technology Conference and Exposition, American Water Works Association, Philadelphia, PA.

Kortmann, R. W. (1994), Oligotrophication of Lake Shenipsit by layer aeration, *Lake Reservoir Manage.*, *9*(1), 94-97.

Kortmann, R. W., et al. (1994), Aeration of stratified lakes: Theory and practice, *Lake Reservoir Manage.*, *8*(2), 99-120.

Lappalainen, K. M. (1994), Positive changes in oxygen and nutrient contents in two Finnish lakes induced by Mixox hypolimnetic oxygenation method, *Internat. Vereinigung fuer Theoret. und Angewandte Limnol.*, *25*(4), 2510-2513.

Leifer, I., and R. K. Patro (2002), The bubble mechanism for methane transport from the shallow sea bed to the surface: A review and sensitivity study, *Continental Shelf Research*, *22*, 2409-2428.

Lindenschmidt, K. E., and P. F. Hamblin (1997), Hypolimnetic aeration in Lake Tegel, Berlin, *Water Res.*, *31*(7), 1619-1628.

Little, J. C. (1995), Hypolimnetic aerators: Predicting oxygen transfer and hydrodynamics, *Water Res.*, *29*(11), 2475-2482.

Little, J. C., and D. C. Del Vecchio (1996), Predicting water flow rate in hypolimnetic aerators, paper presented at International Association on Water Quality, Biennial Conference, Singapore.

Little, J. C., and D. F. McGinnis (2001), Hypolimnetic oxygenation: Predicting performance using a discrete-bubble model, *Water Science & Technology: Water Supply*, *1*(4), 185-191.

Little, J. C. (2005), Personal communication, edited by V. Singleton, Blacksburg, VA.

Lorenzen, M. W., and A. W. Fast (1977), A Guide to Aeration/Circulation Techniques for Lake Management, 125 pp, U.S. Environmental Protection Agency Ecol. Res. Serv.

Matinvesi, J. (1996), The change of sediment composition during recovery of two Finnish lakes induced by waste water purification and lake oxygenation, *Hydrobiol.*, *335*(3), 193-202.

Mauldin, G., et al. (1988), Injecting an oxygen fix, *Civ. Eng. CEWRA9*, *58*(3), 54-56.

McGinnis, D. F., and J. C. Little (1998), Bubble dynamics and oxygen transfer in a Speece Cone, *Water Sci. Technol.*, *37*, 285-292.

McGinnis, D. F., et al. (2001), Hypolimnetic oxygenation: Coupling bubble-plume and reservoir models, paper presented at Asian Waterqual 2001: First IWA Asia-Pacific Regional Conference, Intl. Wat. Assoc., Fukuoka, Japan, 12-15 Sept.

McGinnis, D. F., et al. (2004), Interaction between a bubble plume and the near-field in a stratified lake, *Water Resour. Res.*, *40*(10, W10206).

McQueen, D. J., and D. R. S. Lean (1983), Hypolimnetic aeration and dissolved gas concentrations: Enclosure experiments, *Water Res.*, *17*(12), 1781-1790.

McQueen, D. J., et al. (1986), Effects of hypolimnetic aeration on iron-phosphorus interactions, *Water Res.*, *20*(9), 1129-1135.

Mobley, M. H., and W. G. Brock (1995), Widespread oxygen bubbles to improve reservoir releases, *Lake Reservoir Manage.*, *11*(3), 231-234.

Moore, B. C., et al. (1996), A model for predicting lake sediment oxygen demand following hypolimnetic aeration, *Water Resources Bulletin*, *32*(4), 723-731.

Morton, B. R., et al. (1956), Turbulent gravitational convection from maintained and instantaneous sources, *Proceedings of the Royal Society of London. Series A, Mathematical and Physical Sciences*, *234*(1196), 1-23.

Prepas, E. E., and J. M. Burke (1997), Effects of hypolimnetic oxygenation on water quality in Amisk Lake, Alberta, a deep, eutrophic lake with high internal phosphorus loading rates, *Can. J. Fish. Aquat. Sci.*, *54*(9), 2111-2120.

Prepas, E. E., et al. (1997), Introduction to the Amisk Lake Project: oxygenation of a deep, eutrophic lake, *Can. J. Fish. Aquat. Sci.*, *54*(9), 2105-2110.

Rayyan, F., and R. E. Speece (1977), Hydrodynamics of bubble plumes and oxygen absorption in stratified impoundments, *Prog. Water Technol.*, *9*, 129-142.

Singleton, V. L., et al. (2005), Linear bubble plume model for hypolimnetic oxygenation: Full-scale validation and sensitivity analysis, *Accepted for publication in Water Resources Research*.

Soltero, R. A., et al. (1994), Partial and full lift hypolimnetic aeration of Medical Lake, WA to improve water quality, *Water Res.*, *28*(11), 2297-2308.

Søndergaard, M., et al. (2000), Lake restoration in Denmark, *Lakes & Reservoirs: Research and Management*, *5*(3), 151-159.

Speece, R. E. (1996), Oxygen supplementation by U-tube to the Tombigbee River, *Water Science and Technology*, *34*(12), 83-90.

Steinberg, C., and K. Arzet (1984), Impact of hypolimnetic aeration on abiotic and biotic conditions in a small kettle lake, *Environ. Technol. Letters*, *5*(4), 151-162.

Taggart, C. T., and D. J. McQueen (1981), Hypolimnetic aeration of a small eutrophic kettle lake: Physical and chemical changes, *Archiv fur Hydrobiologie*, *91*(2), 150-180.

Taggart, C. T., and D. J. McQueen (1982), A model for the design of hypolimnetic aerators, *Water Res.*, *16*, 949-956.

Taggart, C. T. (1984), Hypolimnetic aeration and zooplankton distribution: A possible limitation to the restoration of cold-water fish production, *Can. J. Fish. Aquat. Sci.*, *41*(1), 191-198.

Thomas, J. A., et al. (1994), Short term changes in Newman Lake following hypolimnetic aeration with the Speece Cone, *Lake Reservoir Manage.*, *9*(1), 111-113.

Wirth, T. L., et al. (1975), Total and hypolimnetic aeration of lakes in Wisconsin, *Verhandlungen Internationale Vereinigung Limnologie*, *19*, 1960-1970.

Wüest, A., et al. (1992), Bubble plume modeling for lake restoration, *Water Resour. Res.*, *28*, 3235-3250.

CHAPTER 3. LINEAR BUBBLE PLUME MODEL FOR HYPOLIMNETIC OXYGENATION: FULL-SCALE VALIDATION AND SENSITIVITY ANALYSIS

V. L. Singleton, P. Gantzer, and J. C. Little[a]

418 Durham Hall, Department of Civil and Environmental Engineering, Virginia Polytechnic Institute and State University, Blacksburg, VA 24061-0246, U.S.A. ([a]corresponding author)

Published in 2007 in Water Resources Research, Volume 43, W02405

Abstract

An existing linear bubble plume model was improved, and data collected from a full-scale diffuser installed in Spring Hollow Reservoir, VA, U.S.A. were used to validate the model. The depth of maximum plume rise was simulated well for two of the three diffuser tests. Temperature predictions deviated from measured profiles near the maximum plume rise height, but predicted dissolved oxygen profiles compared very well to observations. A sensitivity analysis was performed. The gas flow rate had the greatest effect on predicted plume rise height and induced water flow rate, both of which were directly proportional to gas flow rate. Oxygen transfer within the hypolimnion was independent of all parameters except initial bubble radius and was inversely proportional for radii greater than approximately 1 mm. The results of this work suggest that plume dynamics and oxygen transfer can successfully be predicted for linear bubble plumes using the discrete-bubble approach.

Keywords

Hypolimnetic oxygenation; hypolimnetic aeration; bubble plume; oxygen transfer; line diffuser; reservoir.

Introduction

Bubble plumes are used in a variety of industrial and environmental applications including mixing in chemical reactors, stripping of dissolved gases, containment of spills, prevention of ice formation, protection of harbors from damaging waves [*Fanneløp et al.*, 1991],

and destratification of lakes and reservoirs [*Schladow*, 1992]. In addition to airlift aerators [*Burris et al.*, 2002] and Speece Cones [*McGinnis and Little*, 1998], bubble plumes are commonly used for hypolimnetic aeration and oxygenation, which preserves stratification of water bodies while adding oxygen to the deepest layer. Hypolimnetic anoxia negatively affects the drinking-water treatment process, cold-water fisheries, and water quality downstream of hydropower reservoirs. In the U.S., releases from hydropower reservoirs typically must comply with state water quality criteria for minimum dissolved oxygen (DO) concentrations [*Peterson et al.*, 2003]. Oxygen depletion may lead to increases in hydrogen sulfide, ammonia, and phosphorus, and the release of reduced iron and manganese from the sediments. Hydrogen sulfide, iron, and manganese in drinking water usually require additional treatment [*Cooke and Carlson*, 1989]. Finally, hypoxia can affect sex differentiation and development, resulting in male-dominated populations with reduced reproductive success [*Shang et al.*, 2006].

A bubble plume model to predict oxygen transfer from linear diffuser systems was presented by *McGinnis et al.* [2001], based on the model for a circular diffuser developed earlier by *Wüest et al.* [1992]. While several models for point-source or circular bubble plumes have been proposed [*Asaeda and Imberger*, 1993; *Brevik and Kluge*, 1999; *Ditmars and Cederwall*, 1974; *Fanneløp and Sjøen*, 1980; *Johansen*, 2000; *Kobus*, 1968; *McDougall*, 1978; *Milgram*, 1983; *Rayyan and Speece*, 1977; *Sahoo and Luketina*, 2003; *Schladow*, 1992; *Wüest et al.*, 1992; *Zheng et al.*, 2002] less work has been conducted on linear (also referred to as line, two-dimensional, or planar) bubble plumes. *Kobus* [1968] developed one of the first analytical models for linear bubble plumes, which uses an empirical correlation to calculate buoyancy flux. *Ditmars and Cederwall* [1974] presented a model similar to that of *Kobus* [1968], but included bubble slip velocity. *Brevik* [1977] proposed a phenomenological theory for two-dimensional bubble plumes comparable to that of *Ditmars and Cederwall* [1974], except that kinetic energy was used to predict entrainment. *Wilkinson* [1979] proposed that full-scale linear plumes could be characterized by a Weber number. *Laureshen and Rowe* [1987] presented a model for two-dimensional bubble plumes in which plume spreading, entrainment, and momentum amplification were assumed to be functions of the plume Weber number and empirical constants. *Fanneløp et al.* [1991] developed a model for linear plumes in shallow water and studied the resulting surface currents and recirculation cells. Lastly, *Brevik and Kluge* [1999] expanded an existing model for linear bubble plumes to account for vertical turbulence. Although much

insight into plume dynamics was gained, none of these models for linear or two-dimensional bubble plumes accounted for ambient stratification or gas transfer. The first linear bubble plume model to include gas transfer was presented by *McGinnis et al.* [2001], who converted the circular bubble plume model of *Wüest et al.* [1992] to linear geometry. The incorporation of gas transfer is critical because the rapid dissolution rate of oxygen, and nitrogen when compressed air is used, strongly influences the buoyancy of the plume [*Wüest et al.*, 1992]. Gas transfer is especially important in deep water bodies and for weak plumes because of the increased contact time allows greater gas exchange. Lastly, the prediction of oxygen addition from hypolimnetic oxygenation systems is facilitated. Despite the usefulness of the linear bubble plume model, it has not yet been validated at full-scale and over a range of operating conditions.

Using extensive, high spatial-resolution CTD (**c**onductivity and **t**emperature as a function of **d**epth) transect data collected in Spring Hollow Reservoir (SHR), VA, U.S.A. during diffuser operation in 2003 and 2004, the performance of the linear bubble plume model is evaluated. The motivation for this work includes verification of model performance prior to use for design and investigation of critical model parameters through sensitivity analysis. Also, the accuracy of model predictions for depth of maximum plume rise (DMPR) and induced water flow rate should be assessed prior to coupling with lake/reservoir hydrodynamic and water quality models, such as CE-QUAL-W2 [*McGinnis et al.*, 2001]. In this paper, an improved linear bubble plume model is presented, observations and model predictions are compared, and results of a sensitivity analysis are discussed.

Bubble Plumes in Stratified Waterbodies

During hypolimnetic oxygenation with bubble plumes, compressed gas is continually supplied to diffusers, usually located immediately above the sediments, and is allowed to bubble freely. A gas-water plume mixture that is less dense than the ambient water is created, which causes the mixture to ascend through the hypolimnion. As the mixture rises, ambient water is entrained into the plume, and the plume width increases. The entrained fluid produces a double-plume structure, consisting of an inner core that contains the bubble-water mixture surrounded by an outer annulus that contains plume water relatively free of bubbles [*McDougall*, 1978]. As the outer annulus entrains stratified hypolimnetic water, the plume width increases and the density decreases. When the negative buoyancy of the entrained fluid exceeds the positive

buoyancy imparted by the bubbles, the plume detrains water at a rate nearly equal to that previously entrained [*Lemckert and Imberger*, 1993]. At this depth, the velocity of the relatively dense water within the plume decreases to zero, and the plume stops rising. The detraining plume water then forms an annular downward flow immediately outside the outer annulus of the upward flowing plume water. The detraining plume water entrains ambient water until a depth of neutral buoyancy is reached, where a horizontal intrusion is created into the hypolimnion [*Asaeda and Imberger*, 1993]. The undissolved bubbles remaining in the bubble-water mixture separate from the inner core flow and continue to rise to the surface, repeating the entire process.

Linear Bubble Plume Model

The linear bubble plume model utilizes the discrete-bubble approach, which has also been applied to the airlift aerator and Speece Cone and was recently reviewed in detail by Singleton and Little [2006]. The linear bubble plume model is composed of horizontally-integrated equations based on the conservation of mass, momentum, and heat. Eight flux equations are solved simultaneously to predict water flow rate, plume temperature, oxygen and nitrogen transfer and concentration, salinity, and plume rise height, given diffuser geometry and depth, applied gas flow rate, and initial bubble size (Tables 9 and 10). The model accounts for density stratification due to vertical temperature and salinity gradients. Entrainment is assumed to be proportional to the local (with respect to depth) plume water velocity and perimeter. Bubble size varies as the bubbles rise due to expansion and dissolution, and bubble slip velocity and gas transfer coefficients are functions of bubble radius [*Wüest et al.*, 1992]. Also, Henry's constants for oxygen and nitrogen are functions of temperature [*Wüest et al.*, 1992]. The bubble plume model equations were originally developed by *Wüest et al.* [1992] for circular geometry, but were modified by *McGinnis et al.* [2001] for the linear geometry of the system installed in SHR. The equations that include the spreading coefficient (λ) were recently refined [*Singleton and Little*, 2005] to more accurately reflect the geometry of the plume at the ends of the linear diffuser (Tables 9 and 10), which is approximated in plan view as a long thin rectangle. Additional refinements to the model of *McGinnis et al.* [2001], which are detailed in the following paragraphs, include use of a correlation to calculate initial bubble size [*McGinnis and Little*, 2002], correction of the entrainment coefficient (α) and λ for top-hat profiles, and use of a Froude number (*Fr*) to calculate initial water velocity [*Fischer et al.*, 1979; *Wüest et al.*, 1992].

Also, water quality profiles from the plume near-field, as opposed to the reservoir far-field, were used as boundary conditions [*McGinnis et al.*, 2004].

The entrainment coefficient and λ were set at 0.11 and 0.93, respectively. These values were derived by *Fanneløp et al.* [1991] by fitting Gaussian profiles to laboratory data and were modified for the top-hat profile assumption of the model using [*Fanneløp and Sjøen*, 1980]:

$$\alpha_T = \sqrt{2}\,\alpha_G \tag{1}$$

$$\lambda_T = \sqrt{\frac{\lambda_G{}^2 + 1}{2}} \tag{2}$$

where the subscripts T and G refer to top-hat and Gaussian profiles, respectively. For simplicity, top-hat or uniform profiles are assumed for water velocity, temperature, salinity, dissolved and gaseous constituents, and bubble velocity [*Wüest et al.*, 1992]. Other model assumptions are as follows: 1) the linear plume width W for temperature and dissolved constituents is equal to the width of the plume velocity profile, whereas the bubbles are confined to an inner core of width λW (λ<1); 2) ambient currents are negligible; 3) the diffuser produces bubbles at a constant rate and uniform size that are evenly distributed over the cross-section of initial width λW_o; 4) bubble coalescence is neglected; 5) initial water properties of the plume are those of ambient water at the diffuser depth; and 6) exchange of gases other than oxygen and nitrogen is not considered.

The model predictions are strongly dependent on the initial plume conditions and the plume boundary conditions of temperature, dissolved oxygen, and salinity. Initial conditions for the bubble plume model were determined as detailed by *Wüest et al.* [1992], except for the following deviations. Initial bubble size is calculated using the correlation developed by *McGinnis and Little* [2002] for the type of linear diffuser installed in SHR:

$$d_{3,2} = 1.12 + 0.938q \tag{3}$$

The correlation was determined using measured Sauter-mean bubble diameter ($d_{3,2}$) values of 1.1–2.2 mm collected over actual unit gas flow rates q of 0.08–0.88 m^2/hr at the diffuser.

For the circular bubble plume model, *Wüest et al.* [1992] proposed that the induced vertical water velocity v at the diffuser depth is equivalent to the initial plume water velocity. To estimate the initial velocity, *Wüest et al.* [1992] defined a densimetric Fr and utilized a relationship between the local Richardson number (Ri) and Fr derived by *Fischer et al.* [1979] for single-phase, round buoyant jets discharging vertically. The circular bubble plume model was recently validated by *McGinnis et al.* [2004], so a similar procedure was employed to determine the initial plume velocity for the linear bubble plume. Corresponding equations for Fr were derived for planar or linear plumes using relationships presented by *Fischer et al.* [1979] to obtain:

$$Fr = Ri^{-\frac{3}{4}} \tag{4}$$

$$Fr = \frac{v}{\left[\lambda W g\left(\rho_a - \rho_p\right)/\rho_p\right]^{\frac{1}{2}}} \tag{5}$$

where g is gravitational acceleration, ρ_a is the ambient water density, and ρ_p is the bubble plume density. The local Ri for planar jets has a constant value of 0.735 at distances from the source where the flow is more like a plume [*Fischer et al.*, 1979]. Consequently, Fr for a planar or linear plume is equal to 1.26, except close to the source. *Wüest et al.* [1992] assumed that the bubble slip velocity near the source was relatively low, so the initial Froude number (Fr_o) should be equal to the value for a single-phase plume. Unlike the circular plume model, the Fr profiles predicted by the linear bubble plume model continually increase with depth for the diffuser installed in SHR (not shown). For $Fr_o \leq 2.0$, the plume velocity initially increases with decreasing depth immediately above the linear diffuser (Figure 11a). This effect was also predicted by *Fanneløp and Webber* [2003] for buoyant plumes rising from areal sources, where a point of maximum velocity occurred above the source. Additionally, the plume neck (point of minimum radius or width) is always below the point of maximum velocity in the plume [*Fanneløp and Webber*, 2003]. A neck is not predicted for the linear bubble plume when Fr_o=2.0 (Figure 11b). However, necking or contraction will only occur when the momentum immediately above the source is relatively low and/or the entrainment coefficient is relatively

low [*Fanneløp and Webber*, 2003]. Also, *Wüest et al.* [1992] reasoned that a plume from an open source (diffuser above sediments) may not contract because initially entrained water is not obstructed. Therefore, Fr_o for an open source will likely be higher than that for a closed source (diffuser resting on sediments). Because the linear diffuser in SHR is an open source (Figure 12), Fr_o for the linear bubble plume was assumed to be 2.0, and a sensitivity analysis was conducted to determine the effect of varying Fr_o.

The differential flux equations of the linear bubble plume model (Table 10) were solved numerically using the fourth-order Runge-Kutta method. Further information on the general solution procedure, equations of state, and model assumptions is provided by *Wüest et al.* [1992] and *McGinnis et al.* [2004]. The model calculations are only valid over the plume rise height, up to the DMPR. When the plume stops rising, a secondary plume may form above as bubbles that are not completely dissolved continue to rise [*Asaeda and Imberger*, 1993; *McDougall*, 1978; *Schladow*, 1992]. This phenomenon can occur when a bubble plume is released into strong density stratification.

Application to Spring Hollow Reservoir, VA, U.S.A.

Field Data Collection

To fully evaluate the linear bubble plume model, experimental data for boundary conditions, rise height, and in-plume constituent profiles are required. Testing was conducted using a full-scale linear diffuser (Figure 12) installed in Spring Hollow Reservoir, VA, U.S.A. (Figure 13). Constructed in 1995, SHR is a small monomictic, mesotrophic side-stream reservoir that is generally stratified from May to December. The reservoir is managed by the Western Virginia Water Authority and serves as one of the principle drinking water sources for Roanoke County. The water body has a maximum depth of 65 m and a maximum surface elevation of 431 m. The approximate surface area and volume are 0.54 km^2 and 12.4×10^6 m^3, respectively. To prevent anoxia in the hypolimnion and the associated deterioration of raw water quality, a linear diffuser equipped with fine-bubble porous hoses was installed in 1997 (Figure 13). The 305-m long diffuser can be supplied with compressed air or pure oxygen at various gas flow rates and is located in the deepest portion of the reservoir (368–372 m elevation). Based on an average

surface elevation of 430 m, the depth of the diffuser during testing ranged from 58 to 62 m along its length. Table 11 provides the diffuser operating parameters in 2003 and 2004.

Diffuser tests were performed in 2003 using compressed air (21% O_2) supplied at a high gas flow rate (45 Nm^3/hr average) during 29 June–14 July and pure oxygen (97% O_2) supplied at a low flow rate (11 Nm^3/hr average) during 14–26 August. A third test was conducted in 2004 using pure oxygen, but at a higher gas flow rate (40 Nm^3/hr maximum) during 22 October–5 November. In 2003, the diffuser quickly mixed the rather small hypolimnetic volume during both tests, and the water quality conditions on the dates of data collection (2 July and 17 August for compressed air and pure oxygen, respectively) were by that time relatively homogeneous as a result of plume-induced mixing. One of the primary objectives of the 2004 experiments was to maximize the plume signature in the hypolimnion and to increase confidence in the linear plume model validation under a different set of boundary conditions. In 2004, the data were therefore collected on October 24, soon after start of diffuser operation. Additionally, the 2004 test was performed later in the stratified season to maximize the ambient DO and temperature gradients in the hypolimnion.

To establish appropriate boundary conditions for the plume model, characterization of the plume near-field environment is necessary [*McGinnis et al.*, 2004]. Therefore, the data collected included numerous high spatial-resolution CTD (Sea-Bird Model SBE 19plus; 4 Hz sampling rate) transects measured almost daily before, during, and after diffuser operation. The CTD profiler was also equipped with a DO probe (1.4 second response time measured at 20 °C). Profiles were obtained laterally across the diffuser at 0.5 m increments for 0-10 m, 2 m increments for 10-20 m, and 5 m increments for 20-40 m from the centerline of the diffuser in both directions (Figures 13 and 14). [Note: The diffuser centerline location is shifted to the left for 2004 (Figures 14e and f) because the diffuser was repositioned earlier in the year. Also, the operational length of the diffuser was decreased for that year (Table 11).]

The geometry of SHR affects the extent and rate of circulation within the hypolimnion induced by the bubble plume. Due to the relatively small size of SHR, operation of the linear diffuser created uniform conditions below the thermocline within days after startup. While SHR bathymetry influences plume-induced mixing in the hypolimnion, the effect on short-term plume operation is negligible because the time that individual bubbles spend in the hypolimnion is on the order of minutes. The bubbles and resulting plume experience a pseudo-steady-state with

respect to ambient conditions. Effects on data collection due to the ends of the linear diffuser were assumed to be negligible because the lateral profile location was over 150 m from a diffuser end (Figure 13), and the diffuser is designed to release a uniform gas flow along its length.

Observations and Model Application

Plume rise height, spreading, and constituent profiles predicted by the linear bubble plume model were compared to experimental observations. Critical model input parameters for the three test conditions (2 July 2003, 17 August 2003, and 23 October 2004) are shown in Table 11. The boundary conditions were obtained from averaged near-field lateral profiles [*McGinnis et al.*, 2004] (±2 m and ±1 m from plume centerline for 2003 and 2004, respectively) and differed significantly between 2003 and 2004 (Figure 15). (Note: The presence of two thermoclines in 2003 is due to the pumped reservoir inflow that discharges at 396 m elevation, which corresponded to approximately 34 m depth during diffuser testing. The lower thermocline delineates the effective hypolimnion for the oxygenation system.)

Measured contours of temperature and DO are shown in Figure 14, along with corresponding model predictions for plume width and the DMPR. The actual plume boundaries are not well defined in the contour plots, so comparison to predicted plume widths is difficult. The lack of distinct plume boundaries was due to the almost well-mixed conditions in the hypolimnion as a result of diffuser operation, particularly for 2003 (Figures 14a–d). Also, use of compressed air did not produce a strong DO plume signature for the July test compared to the August and October tests with pure oxygen. The actual plume rise height is easier to distinguish, especially in the DO contours for August and October. The predicted depths of maximum plume rise are 38.2 m, 46.1 m, and 48.8 m for July, August, and October, respectively. For July and October, the DMPR is simulated well by the model (Figures 14a, b, e, and, f). However, the model appears to underestimate the plume rise height for August, when the gas flow rate was comparatively low (Table 11). The under-predicted DMPR may have been due to an overestimated value for α. In a detailed study of round plumes, *Milgram* [1983] found that α is directly proportional to the plume gas holdup or fraction. However, the linear bubble-plume model assumes that α is constant (Table 11).

The structure of the plumes is similar to those observed by *Asaeda and Imberger* [1993] for round bubble plumes in weak stratification (Figure 14). Depending on the gas flow rate and

stratification strength, three types of horizontal intrusions from the plume were reported. The pattern of the DO contours for October (Figure 14f) closely resembles Type 1, which corresponds to a high gas flow rate or weak stratification [*Asaeda and Imberger*, 1993]. This is similar to a single plume impinging on a free surface, which is analogous to the thermocline in SHR. Although the plume for July is not easily discerned from the temperature or DO contours, the structure is most likely similar to a Type 1 plume. The July plume appears to detrain primarily at the lower thermocline with one strong intrusion, as evidenced by accumulation of higher oxygenated water near the top of the plume (Figure 14b). The plume for August is best classified as Type 3, which is for low gas flow rates or strong density stratification [*Asaeda and Imberger*, 1993]. Type 3 plumes do not have steady intrusions, but instead are characterized by alternating, collapsing eddies that cause the plume to meander.

Referring to the October test (Figure 14f), the higher DO concentrations at lower depths adjacent to both sides of the plume were likely the result of detrained water that sinks past the equilibrium depth due to momentum. The temperature isotherms were also depressed immediately beside the plume (Figure 14e). This phenomenon was also observed by *McGinnis et al.* [2004]. The DO concentration immediately above the predicted DMPR and near the vertical plume centerline for October 2004 is higher than the ambient concentration (Figure 14f). This could have been caused by the formation of a secondary plume above the DMPR resulting from incompletely dissolved bubbles. The model estimates that the bubble size at the top of the first plume was about 5×10^{-5} m for October 2004, which is relatively large compared to July 2003 and August 2003 (Figure 16f). These undissolved bubbles could have created a secondary plume, which entrained oxygenated water from the detrainment of the first plume and carried it higher into the water column.

Vertical profiles of constituents and properties within the plumes were also predicted for the three diffuser tests (Figure 16). For the July test with compressed air, the higher gas flux creates a greater buoyancy flux and a higher initial plume water velocity (Figure 16d). Also, the concentration driving force for oxygen transfer is lower compared to pure oxygen, which decreases the rate of bubble dissolution with depth (Figure 16f). These effects result in a higher DMPR for July compared to August (Figures 14 and 16). The model predictions for 2004 differ from those of 2003 because of the differing boundary conditions (Figure 15). The plume rise height for the October test with pure oxygen is less than that for August, even though the gas

flux was more than tripled (Table 11). The ambient temperature, and hence density, stratification was stronger in 2004, which provided greater negative buoyancy to decrease plume momentum. The stronger ambient density stratification also caused the plume velocity to decrease more rapidly with depth in 2004 despite a higher initial velocity from the diffuser (Figure 16d). The lower plume rise height in October resulted in lower plume water flow rates than July (Figure 16e), even with comparable gas fluxes applied (Table 11).

Average temperature, DO, and density profiles within the plumes were also measured (Figures 16a–c). The temperature, and consequently density, predictions for July and October deviate from the measured profiles where the plumes reach the top of the hypolimnion (Figures 16a and c), or where the rate of plume spreading is greatest (Figure 14). The model underpredicts the final plume temperature by approximately 0.3 and 0.2 °C for July and October, respectively. One reason for the discrepancy may be that the model assumes α is constant. In addition to the dependence on plume gas holdup, *Milgram* [1983] also found that α for a circular plume is directly proportional to the local plume radius. As the plume approaches its maximum rise height, the width increases rapidly (Figure 14). If linear plume dynamics are similar to circular plumes, then α for linear plumes may also increase as the plume width increases. Additionally, the boundary profiles selected may not accurately reflect the actual ambient conditions immediately adjacent to the plume along its entire rise height. Measured vertical CTD profiles at the estimated plume width were averaged and used for boundary conditions. However, the plume width varies greatly with depth (Figure 14), so use of vertical profiles at a single lateral distance from the diffuser is not appropriate. Also, the average plume width was visually estimated from the temperature and DO contour plots (Figure 14), but the actual plume boundaries are not well defined.

The model predicts the plume DO profiles well for all three diffuser tests (Figure 16b). For July and August, the model characterizes the initial increase in DO immediately above the diffuser quite accurately. The initial rapid increase in DO for August and October is due to the higher oxygen saturation concentration at depth with the use of pure oxygen. The high hydrostatic pressure causes the oxygen transfer rate to be almost independent of the ambient DO concentration at the depth of diffuser. By contrast, the initial DO increase for the July test with compressed air is more modest (Figure 16b). The shape of the predicted DO profile for October differs somewhat from the experimental data, even though the final values at the DMPR differ by

only 0.3 g/m^3. The hypolimnion and, hence, plume near-field were more heterogeneous in 2004 than 2003, which may have contributed to the overprediction at lower depths if the selected boundary profiles did not accurately represent water entrained into the plume.

Another source of inaccuracy could be the correlation equation used to calculate initial bubble size (Equation 3). This relationship was developed using data collected over actual air flow rates per unit length of diffuser of 0.08–0.88 m^2/hr [*McGinnis and Little*, 2002]. The actual gas flow rates per unit length of diffuser for the July, August, and October tests were 0.019, 0.0063, and 0.024 m^2/hr, respectively. Therefore, the initial bubble diameters used in the model were extrapolated beyond the valid correlation range.

Sensitivity Analysis

A sensitivity analysis was performed with the linear bubble plume model to determine the effects on plume rise height, oxygen transfer efficiency, and induced water flow rate, because these parameters are important for design and operation of hypolimnetic aeration/oxygenation systems. Parameter perturbation was employed, in which input variables are independently adjusted to determine their individual effects on model predictions. The model variables investigated are either difficult to measure or can be controlled through system design or operation (Table 11). Currently, α and λ for the linear plume model are empirical constants [*Fanneløp et al.*, 1991], and the initial plume water velocity is calculated using a densimetric *Fr* [*Wüest et al.*, 1992]. The initial plume area, gas flow rate, and, to a lesser extent, initial bubble size can be controlled through diffuser design and operation. The sensitivity of model predictions to ambient dissolved nitrogen was also examined for the standard case using compressed air (2 July 2003). The model assumes that the background dissolved nitrogen concentration is equivalent to the saturated value at atmospheric partial pressure and the average hypolimnetic water temperature.

The DMPR is most influenced by gas flow rate and initial bubble radius (Figures 17e and f). The gas flow rate is directly related to the density of the plume bubble-water mixture and, subsequently, the positive buoyancy and upward momentum of the plume (Table 10). For gas flow rates greater than approximately 100 Nm^3/hr, the plume rise height is controlled more by the depth of the thermocline in SHR (Figure 15a). As the plume rise height approaches the thermocline, further increases in the buoyancy and momentum fluxes can not overcome the

strong ambient density stratification. The 2003 predictions are more a function of gas flow rate than those for October 2004 because of differing boundary conditions (Figure 15).

The plume rise height is moderately sensitive to initial bubble radius (Figure 17f). For initial radii less than about 1 mm, the DMPRs are nearly independent of bubble size. As initial bubble sizes increase, the plumes ascend higher and reach a maximum height for a radius of about 6 mm for each diffuser test. The shapes of the curves can be attributed to the dependence of bubble rise velocity and gas transfer coefficients on bubble radius [*Wüest et al.*, 1992]. The DMPR predictions for August are more sensitive to initial bubble radius than those for July and October (Figure 17f). The plume on 17 August 2003 did not have sufficient buoyancy and momentum to rise to the thermocline because a relatively low gas flow rate was applied (Figure 14c and Table 11). By contrast, the plume dynamics for July and October were influenced to a greater degree by the thermocline, which in effect damped the sensitivity of plume rise height to the initial bubble radius.

The predicted DMPR for the linear bubble plume is virtually independent of Fr_o and λ over the ranges analyzed (Figures 17b and c). The plume rise height is moderately sensitive to α. Entrainment into the plume is a function of plume size, water velocity, and α (Table 9), and entrainment of ambient water decelerates the plume. Plume rise is influenced to a somewhat greater degree by the initial plume area. As the plume area is increased, the buoyancy flux decreases because the gas flow rate is constant. Plume rise height was unaffected by variations in the ambient dissolved nitrogen concentration from 50–200 percent saturation in the hypolimnion for the 2 July 2003 diffuser test. Similar to the analysis for DMPR, induced water flow rate at the top of the plume was found to be insensitive to Fr_o and λ and somewhat more sensitive to α and the initial plume area (results not shown). Plume water flow rate is most influenced by gas flow rate and initial bubble radius. Higher gas flow rates produce greater buoyancy and momentum fluxes, which results in greater plume rise heights and increased entrainment.

Oxygen transfer efficiency (total mass of oxygen transferred relative to initial mass of oxygen in bubbles) within the hypolimnion was independent of all parameters except initial bubble radius, decreasing from nearly 100 percent to around 20 percent for air and pure oxygen as the initial radii increased from approximately 1 mm to 1 cm (Figure 18). Oxygen transfer can continue above the DMPR if the bubbles are not dissolved. However, secondary plumes are not

accounted for in the model. Even though undissolved bubbles at the top of the plume may continue to transfer oxygen during ascent, the oxygen may not be added at the desired depth (i.e., below the thermocline). A local minimum with respect to induced water flow rate at the top of the plume is predicted for a bubble radius of about 1 mm for the conditions in SHR (not shown). This suggests that while maximum oxygen transfer efficiency can be achieved with a 1 mm initial bubble radius, vertical water circulation, and hence oxygen distribution in the hypolimnion, will not be optimized. As the bubble radius is increased from 1 mm, induced water flow rate increases as well for radii up to 5 mm, but oxygen transfer efficiency decreases rapidly within this range (Figure 18).

Comparison of Linear and Circular Bubble Plume Models

The primary difference between the linear and circular bubble plume models is the plume geometry. For a given plume cross-sectional area, the perimeter of a linear plume is much greater than for a circular or round plume. The initial estimated plume area and perimeter of the linear diffuser in SHR for July 2003 was about 50 m^2 and 600 m, respectively (Table 11). This corresponds to an equivalent radius and perimeter of approximately 4 m and 25 m, respectively, for a circular plume. In this case, the perimeter of the linear plume is 24 times greater than for the circular plume. For both the linear and circular plume models, entrainment of ambient water is directly proportional to local plume perimeter, local plume water velocity, and α (Table 9). The larger perimeter of the linear plume greatly increases ambient entrainment, which contributes to the negative buoyancy of the plume and causes the plume to decelerate more rapidly. This results in a lower plume rise height compared to the circular plume.

The sensitivity of the linear bubble plume model to various parameters was comparable to results for the circular bubble plume model analysis. Gas flow rate had the greatest effect on DMPR predictions by both models, and the linear plume model was less sensitive to initial bubble radius than the circular plume model [*Wüest et al.*, 1992]. The latter may be due to differences between temperature boundary conditions, which caused plume dynamics in SHR to be more influenced by thermocline depth. Initial bubble size greatly affected oxygen transfer efficiency for both diffuser geometries, decreasing rapidly as the radii increased beyond 1 mm and 3 mm for the linear and circular plumes, respectively. Both the linear and circular plume model predictions for DMPR were relatively insensitive to Fr_o and initial plume area {Figure 17

and [*Wüest et al.*, 1992]}. However, circular model predictions for DMPR were more sensitive to α. Overall, the linear model was less sensitive to input parameters than the circular model, but this insensitivity is probably due to the relatively homogeneous boundary conditions in the hypolimnion of SHR caused by diffuser mixing.

Summary and Conclusions

In the current work, the linear bubble plume model of *McGinnis et al.* [2001] was improved, and the updated model was evaluated using data collected from a full-scale hypolimnetic oxygenation system installed in Spring Hollow Reservoir, VA, U.S.A. Three diffuser experiments were conducted using compressed air and pure oxygen over a range of flow rates. Predicted plume rise height, spreading, and constituent profiles were compared to experimental observations. For July 2003 and October 2004, the DMPR was simulated well by the model. However, the model underestimated the plume rise height for August 2003, when the gas flow rate was comparatively low. The model underpredicted the final plume temperature by approximately 0.3 and 0.2 °C for July 2003 and October 2004, respectively. The model predicted the plume DO profiles very well for all three diffuser tests, including simulating the initial rapid transfer of oxygen immediately above the diffuser.

A sensitivity analysis was performed to determine the effect of various model input parameters. The DMPR and induced water flow rate were most influenced by gas flow rate and initial bubble radius, moderately sensitive to α and the initial plume area, and insensitive to Fr_o, λ, and ambient dissolved nitrogen. Oxygen transfer within the hypolimnion was independent of all parameters except initial bubble radius, decreasing from nearly 100 percent to around 20 percent for air and pure oxygen as the initial radii increased from approximately 1 mm to 1 cm.

The linear bubble plume model for hypolimnetic oxygenation has been successfully validated. The model can be used to design lake and reservoir oxygenation systems and to optimize existing systems to maximize oxygen addition. Application of the linear plume model requires knowledge of the gas flow rate, initial bubble radius, initial plume area, and near-field constituent profiles (boundary conditions). Additionally, several empirical parameters must be estimated including α and λ. Even though all of the model inputs may not be known with certainty for a given aeration or oxygenation system, the model can be used for preliminary

design and coarse optimization. Also, plume rise height, water flow rate, and oxygen transfer efficiency were found to be primarily dependent on gas flow rate and initial bubble radius.

Operation of bubble plumes for hypolimnetic oxygenation usually alters the ambient temperature and DO conditions of a waterbody. Plume dynamics and oxygen transfer are strongly related to the near-field water column properties, establishing a feedback loop that continually changes plume dynamics. This complex plume-lake interaction should be accounted for in the design and operation of bubble plume diffusers. *McGinnis et al.* [2001] performed a preliminary coupling of the linear bubble plume model with an existing reservoir model, CE-QUAL-W2 [*Cole and Wells*, 2003], and obtained encouraging results. Efforts are currently underway to further develop the coupled model to predict plume performance and the near- and far-field reservoir responses. In the absence of near-field boundary profiles, far-field or simulated constituent profiles can be used to provide a reasonable estimate of plume performance.

Acknowledgements

The authors thank Daniel McGinnis for his valuable technical assistance. Financial support was generously provided by the U. S. National Science Foundation (Grant No. BES 0202034) and the Western Virginia Water Authority.

Notation

b plume radius (circular bubble plume), m.

d bubble diameter, mm.

C dissolved concentration, mol/m^3.

E entrainment factor, m^2/s.

F_D dissolved species flux, mol/s.

F_G gaseous species flux, mol/s.

F_S salinity flux, kg/s.

F_T temperature flux, $^\circ$C m^3/s.

Fr Froude number,-.

g gravitational acceleration, m/s^2.

H Henry's constant, mol/m^3/bar.

K_L mass transfer coefficient, m/s.

L plume length, m.

M water momentum, m^4/s^2.

N number flux of bubbles, 1/s.

P pressure, bar.

Q plume flow rate, m^3/s.

q actual gas flow rate per unit diffuser length, m^2/h.

Ri Richardson number,-.

R bubble radius, m.

S salinity, g/kg.

T temperature, $^{\circ}C$.

v velocity, m/s.

W plume width, m.

y gaseous concentration, mol/m^3.

Z depth, m.

Greek letters

α entrainment coefficient, -.

λ spreading coefficient, -.

ρ density, kg/m^3.

Subscripts

3,2 Sauter-mean

G Gaussian profile

O oxygen

N nitrogen

T top-hat profile

a ambient water

b bubble

i gas species, oxygen or nitrogen

o initial

p	plume water and gas mixture
w	plume water

References

Asaeda, T., and J. Imberger (1993), Structure of bubble plumes in linearly stratified environments, *J. Fluid Mech.*, *249*, 35-57.

Brevik, I. (1977), Two-dimensional air-bubble plume, *J. Waterway, Port, Coastal, and Ocean Div., Proc. Am. Soc. Civil Engineers*, *103*, 101-115.

Brevik, I., and R. Kluge (1999), On the role of turbulence in the phenomenological theory of plane and axisymmetric air-bubble plumes *Internat. J. Multiphase Flow*, *25*, 87-108.

Burris, V. L., D. F. McGinnis, and J. C. Little (2002), Predicting oxygen transfer and water flow rate in airlift aerators, *Water Res.*, *36*, 4605-4615.

Cole, T. M., and S. A. Wells (2003), CE-QUAL-W2: A Two-Dimensional, Laterally Averaged, Hydrodynamic and Water Quality Model, Version 3.2, U.S. Army Engineering and Research Development Center, Vicksburg, MS.

Cooke, G. D., and R. E. Carlson (1989), *Reservoir Management for Water Quality and THM Precursor Control*, 387 pp., American Water Works Association Research Foundation, Denver, CO.

Ditmars, J. D., and K. Cederwall (1974), Analysis of air-bubble plumes, paper presented at 14th Coastal Engineering Conference, American Society of Civil Engineers, Copenhagen, Denmark.

Fanneløp, T. K., and K. Sjøen (1980), Hydrodynamics of underwater blowouts, *Norweg. Maritime Res.*, *4*, 17-33.

Fanneløp, T. K., S. Hirschberg, and J. Kueffer (1991), Surface current and recirculating cells generated by bubble curtains and jets, *J. Fluid Mech.*, *229*, 629-657.

Fanneløp, T. K., and D. M. Webber (2003), On buoyant plumes rising from area sources in a calm environment, *J. Fluid Mech.*, *497*, 319-344.

Fischer, H. B., E. J. List, R. C. Y. Koh, J. Imberger, and N. H. Brooks (1979), *Mixing in Inland and Coastal Waters*, 483 pp., Academic Press, Inc., San Diego, California.

Johansen, O. (2000), DeepBlow - a Lagrangian plume model for deep water blowouts, *Spill Sci. & Tech. Bull.*, *6*, 103-111.

Kobus, H. E. (1968), Analysis of the flow induced by air-bubble systems, paper presented at 11th Coastal Engineering Conference, American Society of Civil Engineers, London.

Laureshen, C. J., and R. D. Rowe (1987), Modeling of plane bubble plumes, paper presented at Buoyant Plumes, The 24th National Heat Transfer Conference and Exhibition, 9-12 August.

Lemckert, C. J., and J. Imberger (1993), Energetic bubble plumes in arbitrary stratification, *J. Hydraul. Eng.*, *119*, 680-703.

McDougall, T. J. (1978), Bubble plumes in stratified environments, *J. Fluid Mech.*, *85*, 655-672.

McGinnis, D. F., and J. C. Little (1998), Bubble dynamics and oxygen transfer in a Speece Cone, *Water Sci. Technol.*, *37*, 285-292.

McGinnis, D. F., J. C. Little, and A. Wuest (2001), Hypolimnetic oxygenation: Coupling bubble-plume and reservoir models, paper presented at Asian Waterqual 2001, First IWA Asia-Pacific Regional Conference, Fukuoka, Japan.

McGinnis, D. F., and J. C. Little (2002), Predicting diffused-bubble oxygen transfer rate using the discrete-bubble model, *Water Res.*, *36*, 4627-4635.

McGinnis, D. F., A. Lorke, A. Wüest, A. Stöckli, and J. C. Little (2004), Interaction between a bubble plume and the near-field in a stratified lake, *Wat. Resour. Res.*, *40*.

Milgram, J. H. (1983), Mean flow in round bubble plumes, *J. Fluid Mech.*, *133*, 345-376.

Peterson, M. J., G. F. Cada, M. J. Sale, and G. K. Eddlemon (2003), Regulatory Approaches for Addressing Dissolved Oxygen Concerns at Hydropower Facilities, 38 pp, U.S. Department of Energy, Energy Efficiency and Renewable Energy, Wind and Hydropower Technologies

Rayyan, F., and R. E. Speece (1977), Hydrodynamics of bubble plumes and oxygen absorption in stratified impoundments, *Prog. Water Technol.*, *9*, 129-142.

Sahoo, G. B., and D. Luketina (2003), Modeling of bubble plume design and oxygen transfer for reservoir restoration, *Water Res.*, *37*, 393-401.

Schladow, S. G. (1992), Bubble plume dynamics in a stratified medium and the implications for water quality amelioration in lakes, *Wat. Resour. Res.*, *28*, 313-321.

Shang, E. H. H., R. M. K. Yu, and R. S. S. Wu (2006), Hypoxia Affects Sex Differentiation and Development, Leading to a Male-Dominated Population in Zebrafish (Danio rerio), *Environ. Sci.Tech.*, *40*, 3118-3122.

Singleton, V. L., and J. C. Little (2005), Linear bubble plume model for hypolimnetic oxygenation: Full-scale evaluation and sensitivity analysis, paper presented at 9th

Workshop on Physical Processes in Natural Waters, Lancaster University, Lancaster, United Kingdom, 4-6 September.

Singleton, V. L., and J. C. Little (2006), Designing hypolimnetic aeration and oxygenation systems - A review, *Environ. Sci. Technol.*, DOI:10.1021/es060069s.

Wilkinson, D. L. (1979), Two-dimensional bubble plumes, *J. Hydraul. Div., Proc. Am. Soc. Civil Engineers*, *105*, 139-154.

Wüest, A., N. H. Brooks, and D. M. Imboden (1992), Bubble plume modeling for lake restoration, *Wat. Resour. Res.*, *28*, 3235-3250.

Zheng, L., P. D. Yapa, and F. Chen (2002), A model for simulating deepwater oil and gas blowouts–Part I: theory and model formulation *J. Hydraul. Res.*, *41*, 339-351.

Table 9. Key variables of the linear bubble plume model (revised from McGinnis et al., 2001).

Variable	Formula	Units
Entrainment factor	$E = 2(L+W)\alpha v$	m^2/s
Plume water volume flux	$Q = LWv$	m^3/s
Momentum flux	$M = LWv^2$	m^4/s^2
Temperature flux	$F_T = QT_p$	°C m^3/s
Dissolved solids flux	$F_s = QS\rho_w$	kg/s
Dissolved O_2 and N_2 fluxes	$F_{D_i} = QC_i$	mol/s
Gaseous O_2 and N_2 fluxes	$F_{G_i} = \lambda W\left(L - W + \lambda W\right)\left(v + v_b\right)y_i$	mol/s

Table 10. Non-linear differential flux equations of the linear bubble plume model (revised from McGinnis et al., 2001).

Water volume flux	$\frac{dQ}{dz} = E$
Momentum flux	$\frac{dM}{dz} = \frac{\rho_a - \rho_w}{\rho_p} gLW + \frac{\rho_w - \rho_p}{\rho_p} g\lambda W\left[L - W(1-\lambda)\right]$
Temperature flux	$\frac{dF_T}{dz} = ET_a$
Salinity flux	$\frac{dF_s}{dz} = E\rho_a S_a$
Dissolved gas flux	$\frac{dF_{D_i}}{dz} = EC_a + \frac{4\pi r^2 N}{v + v_b} K_L(H_i P_i - C_i)$
Gas flux	$\frac{dF_{G_i}}{dz} = -\frac{4\pi r^2 N}{v + v_b} K_L(H_i P_i - C_i)$

Table 11. Conditions for linear bubble plume model application and sensitivity analysis for Spring Hollow Reservoir, VA, U.S.A. Reservoir conditions on testing days are also included.

Parameter	2 July 2003	17 Aug 2003	23 Oct 2004	Sensitivity Range
Oxygen in gas supply (%)	21	97	97	n/a
Entrainment coefficient (-)	0.11	0.11	0.11	0.05 – 0.2
Spreading coefficient (-)	0.93	0.93	0.93	0.5 – 1.0
Initial Froude number (-)	2.0	2.0	2.0	1.0 – 3.0
Operational diffuser length (m)	300	300	250	60–625
Initial plume width (m)	0.16	0.16	0.16	n/a
Initial plume area (m^2)	50	50	42	10 – 100
Gas flow rate (Nm^3/hr)[a]	38	13	40	1 – 400
Initial gas flux (m/hr)[b]	0.76	0.26	0.96	0.02 – 9.5
Initial bubble radius (m)	5.7×10^{-4}	5.6×10^{-4}	5.7×10^{-4}	$10^{-4} – 10^{-1}$
Diffuser depth (m)[c]	60	60	59	n/a
Reservoir maximum depth (m)	64	65	64	n/a
Reservoir surface area (10^6 m^2)	0.53	0.53	0.53	n/a
Reservoir total volume (10^6 m^3)	12	12	12	n/a

[a]1 Nm^3 denotes 1 m^3 of gas at 1 bar and 0 °C.

[b]Sensitivity analysis range refers to varying gas flow rate while maintaining constant initial plume area.

[c]Depth at location of lateral CTD transect.

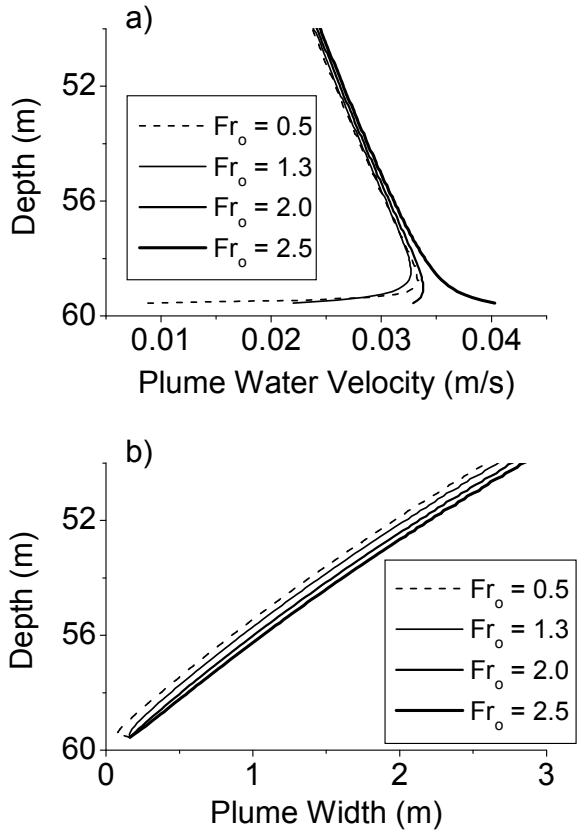

Figure 11. Effect of initial Froude number (Fr_o) on predictions of plume water velocity and plume width using linear bubble plume model.

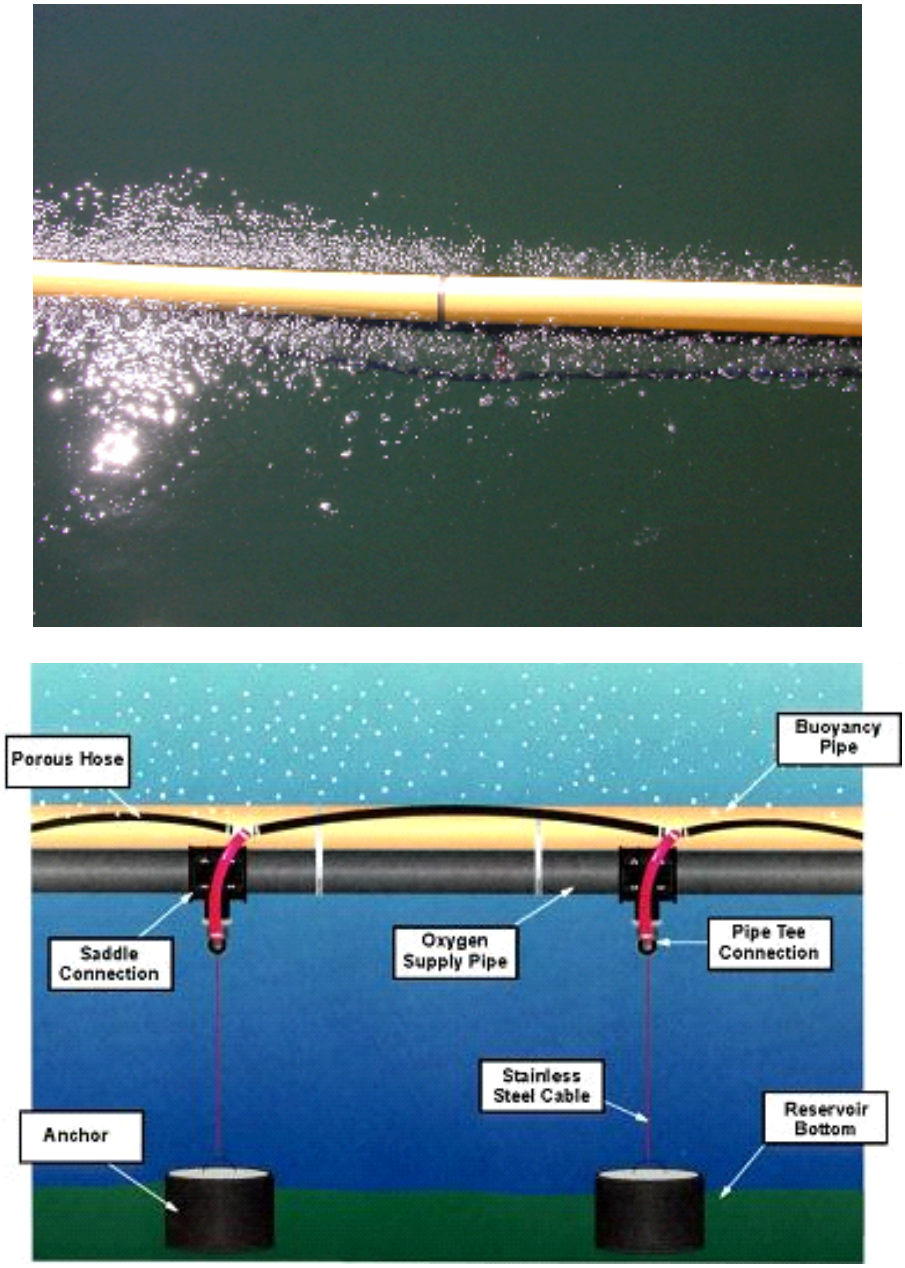

Figure 12. Photograph and schematic of linear bubble plume diffuser in Spring Hollow Reservoir, VA, U.S.A. (Courtesy of Mark Mobley, Mobley Engineering, Inc.).

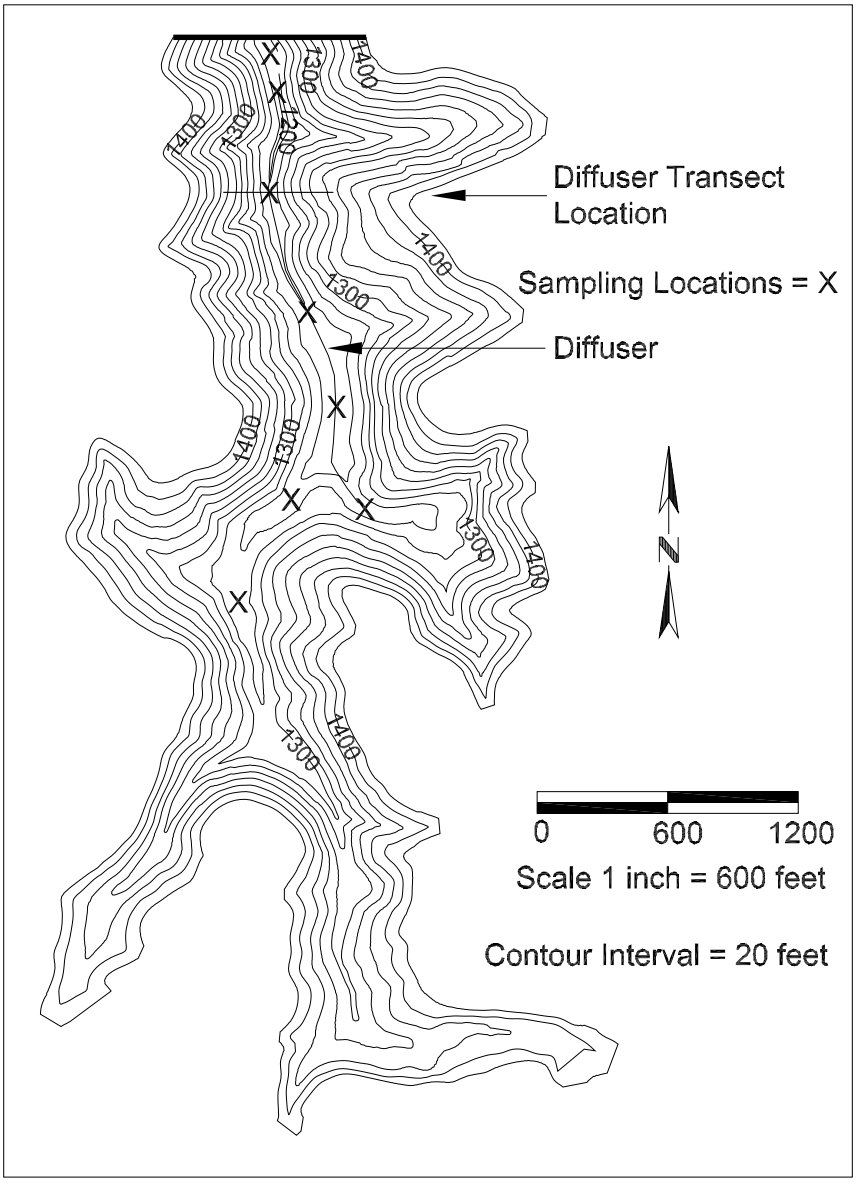

Figure 13. Bathymetric map of Spring Hollow Reservoir, VA, U.S.A. showing locations of linear bubble plume diffuser and lateral CTD transects.

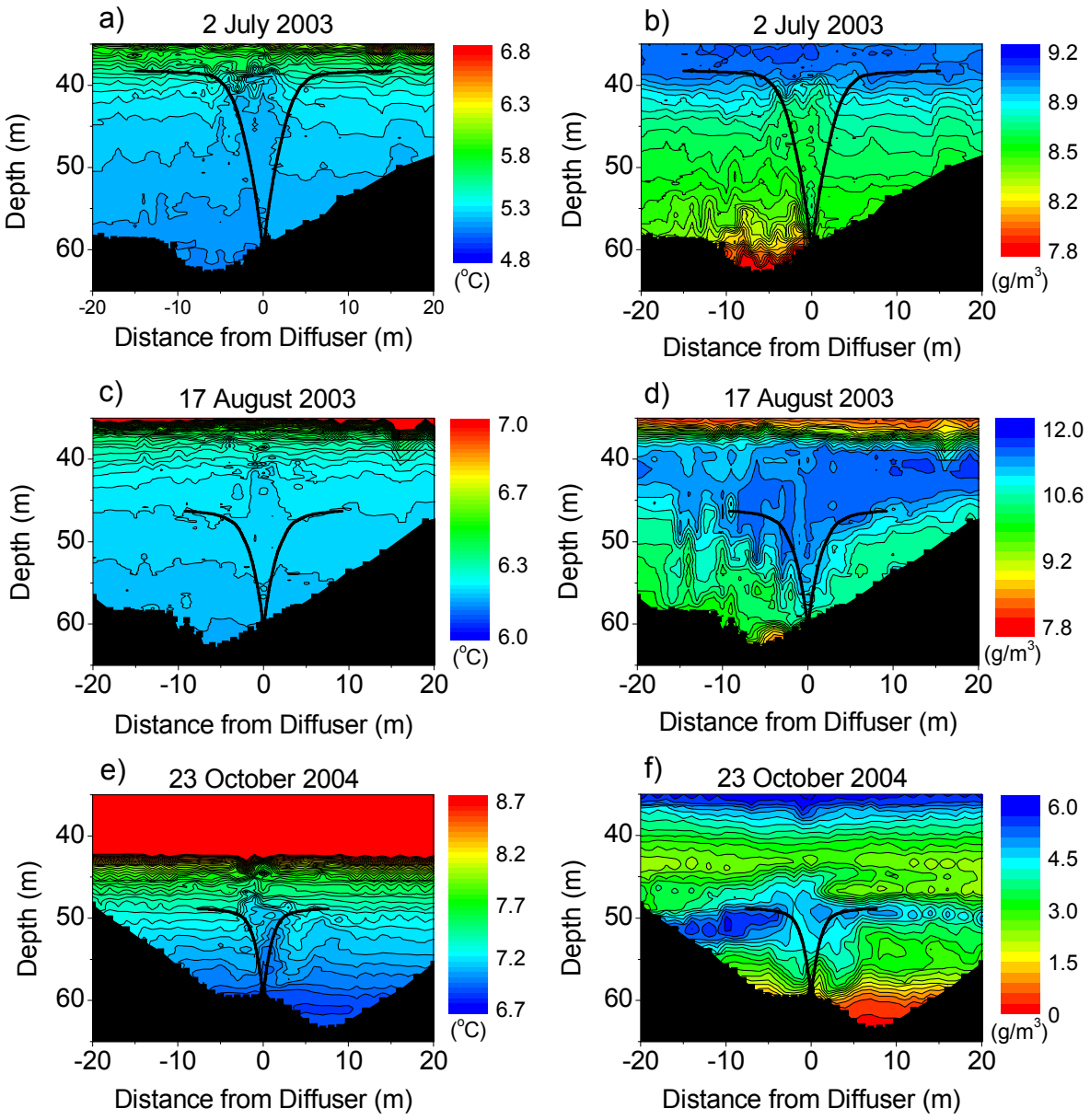

Figure 14. Measured plume temperature (°C) (left) and DO (g/m^3) (right) contours with linear bubble plume model predictions for diffuser operation with air (2 July 2003) and pure oxygen (17 August 2003 and 23 October 2004) in Spring Hollow Reservoir, VA, U.S.A. Contours were interpolated from CTD profiles collected at locations indicated by small black squares along the bottom of each plot.

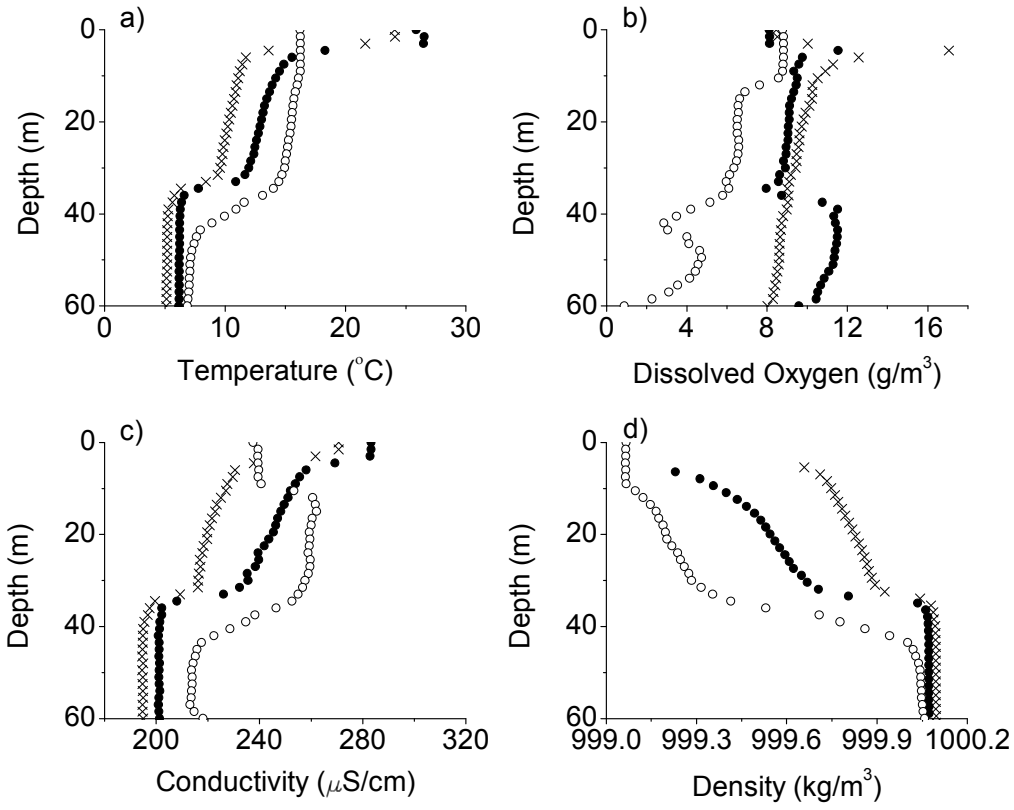

Figure 15. Input boundary conditions for linear bubble plume model evaluation and sensitivity analysis. Data collected from Spring Hollow Reservoir, VA, U.S.A. during diffuser operation with compressed air [2 July 2003 (×)] and pure oxygen [17 August 2003 (●) and 23 October 2004 (○)].

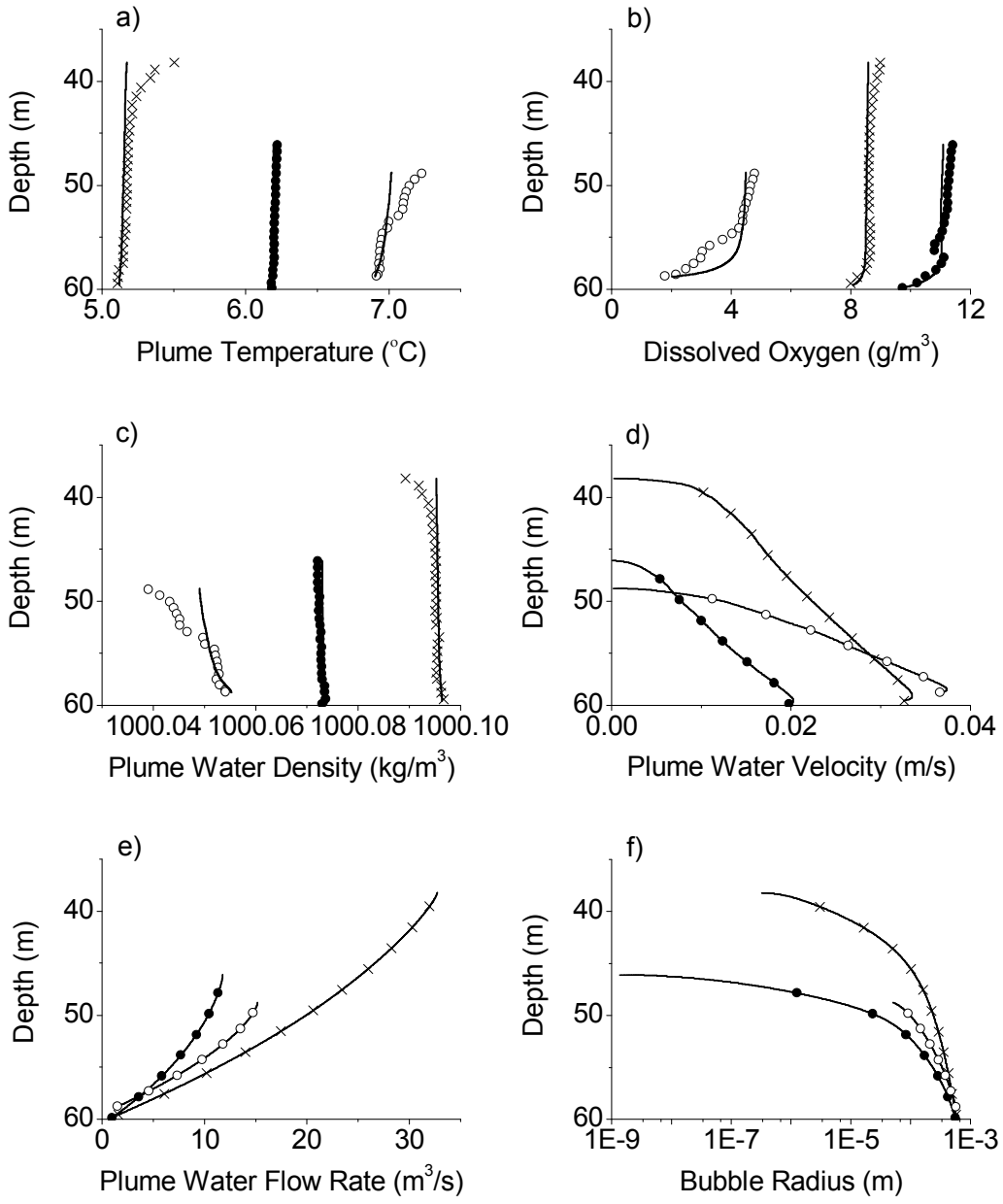

Figure 16. In-plume profiles predicted by linear bubble plume model, represented as solid lines (a–c) and as solid lines and symbols (d–f). Input data collected from Spring Hollow Reservoir, VA, U.S.A. during diffuser operation with compressed air [2 July 2003 (×)] and pure oxygen [17 August 2003 (●) and 23 October 2004 (○)]. Measured average in-plume temperature, DO, and plume water density represented as symbols (a–c).

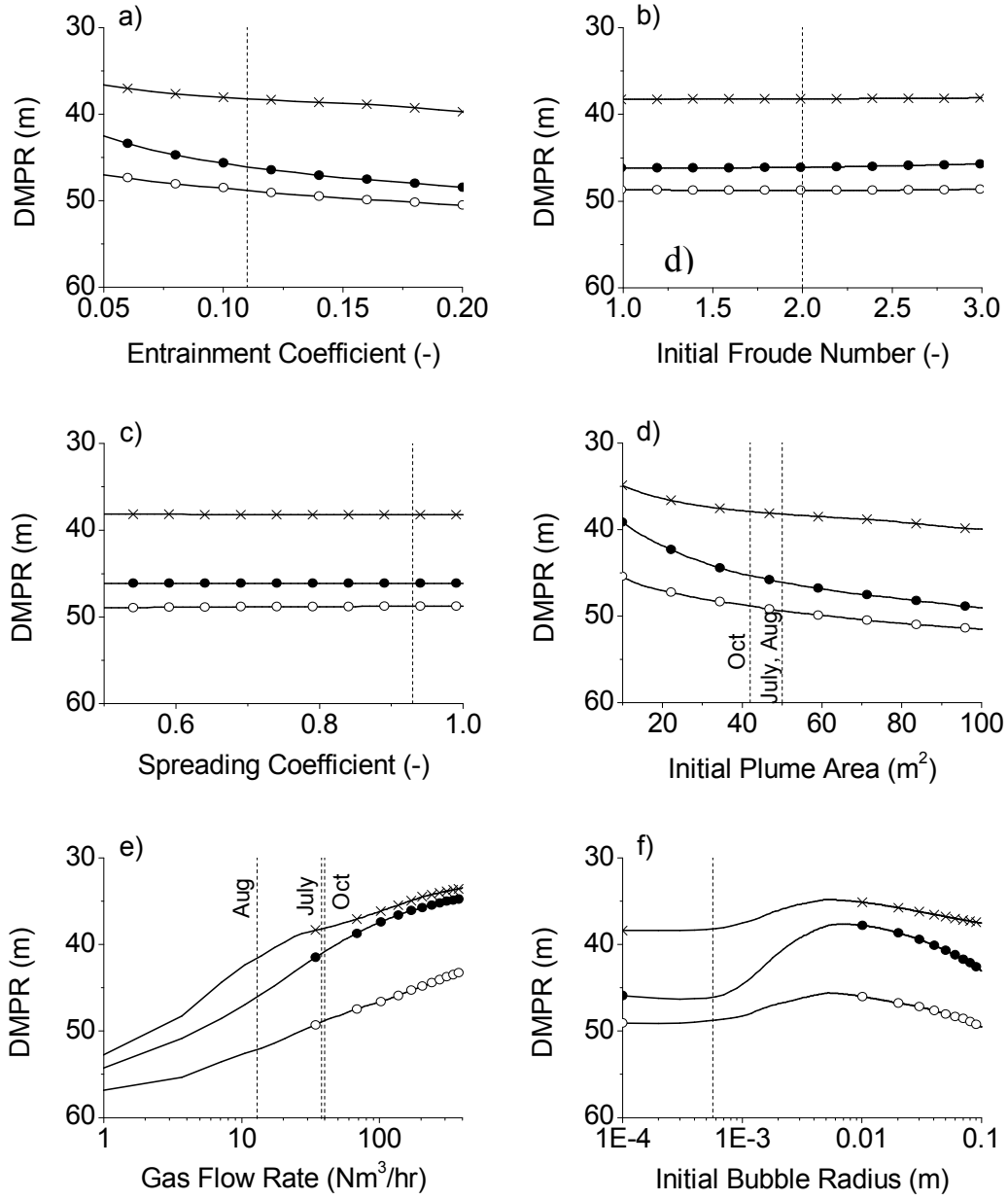

Figure 17. Effect of linear bubble plume model parameters on depth of maximum plume rise (DMPR). Standard values for each parameter are indicated by the vertical dashed lines. Input data collected from Spring Hollow Reservoir, VA, U.S.A. during diffuser operation with compressed air [2 July 2003 (×)] and pure oxygen [17 August 2003 (●) and 23 October 2004 (○)].

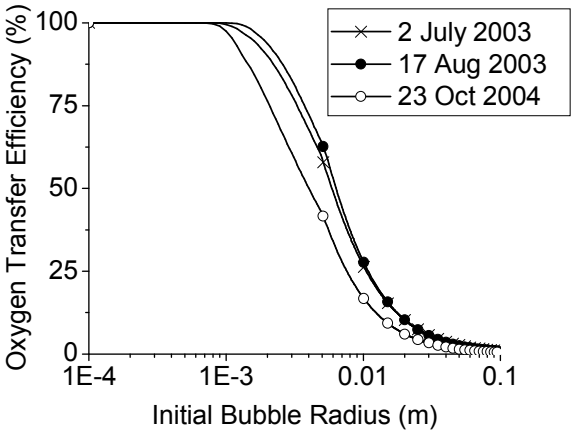

Figure 18. Effect of initial bubble radius on oxygen transfer efficiency predicted by linear bubble plume model. Input data collected from Spring Hollow Reservoir, VA, U.S.A. during diffuser operation with compressed air (2 July 2003) and pure oxygen (17 August 2003 and 23 October 2004).

CHAPTER 4. COUPLED BUBBLE PLUME/RESERVOIR MODELS FOR HYPOLIMNETIC OXYGENATION

V. L. Singleton[a], F. J. Rueda[b], D. F. McGinnis[c] and J. C. Little[a,d]

[a]*418 Durham Hall, Department of Civil and Environmental Engineering, Virginia Polytechnic Institute and State University, Blacksburg, VA 24061-0246, U.S.A. ([d]corresponding author)*

[b]*Instituto del Agua y Dpto. Ingeniería Civil, Universidad de Granada, C/Ramón y Cajal, 4 - 18071 Granada, Spain*

[c]*Surface Waters - Research and Management, Federal Institute for Environmental Science and Technology (Eawag), Kastanienbaum, CH-6047, Switzerland*

Target publication for manuscript: Water Resources Research

Abstract

A model for a linear bubble plume used for hypolimnetic oxygenation was coupled to two reservoir models [CE-QUAL-W2 (W2) and Si3D] to simulate their complex interaction. In simulations with a rectangular basin, predicted oxygen addition was directly proportional to the update frequency of the plume model. W2 calculated less oxygen input to the basin than Si3D and significantly less mixing within the hypolimnion. With a plume update period of 0.5 hr, the coupled models were then applied to a simplified test of a full-scale linear diffuser. Both the W2 and Si3D coupled models predicted bulk hypolimnetic DO concentrations well. Warming within the hypolimnion was overestimated by both models, but more so by W2. The coarser vertical resolution of the reservoir grid in W2 caused the plume rise height to be over-predicted, enhancing erosion of the thermocline.

Keywords

Hypolimnetic oxygenation; hypolimnetic aeration; model coupling; bubble plume; oxygen transfer; line diffuser; reservoir.

Introduction

Hypolimnetic anoxia, the depletion of dissolved oxygen (DO) in the bottom layers of lakes and reservoirs, can result in severe water quality degradation. Anoxia within lake sediments can increase the rate of soluble phosphorus release [*Bostrom et al.*, 1988], triggering the growth of nuisance algal blooms [*French and Petticrew*, 2007]. Oxygen depletion within the hypolimnion may also lead to increases in reduced species such as hydrogen sulfide and ammonia, and the release of soluble iron and manganese from the sediments. Hydrogen sulfide, iron, and manganese in raw water used for potable purposes typically requires additional treatment [*Cooke and Carlson*, 1989], and elevated ammonia concentrations can be toxic to aquatic organisms. The effects of low DO levels on fish have been studied for decades and include mass mortalities, ecological disruption, physiological stress, and modification of complex behaviors such as schooling, swimming, and reproduction [*Pollock and Dubé*, 2007]. Methylation of inorganic mercury by microorganisms to a soluble and more bioavailable form is enhanced under anoxic conditions [*Mailman et al.*, 2006]. Lastly, anoxic water has been shown to greatly increase the release of major greenhouse gasses such as methane and carbon dioxide from lake sediments [*Liikanen et al.*, 2002].

Bubble plumes are commonly used for hypolimnetic aeration and oxygenation, which adds oxygen to the deepest layer while preserving stratification [*Singleton and Little*, 2006]. The plume is in intimate contact with the ambient water and is strongly influenced by the local density profile. While bubble plumes are successful at adding oxygen, the added energy may induce large-scale hypolimnetic mixing. Plume-induced mixing alters the density structure of the reservoir, while the plume performance depends strongly on the density gradient, establishing a feedback loop that continually changes plume behavior [*McGinnis et al.*, 2004]. Mixing may partially erode the thermocline and subsequently lead to warming of the hypolimnion and even premature destratification of the reservoir. Higher hypolimnetic temperatures and plume-induced mixing may also be responsible for increased sediment oxygen uptake (SOU). A number of studies have reported that small increases in water velocity above lake sediments can significantly increase SOU [*Arega and Lee*, 2005; *Beutel*, 2003; *Hondzo*, 1998; *Josiam and Stefan*, 1999; *Lorke et al.*, 2003; *Mackenthun and Stefan*, 1998]. Because the sediment is the largest sink of oxygen in most reservoirs, the effect of plume-induced mixing must be included to avoid serious under-sizing of oxygenation systems. The specific plume-induced mixing

mechanisms should be identified and incorporated in a coupled bubble-plume/reservoir model for successful design and operation.

A number of models for predicting plume dynamics and/or oxygen transfer from bubble-plumes have been developed [*Singleton and Little*, 2006], but less research has focused on modeling the interaction between bubble-plumes and ambient water bodies. Most of the coupled bubble-plume/reservoir models proposed in the literature involve whole-lake artificial circulation or destratification systems and, consequently, do not account for oxygen transfer from the bubbles [*Johnson et al.*, 2000; *Schladow*, 1993; *Zic and Stefan*, 1994]. Similar to *Schladow* [1993], *Lindenschmidt and Hamblin* [1997] coupled the one-dimensional hydrodynamic model DYRESM with stirrer and bubbler modules to simulate mixing induced by Limnox hypolimnetic aerators, an enclosed type of aeration device. To analyze the effectiveness of bubble-plume destratification on reducing algal blooms, *Imteaz and Asaeda* [2000] coupled DYRESM with a bubble plume model and an ecological model that tracks factors related to phytoplankton growth. *Bravo et al.* [2007] used a comprehensive and commercially available hydrodynamic model, FLUENT, and constructed a two-fluid, dispersed turbulence model to simulate bubble plume dynamics. However, none of these coupled models included mass transfer between the bubbles and water, which is critical to predicting the performance of hypolimnetic oxygenation systems.

To address this shortcoming, this work presents the coupling of a linear bubble plume model that includes gas transfer with two different reservoir models, CE-QUAL-W2 (W2) Version 3.2 and Si3D. The coupled models are used to predict plume dynamics, induced mixing, and oxygen addition from a linear diffuser used for hypolimnetic oxygenation. W2 is a two-dimensional (2D), laterally averaged hydrodynamic and water quality model, and Si3D is a three-dimensional (3D) hydrodynamic model. In this paper, the components of the coupled models and the coupling procedures are described, results from simulations using a rectangular basin are discussed, and field data from a full-scale system are compared to model predictions.

Description of Coupled Models

The primary components of each coupled model are the bubble plume model and a reservoir model, either W2 or Si3D. Generally, the coupling procedure was as follows. Using measured temperature and DO profiles as initial boundary conditions, plume model simulations were performed to estimate the flow rate of ambient water entrained as the plume rises, and the

plume flow rate, temperature, and gas concentrations of the water that is detrained upon reaching the depth of maximum plume rise. Each reservoir model was then used to simulate reservoir response over a short time step, and the predicted ambient temperature and DO profiles obtained at the end of the simulation were then used as the new input to the plume model to generate the next set of predicted plume entrainment and detrainment flows.

Linear Bubble Plume Model

The linear bubble plume model was recently validated by *Singleton et al.* [2007] using full-scale diffuser data collected from Spring Hollow Reservoir (SHR), Virginia, U.S.A (refer to Chapter 3 of this dissertation). The model utilizes the discrete-bubble approach, which has been successfully applied to other hypolimnetic oxygenation devices and was reviewed in detail by *Singleton and Little* [2006]. The linear bubble plume model is derived from the circular model of *Wüest et al*. [1992] and is composed of horizontally-integrated equations based on the conservation of mass, momentum, and heat. Eight flux equations are solved simultaneously to predict water flow rate, temperature, oxygen and nitrogen transfer and concentration, salinity, and rise height, given diffuser geometry and depth, applied gas flow rate, and initial bubble size [*Singleton et al.*, 2007]. The model accounts for vertical density gradients due to temperature and salinity. Entrainment is assumed to be proportional to the local (with respect to depth) plume water velocity. Bubble size varies as the bubbles rise due to expansion and dissolution, and bubble slip velocity and gas transfer coefficients are functions of bubble radius [*Wüest et al.*, 1992]. Henry's constants for oxygen and nitrogen are functions of temperature [*Wüest et al.*, 1992]. The bubble plume model equations were originally developed by *Wüest et al.* [1992] for circular geometry, but were modified by *McGinnis et al.* [2001] for the linear geometry of the system installed in SHR. *Singleton et al.* [2007] improved the linear bubble plume model by use of a correlation to calculate initial bubble size [*McGinnis and Little*, 2002], correction of the entrainment coefficient (α) and spreading coefficient (λ) for top-hat profiles [*Fanneløp and Sjøen*, 1980], and use of a Froude number (*Fr*) to calculate initial water velocity [*Fischer et al.*, 1979; *Wüest et al.*, 1992]. Except as noted previously, initial conditions for the bubble plume model were determined as detailed by *Wüest et al.* [1992]. The α and λ were set at 0.11 and 0.93, respectively [*Fanneløp et al.*, 1991]. The initial *Fr* for the linear bubble plume was taken as 2.0 [*Singleton et al.*, 2007]. The model calculations are only valid over the plume rise height, up to

the depth of maximum plume rise. When the plume stops rising, a secondary plume may form above as bubbles that are not completely dissolved continue to rise [*Asaeda and Imberger*, 1993; *McDougall*, 1978; *Schladow*, 1992].

Reservoir Models

CE-QUAL-W2 (W2)

W2 is a laterally-averaged, two-dimensional hydrodynamic and water quality model that was developed by the U.S. Army Corps of Engineers [*Cole and Wells*, 2003]. Because the model assumes lateral homogeneity, it is most applicable to relatively long and narrow water bodies with longitudinal and vertical gradients. W2 models basic eutrophication processes such as temperature, nutrients, algae, dissolved oxygen, organic matter, and sediment relationships. W2 includes horizontal, but not vertical momentum, and accounts for momentum transfer from inflowing branches. A principal aspect of the model is the ability to calculate the two-dimensional velocity field in stratified reservoirs. The ability to simulate transport accurately can be as critical as kinetics in properly estimating water quality [*Wells*, 2000] and is especially important for predicting the distribution of oxygen added by the bubble-plume. Input data required for application of W2 are geometric data (bathymetry), initial and boundary conditions, hydraulic and kinetic parameters, and calibration data. Initial conditions include starting temperature and constituent profiles, and boundary conditions include inflows, outflows, and meteorological data. For this work, default hydrodynamic and water quality coefficients were used in W2 [*Cole and Wells*, 2003], except where noted. Lastly, the W2N (W2 with Nickuradse mixing length) formulation was selected for the vertical turbulence closure algorithm, and the vertical eddy viscosity was calculated implicitly.

Si3D

Si3D is a three-dimensional free surface hydrodynamic model, which has been extensively validated against analytical solutions and field observations [*Rueda and Schladow*, 2002a; *Rueda and Schladow*, 2003; *Rueda et al.*, 2003; *Rueda and Cowen*, 2005]. The model is based on the continuity equation for incompressible fluids, the Reynolds-averaged form of the Navier-Stokes equations for momentum, and the transport equation for temperature. Turbulent mixing in the vertical is represented in the 3D model following the level 2.5 Mellor-Yamada

hierarchy of turbulence closure models [*Kantha and Clayson*, 1994]. Horizontal mixing of momentum and scalars is parameterized using a constant mixing coefficient. Further details of the algorithms used in the model are presented by *Smith* [1997], *Rueda* [2001], and *Rueda and Schladow* [2002b]. Lastly, to make Si3D more comparable to W2, surface boundary conditions (meteorology) and open boundary condition flows were incorporated into the hydrodynamic model for this work.

Coupling Bubble Plume and Reservoir Models

W2

To couple the bubble-plume model with W2, the diffuser is represented as individual segments that span consecutive columns in the discretized bathymetry. This facilitates varying the depth of the diffuser along its length, such as for a sloping reservoir bottom (Figure 19). The plume model is used to compute the flow rate of ambient water entrained as the plume rises, and the flow rate, temperature, DO concentration, and discharge depth of the water detrained at the top of the plume. Entrainment removes water of known temperature and oxygen concentration from a range of depths, while detrainment returns the total volume of entrained water at the specified discharge depth after adding the predicted mass of oxygen. In W2, plume entrainment is represented as individual lateral withdrawals from each cell in the entrainment zone above each diffuser segment. The flow rate of each lateral withdrawal varies up the plume based on the predicted entrainment for the corresponding plume slice (delta Q/ delta z). Plume rise height fluctuated slightly during the course of the coupled model runs, but generally increased as plume operation continually eroded the thermocline. Detrainment for each diffuser segment is represented as tributary inflows in W2, with discharge depth, temperature, and DO as predicted by the plume model. Detrainment is returned to the basin within a single layer, which means that the initial plume detrainment thickness is equivalent to the height of this layer in the model grid.

The bubble plume model/W2 manual coupling procedure was completed as follows. Using the initial reservoir conditions prior to diffuser startup, the plume model was run for each diffuser segment, accounting for varying diffuser elevations if applicable. Using the predicted plume data for each diffuser segment, the coupled plume/W2 model was then run for a selected plume-update time period (which remained constant during the run). The predicted ambient temperature and DO profiles obtained at the end of this iteration were then used as input

boundary conditions for the plume model to generate the next set of predicted plume entrainment and detrainment data for each diffuser segment. The entire procedure was repeated in increments of the selected plume update period until the end of diffuser operation. Currently, the exchange of information between the bubble plume model and W2 is preformed manually, although many steps of the procedure have been automated within the plume model code.

Si3D

To incorporate the bubble plume model into Si3D, the governing equations were modified to incorporate source-sink terms. The equations were adapted from *Lynch* [1986] and are given by:

$$\frac{\partial \zeta}{\partial t} + \frac{\partial}{\partial x}\left[\int_{-H}^{\zeta} u dz\right] + \frac{\partial}{\partial y}\left[\int_{-H}^{\zeta} v dz\right] = 0 \tag{1}$$

$$\frac{\partial u}{\partial t} + u\frac{\partial u}{\partial x} + v\frac{\partial u}{\partial y} + w\frac{\partial u}{\partial z} - fv = -\left(g\frac{\partial \zeta}{\partial x} + g\frac{1}{\rho_0}\int_{z}^{\zeta}\frac{\partial \rho}{\partial x}dz'\right) + \frac{\partial}{\partial x}\left(A_h\frac{\partial u}{\partial x}\right) + \frac{\partial}{\partial y}\left(A_h\frac{\partial u}{\partial y}\right) + \frac{\partial}{\partial z}\left(A_v\frac{\partial u}{\partial z}\right) + S(u - u_0) \tag{2}$$

$$\frac{\partial v}{\partial t} + u\frac{\partial v}{\partial x} + v\frac{\partial v}{\partial y} + w\frac{\partial v}{\partial z} + fu = -\left(g\frac{\partial \zeta}{\partial y} + g\frac{1}{\rho_0}\int_{z}^{\zeta}\frac{\partial \rho}{\partial y}dz'\right) + \frac{\partial}{\partial x}\left(A_h\frac{\partial v}{\partial x}\right) + \frac{\partial}{\partial y}\left(A_h\frac{\partial v}{\partial y}\right) + \frac{\partial}{\partial z}\left(A_v\frac{\partial v}{\partial z}\right) + S(v - v_0) \tag{3}$$

$$\frac{\partial \theta}{\partial t} + u\frac{\partial \theta}{\partial x} + v\frac{\partial \theta}{\partial y} + w\frac{\partial \theta}{\partial z} = D_h\frac{\partial^2 \theta}{\partial x^2} + D_h\frac{\partial^2 \theta}{\partial y^2} + \frac{\partial}{\partial z}\left(D_v\frac{\partial \theta}{\partial z}\right) + \frac{H}{\rho c_p} + \frac{S}{\rho_0}\theta_0 \tag{4}$$

$$\frac{\partial O}{\partial t} + u\frac{\partial O}{\partial x} + v\frac{\partial O}{\partial y} + w\frac{\partial O}{\partial z} = D_h\frac{\partial^2 O}{\partial x^2} + D_h\frac{\partial^2 O}{\partial y^2} + \frac{\partial}{\partial z}\left(D_v\frac{\partial O}{\partial z}\right) + \frac{S}{\rho_0}O_0 \tag{5}$$

$$\frac{\partial u}{\partial x} + \frac{\partial v}{\partial y} + \frac{\partial w}{\partial z} = \frac{S}{\rho_0} \tag{6}$$

The ratio S/ρ, for a given computational source cell of nominal volume V = (Δx x Δy x Δz), represents the volume of water added per unit time, divided by the volume of the cell. Note that no source terms are included in the depth-integrated form of the continuity equation (Equation 1). This approximation is valid for plumes, since all water entrained into the rising

plume appears again in the detrainment cell at the top of the plume. Hence, water is only relocated in the water column.

The coupling is performed on a water column by water column basis for each diffuser segment (Figure 20). Si3D provides boundary conditions (temperature and DO profiles) to the bubble plume model. Using those boundary conditions, the bubble plume model predicts the detrainment volumetric flow rate Q_d, depth, temperature, and DO concentration. From those predictions, the detrainment cell (DC) is selected. For the DC, the source strength term S/ρ is positive and defined as Q_d/V. All other cells below the DC are considered entrainment (sink) cells (ECs). For the ECs, the source strength terms S/ρ are negative and vary up the plume, as predicted by the bubble plume model. The frequency with which information is exchanged between the linear bubble plume model and Si3D is selected at the start of the simulations, and the plume parameters are updated automatically at this frequency as the coupled model runs.

Application of Coupled Models

Rectangular Basin

The performance of the coupled models was initially tested in a narrow and elongated basin with a flat bottom and vertical sides. Using this rectangular basin, a number of model runs were conducted to evaluate the major parameters affecting oxygen addition from the diffuser. The rectangular basin simulations also facilitated comparison of basic hydrodynamic differences between the two coupled models, including two-dimensional versus three-dimensional representation. The length, width, and depth of the basin were 360, 50 and 52 m, respectively. The basin length and depth were selected to correspond to the diffuser length and reservoir maximum depth of a full-scale installation (refer to next section). The basin was assumed to be horizontally homogeneous with respect to temperature and DO at the start of the simulations. The initial temperature and DO profiles were assumed to be equivalent to data collected on September 28, 1998, in SHR. The lake surface was initially horizontal, and the water was at rest. Lake circulation and mixing was forced only through operation of the diffuser, which was located along the longitudinal axis of the basin. Two different diffuser lengths, 60 and 360 m, were used and supplied with the same air flow rate (Table 12) to examine the effect of varying initial buoyancy fluxes on plume dynamics. The gas flow rate and composition were the same as

those used during diffuser testing in SHR in 1998. The length of the simulations was set at seven days. For W2, the horizontal dispersion coefficients for momentum and constituents, Ax and Dx, were both 1.0 m^2/s. For Si3D, the horizontal dispersion coefficients for momentum and constituents, A_h and D_h, were 0.5 m^2/s and of the same order of magnitude as reference values proposed by *Madsen et al.* [1988].

To focus on the effects of the bubble plume, surface boundary conditions (meteorology), inflows and outflows, and SOD were excluded from the simulations. Therefore, all temperature changes within the hypolimnion were due to plume-induced mixing. In W2, all of the water quality constituent calculations were turned off except DO. The only source of DO was the bubble plume, and there were no sinks for DO.

Results and Discussion

Because the bubble-plume/Si3D coupled model is fully automated, it was primarily used instead of the bubble-plume/W2 coupled model to test the effect of various parameters on oxygen addition to the rectangular basin. Based on previous work with the W2 coupled model by *McGinnis et al* [2001], a plume update period of six hours was initially used. In other words, the plume model was run and the output parameters of detrainment depth, flow rate, temperature, and DO concentration and height-varying entrainment flow rate were updated for every six hours of simulation time in the reservoir models. This assumes that the plume near-field was in a quasi-steady state condition and did not vary significantly during each six-hour period. Both the W2 and Si3D coupled models were run with a six-hour plume update period for each diffuser length, and the mass of DO added to the entire basin over the course of each seven-day diffuser operating period was calculated. However, DO addition was consistently under-predicted for both coupled models (Table 13), assuming 100 percent oxygen transfer efficiency from the bubble plume. (Note: the oxygen transfer efficiency predicted by the bubble plume model was essentially 100 percent for each plume update period.) Because of these discrepancies and in an attempt to increase predicted oxygen addition, the Si3D coupled model was run using plume update periods that varied from three hours down to five minutes (Table 13). The DO input predicted by the plume/Si3D model was directly proportional to the plume update period for both diffuser lengths, and was more sensitive to the plume model update frequency for the longer 360 m diffuser. This can be explained by differences in the gas flux between the two diffuser

lengths. Both diffuser lengths were modelled with the same gas flow rate (Table 13), but the initial gas flux for the 60 m diffuser was greater because the initial plume area was smaller. The lower gas flux for the 360 m diffuser added less DO to the plume per unit length, which resulted in a lower final DO concentration increase in the detrainment. The predicted DO concentration within the plume is a function of two variables: mass transfer from the bubbles and entrainment of ambient water into the plume. Because the DO change from gas transfer from the bubbles is more modest for the 60 m diffuser due to the lower gas flux, the final DO of the detrainment is influenced to a greater extent by the ambient DO concentration. This suggests that using the correct near-field boundary conditions may be more critical when predicting oxygen transfer at relatively low gas flow rates and/or when compressed air is used.

To determine if the same trends held true for the coupled bubble-plume/W2 model, runs were performed with a plume update period of one hour for each diffuser length (Table 13). Again, the predicted oxygen addition increased closer to the theoretical value as compared to the runs with a six-hour plume update interval, and the results using the longer diffuser length deviated more from the expected DO mass input. Most of the predicted oxygen input values for the W2 coupled model deviated more from the theoretical value than did the corresponding Si3D results. This is likely due to the lateral-averaging feature in W2, which essentially dilutes the DO added by the plume throughout the entire width of the basin within the detrainment cell. This results in a decreased ambient DO concentration that is entrained into the plume compared to Si3D, in which a DO gradient can exist across the basin. The 3D capability of Si3D allows the plume near-field perpendicular to the linear diffuser to have higher localized DO, and it is from this near-field that the plume boundary conditions are obtained. The oxygen mass balance results from the rectangular basin indicate that a shorter plume update period may be required in the W2 coupled model to achieve the similar oxygen addition predictions as Si3D.

For both coupled models, the plume update frequency directly affects the predicted oxygen addition to the rectangular basin (Table 13). As stated previously, the DO concentration of the plume detrainment is a function of the oxygen transferred from the bubbles and the DO in the water entrained from the plume near-field. *McGinnis et al.* [2004] found that plume model predictions were strongly dependent on near-field boundary conditions. When a given plume update period is selected, it is assumed that the plume is operating in quasi-steady state during that time and that the plume near-field, and associated entrainment variables, do not change

appreciably. When the plume entrainment conditions are not updated frequently enough to capture the DO increase in the plume near-field, the resulting DO concentration in the detrainment is under-estimated and oxygen addition to the basin is underpredicted. Theoretically, the plume near-field changes continuously as the diffuser operates until the entire reservoir is well-mixed and saturated with DO. Although it may be more appropriate to update the plume model boundary conditions after every time step of the reservoir models, it would be very computationally intensive. Additionally, updating the plume model output at such a high frequency would be extremely inefficient for the manual coupling of the bubble-plume/W2 model. Updating the plume model output at a higher frequency can also result in over-estimation of the oxygen addition to the basin (Table 12). This could occur if relatively high DO water from plume detrainment accumulates in the plume near-field and is not dispersed away from the plume quickly enough. In this case, the horizontal dispersion coefficient(s) may need to be adjusted.

The predicted temperature and DO profiles at the center of the rectangular basin for each diffuser length are shown in Figures 21 and 22 for the W2 and Si3D coupled models, respectively. The predicted hypolimnetic warming is greater for the shorter 60 m diffuser because the initial buoyancy flux is greater, resulting in a higher plume rise height. The predicted DO profiles at the end of the operating period on Day 7 reflect the relative oxygen mass additions (Table 13), showing that the case with the 360 m diffuser in W2 was the most underpredicted. The predicted degree of plume-induced mixing, and subsequent warming of the hypolimnion, was greater for the bubble-plume/Si3D coupled model runs, especially for the 60 m diffuser. This can also be attributed to the fact that W2 is laterally-averaged. In W2, the plume detrainment is added into a single cell with a width equal to the basin width, which immediately distributes the momentum across the entire basin. This results in a lower plume-induced velocity for a given diffuser length.

Horizontal and vertical velocity contours predicted by the W2 coupled model are shown in Figure 23, and 2D sectional and planar velocity vector plots of the Si3D predictions are shown in Figures 24 and 25, respectively. Both the W2 and Si3D results indicate that two circulation cells are created in the longitudinal direction on either side of the 60 m diffuser (Figure 23, top left and Figure 24, top). In addition to recirculation of plume detrainment into the hypolimnion below, both model simulations also indicate that a small portion of the detrainment is

recirculated up towards the thermocline after it is deflected by the basin end walls. The Si3D results for the shorter diffuser also show circulation in the lateral direction perpendicular to the diffuser at the approximate detrainment depth (Figure 25, top left). The 2D horizontal velocity induced by plume entrainment for the 60 m diffuser is evident in the vectors from a plane towards the bottom of the plume (Figure 25, bottom left). At 45 m depth, which was 7 m above the diffuser depth, Si3D predicts relatively strong longitudinal and lateral entrainment velocity into the plume. At this lower depth, the plume length and width are shorter than at the higher detrainment depth (Figure 25, top right), which causes the induced velocity field to be more compact (Figure 25, bottom right). Vertical velocity as predicted by W2 for the 60 m diffuser is also presented in Figure 23 (bottom right). For the lower portion of the plume entrainment zone, the calculated velocity is positive or downwards, and the vertical velocity component is upwards for the upper region of the plume. A clear demarcation and region of zero vertical velocity was predicted between the downward and upward velocity zones. This effect is not apparent in the Si3D coupled model velocity vectors (Figure 24, top). The velocity contours and vectors estimated by the W2 and Si3D coupled models for the 360 m diffuser differ significantly from results using the 60 m diffuser. For W2, the predicted horizontal and vertical velocity is much lower for the 360 m diffuser (Figure 23, right). The longer diffuser had a lower buoyancy flux because the same gas flow rate was used, and this resulted in a slower induced plume velocity. For Si3D, the lateral velocity field induced by plume entrainment (Figure 25, bottom right) was weaker than that estimated for detrainment (Figure 25, top right). A similar trend was obtained for the shorter 60 m diffuser (Figure 25, left). These results suggest that the velocity induced by the plume is greater towards the bottom of the hypolimnion, which may cause the localized velocity directly above the sediments to be greater and subsequently lead to increased SOU. Both the W2 and Si3D coupled model simulations produced relatively uniform velocity fields along the longitudinal axis of the basin for the 360m diffuser (Figures 23, right and Figure 24, bottom). The Si3D predictions also indicate a uniform horizontal velocity field laterally across the basin at the detrainment depth as well as within the plume rise height (Figure 25, top right and bottom right, respectively). The distribution of DO within the basin is indicative of velocity and recirculation patterns because it serves as a tracer. Similar to velocity, DO contours predicted by W2 and Si3D were homogeneous longitudinally for the 360 m diffuser, which spanned the entire length of the basin (not shown). Both models also predicted a stronger DO

gradient in the longitudinal and vertical directions for the 60 m diffuser, and these gradients corresponded to predicted flow patterns in the hypolimnion (not shown).

Spring Hollow Reservoir, Virginia, U.S.A.

Using insights gained through simulations with the coupled bubble-plume/reservoir models on the rectangular basin, the models were then applied to a full-scale linear diffuser. The diffuser is installed in a small, controlled reservoir where all major inflows and outflows are measured, which makes it ideal for research. Data collected during a relatively simple and well-defined diffuser test were used to evaluate the coupled models. Based on results from the rectangular basin, a plume update period of 0.5 hours was used. This frequency produced acceptable oxygen mass balance results with the Si3D coupled model (Table 13) and could also be accommodated in the manual coupling procedure for W2.

Field Data Collection

Testing was conducted using a full-scale linear diffuser installed in Spring Hollow Reservoir, VA, U.S.A. (Figure 26). Constructed in 1995, SHR is a small side-stream reservoir that is supplied by water pumped up from the Roanoke River. The reservoir is managed by the Western Virginia Water Authority and serves as one of the principle drinking water sources for Roanoke County. The water body has a maximum depth of 65 m and a maximum surface elevation of 431 m. The approximate surface area and volume are 0.54 km^2 and 12.4 × 106 m^3, respectively. To prevent anoxia in the hypolimnion and the associated deterioration of raw water quality, a linear diffuser equipped with fine-bubble porous hoses was installed in 1997 (Figure 26). The diffuser can be supplied with compressed air or pure oxygen at various gas flow rates and is located in the deepest portion of the reservoir (367–375 m elevation). Diffuser testing using compressed air was conducted from 28 September–13 October 1998, and data collected during that test were used to evaluate the coupled models (Table 12). Based on an average surface elevation of 420 m, the depth of the diffuser during testing ranged from 45 to 53 m along its length. The 1998 data set was selected because no water was pumped from the river into the reservoir during diffuser operation, thereby simplifying reservoir hydrodynamics. The primary hydraulic forcing in the hypolimnion during testing was the linear bubble plume. Temperature and DO profiles were obtained adjacent to the dam, approximately 155 m downstream of the end of the diffuser (Figure 27). Profiles were measured immediately before the diffuser was started

on September 28 and for four additional days during diffuser operation. Profiles were also collected on two dates after the diffuser was turned off on October 13, and the differences between the October 21 and October 28 profiles show the effect of the baseline oxygen demand within the hypolimnion and sediments (Figure 27, right).

Results and Discussion

For application of the bubble-plume/W2 and bubble-plume/Si3D coupled models to SHR, surface boundary conditions and reservoir outflow to the treatment plant were included in the model runs. The plant outflow was the largest measured flow rate from the reservoir. Because it was relatively easy to do with the existing code, seepage through the dam and precipitation were also included in the simulation with the W2 coupled model. In W2, all of the water quality constituent calculations were turned off except DO. Sediment oxygen demand (SOD) was included in the simulations, and an assumed rate of 0.5 $g/m^2/d$ was used because of the lack of measured data for this parameter in SHR. Rates of SOD used in water quality models and reported in the literature range from 0.06 to 2 $g/m^2/d$ [*Chapra*, 1997; *Cole and Wells*, 2003]. Within W2, the main basin of SHR was represented as a single branch, and the three sub-basins were represented as additional branches (Figure 26). The main basin was divided into 18 segments which varied in length from 67 to 95 m (Figure 19). The diffuser for the 1998 test was modeled as five discrete segments in consecutive columns in W2 because its depth varied along the length (Figure 19). The number of lateral withdrawals (plume entrainment cells) per segment ranged from nine to sixteen, depending on diffuser depth and plume rise height. Within Si3D, the bathymetry of SHR was characterized using 15 × 15 × 1 m cells (Figure 28). Similar to the W2 coupled model, the diffuser was represented as twenty-four discrete segments in consecutive cells, which allowed the elevation of each segment to vary along the reservoir bottom.

The evolution of temperature and DO within the hypolimnion as predicted by the coupled bubble-plume/W2 and bubble-plume/Si3D models is shown in Figures 29 and 30, respectively. The W2 coupled model generally over-predicted plume mixing and subsequent hypolimnetic warming, and the effect became more pronounced as the diffuser test progressed (Figure 29, left). DO was under-predicted throughout the run with the W2 coupled model, but the final predicted DO concentration is only slightly less than measured on October 9 (Figure 29, right). Temperature and DO gradients directly above the sediments are reproduced by the coupled

model similar to measured profiles, although further evidence of over-estimated mixing is shown by predicted bottom temperatures and DO concentrations being greater than observed. Possible reasons for this include inaccuracies in the horizontal dispersion coefficient and over-estimation of the induced plume water flow rate. The measured temperature and concentration gradients near the sediment surface were due to the fact that the profiles were collected in the deepest location in the reservoir, which was lower in elevation than the downstream end of the diffuser (Figure 19). The data indicates that, during eleven days of diffuser operation, the bubble plume induced minimal mixing vertically below the diffuser depth, compared to laterally and vertically above the diffuser. The lack of mixing below the diffuser resulted in the added DO not being distributed to the sediment surface, which can negatively affect the performance of an oxygenation system. Increasing the DO concentration in the bulk water facilitates diffusion of oxygen into the sediments, which can suppress the release of reduced compounds into the water column.

The change in the hypolimnetic temperature and DO predicted by the coupled plume/Si3D model was fairly similar to that obtained using the W2 coupled model (Figure 30). Plume-induced mixing and the resulting hypolimnetic temperature increase were over-predicted throughout the diffuser test, with the deviation increasing as the test progressed. However, the predicted temperature profiles from the Si3D coupled model more closely resembled observations, particularly on October 9. The Si3D coupled model did not estimate as much plume-induced mixing as the W2 coupled model. This is evident in the steeper temperature gradient above the sediments for the Si3D results and also in the lower bulk water temperature in the hypolimnion (Figure 30, left). The temperature gradient observed at the top of the hypolimnion during the course of the diffuser test (Figure 27) was also better simulated by Si3D. The Si3D coupled model characterized the DO increase in the hypolimnion quite precisely and predicted the DO decrease towards the reservoir bottom much more accurately than W2 (Figure 30, right). The 3D coupled model also captured the maintenance of relatively low DO at the bottom of the thermocline and above the direct influence of the diffuser. Additionally, the lower extent of mixing predicted by Si3D is supported by the stronger DO gradient above the sediments. Overall, the bubble-plume/Si3D coupled model predictions more closely represented the 1998 SHR diffuser data.

The 2D coupled model calculated a higher degree of plume-induced mixing than the 3D version. A possible explanation for this is the difference in vertical resolution between reservoir grids used in the two models (Table 12). Layer heights in the W2 coupled model were all the same and equal to 1.52 m, while the cell thickness used in the Si3D coupled model was 1.0 m. The greater resolution of the 3D grid in the vertical dimension more accurately characterized temperature gradients in water column, particularly at the interface between the hypolimnion and metalimnion. Measured profiles indicate that the temperature gradient at the top of the hypolimnion at the start of testing was relatively strong, and that the lower depth of the thermocline did not change appreciably during diffuser operation (Figure 27). This effect was better simulated by the Si3D coupled model (Figure 30, left). The lower vertical resolution of the W2 grid averaged water column temperature gradients, which allowed the plume to rise higher into the thermocline. This increased plume rise height eroded the thermocline to a greater extent, which resulted in higher predicted hypolimnetic temperatures in the W2 coupled model (Figure 29).

Distribution of the DO added by a hypolimnetic oxygenation system is of great interest to reservoir managers and design engineers. In some cases, mangers and operators will want the oxygenated water to be distributed as much as possible in order to satisfy an areal oxygen demand such as SOD. In other situations, it is desirable to maintain a localized volume of oxygenated water, such as near a deep dam outlet to ensure that releases meet minimum DO standards or for maintenance of a coldwater fishery during summer months. With this in mind, DO, temperature, and velocity contours predicted by the W2 and Si3D coupled models were analyzed (Figures 31 and 32). Both models simulated a region of higher DO directly above the diffuser, which was located from 0.16 to 0.52 km upstream of the dam (Figure 31b and Figure 32, bottom). The area of the hypolimnion downstream of the diffuser and towards the dam appears to be more oxygenated than upstream of the diffuser. The topography and slope of the reservoir bottom may have contributed to this effect. The distribution of DO around the diffuser correlates with the velocity fields predicted by the coupled models. Both models predicted relatively high velocities above the diffuser where entrainment occurred. Greater velocities were also estimated for the downstream portion of the linear diffuser, which correspond to the higher DO concentrations towards the dam. Plume detrainment is evident in the horizontal velocity results from the W2 coupled model (Figure 31c) and the longitudinal velocity vectors from the

Si3D coupled model at the top of the hypolimnion (Figure 32). The effect of wind-induced mixing within the epilimnion was also captured by both models. The consequences of plume-induced mixing can be seen in the temperature contours predicted by W2, where plume detrainment eroded the thermocline at about 0.4 km from the dam (Figure 31a). Plume detrainment also introduced higher DO concentrations to this region of the hypolimnion (Figure 31b). The temperature within the hypolimnion predicted by the Si3D coupled model (Figure 32, top) appears to be more homogeneous compared to the W2 coupled model results (Figure 31a).

Conclusions

Bubble-plume diffusers are commonly installed to add DO to anoxic bottom layers of lakes and reservoirs. In an attempt to model the complex interaction between the plume and the ambient water body, a bubble-plume model for a linear diffuser was coupled with two different reservoir models, W2 and Si3D. Simulations were run using a rectangular basin, and predicted oxygen addition was found to be directly proportional to the frequency of plume model updates. Using similar basin and diffuser conditions, the W2 coupled model calculated less oxygen input than Si3D. This was likely due to the effects of lateral-averaging, which diluted the near-field DO accumulation. Plume-induced mixing predicted by the Si3D coupled model was greater than for W2, also because of lateral-averaging. Using a plume update period of 0.5 hr, the coupled models were then applied to a simplified test of a full-scale linear diffuser in a water-supply reservoir. Both models reproduced the rate of DO addition by the plume well but over-estimated warming within the hypolimnion. The W2 coupled model over-predicted the extent of plume-induced mixing. This may have been due to the lower vertical resolution of the reservoir grid in W2, which averaged the water column temperature gradient and subsequently decreased the resistance to plume rise. A higher plume rise height results in greater induced circulation and erosion of the thermocline. Using the 1998 data set from SHR, coupling of the linear bubble-plume model with both W2 and Si3D has produced encouraging results. Therefore, the coupled models will be more extensively evaluated using additional diffuser data from SHR collected over a range of operating conditions. This future work will be complicated by the presence of pumped inflow into the reservoir during diffuser testing, which forms a high-flow, underwater plume that discharges vertically. Accurate modeling of this single-phase plume and the ultimate location of its detrainment will be critical to reproducing temperature and DO profiles well. Coupling of the plume model with either W2 or Si3D is promising as an engineering tool for

design and evaluation of hypolimnetic oxygenation systems. As a complement to this, the coupled-models can be used to more thoroughly investigate the effect of plume-induced mixing on a reservoir.

Acknowledgements

Financial support was generously provided by the U. S. National Science Foundation (Grant No. BES 0202034), Western Virginia Water Authority, University of Granada, and Junta de Andalucía. The authors thank Gary Hauser of Loginetics, Inc. for use of W2i and AGPM-2D, pre- and post-processors for CE-QUAL-W2.

Notation

A dispersion coefficient for momentum, m^2/s.

c_p specific heat of water, J/kg/°C

D dispersion coefficient for temperature and constituents, m^2/s.

DC detrainment cell, -.

EC entrainment cell, -.

f body force, Coriolis parameter, 1/s.

g gravitational acceleration, m/s^2.

H source of heat, $J/m^3/s$, or water depth, m.

M mass flow rate, kg/s.

O dissolved oxygen concentration, g/m^3.

Q volumetric flow rate, m^3/s.

S fluid source strength, $kg/m^3/s$

t time, s.

u velocity in x-direction, m/s.

V volume of cell, m^3.

v velocity in y-direction, m/s.

w velocity in z-direction, m/s.

z depth, m.

Greek letters

ζ free surface elevation, m.

θ temperature, $^{\circ}$C.

ρ density, kg/m^3.

Subscripts

0 properties of water being added or removed at a source or sink cell

d detrainment

DO dissolved oxygen

h horizontal

v vertical

References

Arega, F., and J. H. W. Lee (2005), Diffusional mass transfer at sediment-water interface of cylindrical sediment oxygen demand chamber, *J. Environ. Engineer.*, *131*(5), 755-766.

Asaeda, T., and J. Imberger (1993), Structure of bubble plumes in linearly stratified environments, *J. Fluid Mech.*, *249*, 35-57.

Beutel, M. W. (2003), Hypolimnetic anoxia and sediment oxygen demand in California drinking water reservoirs, *Lake Reservoir Manage.*, *19*(3), 208-221.

Bostrom, B., et al. (1988), Exchange of phosphorus across the sediment and water interface, *Hydrobiol.*, *170*, 229-244.

Bravo, H. R., et al. (2007), Development of a commercial-code based two-fluid model for bubble plumes, *Environ. Modelling & Software*, *22*, 536-547.

Chapra, S. C. (1997), *Surface Water-Quality Modeling*, 844 pp., WCB McGraw-Hill, Boston, Massachusetts.

Cole, T. M., and S. A. Wells (2003), CE-QUAL-W2: A Two-Dimensional, Laterally Averaged, Hydrodynamic and Water Quality Model, Version 3.2, U.S. Army Engineering and Research Development Center, Vicksburg, MS.

Cooke, G. D., and R. E. Carlson (1989), *Reservoir Management for Water Quality and THM Precursor Control*, 387 pp., American Water Works Association Research Foundation, Denver, CO.

Fanneløp, T. K., and K. Sjøen (1980), Hydrodynamics of underwater blowouts, *Norweg. Maritime Res.*, *4*, 17-33.

Fanneløp, T. K., et al. (1991), Surface current and recirculating cells generated by bubble curtains and jets, *J. Fluid Mech.*, *229*, 629-657.

Fischer, H. B., et al. (1979), *Mixing in Inland and Coastal Waters*, 483 pp., Academic Press, Inc., San Diego, California.

French, T. D., and E. L. Petticrew (2007), Chlorophyll a seasonality in four shallow eutrophic lakes (northern British Columbia, Canada) and the critical roles of internal phosphorus loading and temperature, *Hydrobiol.*, *575*(1), 285-299.

Hondzo, M. (1998), Dissolved oxygen transfer at the sediment-water interface in a turbulent flow, *Water Resour. Res.*, *34*(12), 3525-3533.

Imteaz, M. A., and T. Asaeda (2000), Artificial mixing of lake water by bubble plume and effects of bubbling operations on algal bloom, *Water Res.*, *34*(6), 1919-1929.

Johnson, G. P., et al. (2000), Methodology, Data Collection, and Data Analysis for Determination of Water-Mixing Patterns Induced by Aerators and Mixers, 48 pp, U.S. Geological Survey.

Josiam, R. M., and H. G. Stefan (1999), Effect of flow velocity on sediment oxygen demand: comparison of theory and experiments, *J. Am. Water Resour. Assoc.*, *35*, 433-439.

Kantha, L. H., and C. A. Clayson (1994), An improved mixed layer model for geophysical applications, *Journal of Geophysical Research*, *99*(C12), 25235-25266.

Liikanen, A., et al. (2002), Gas dynamics in eutrophic lake sediments affected by oxygen, nitrate, and sulfate, *J. Environ. Qual.*, *31*, 338-349.

Lindenschmidt, K. E., and P. F. Hamblin (1997), Hypolimnetic aeration in Lake Tegel, Berlin, *Water Res.*, *31*(7), 1619-1628.

Lorke, A., et al. (2003), Breathing sediments: The control of diffusive transport across the sediment-water interface by periodic boundary-layer turbulence, *Limnol. Oceanogr.*, *48*(6), 2077-2085.

Lynch, D. R. (1986), Basic hydrodynamic equations for lakes, in *Physics-based modelling of lakes, reservoirs and impoundments*, edited by W. G. Gray, pp. 17-53, ASCE, New York.

Mackenthun, A. A., and H. G. Stefan (1998), Effect of flow velocity on sediment oxygen demand: Experiments, *J. Environ. Engineer.*, *124*(3), 222-230.

Madsen, P. A., et al. (1988), Subrid modelling in depth integrated flows, paper presented at 21st Coastal Engineering Conference, ASCE, New York.

Mailman, M., et al. (2006), Strategies to lower methyl mercury concentrations in hydroelectric reservoirs and lakes: A review, *Sci. Tot. Envr.*, *368*, 224-235.

McDougall, T. J. (1978), Bubble plumes in stratified environments, *J. Fluid Mech.*, *85*, 655-672.

McGinnis, D. F., et al. (2001), Hypolimnetic oxygenation: Coupling bubble-plume and reservoir models, paper presented at Asian Waterqual 2001: First IWA Asia-Pacific Regional Conference, Intl. Wat. Assoc., Fukuoka, Japan, 12-15 Sept.

McGinnis, D. F., and J. C. Little (2002), Predicting diffused-bubble oxygen transfer rate using the discrete-bubble model, *Water Res.*, *36*(18), 4627-4635.

McGinnis, D. F., et al. (2004), Interaction between a bubble plume and the near-field in a stratified lake, *Water Resour. Res.*, *40*(10, W10206).

Pollock, L. M. J., and M. G. Dubé (2007), The effects of hypoxia on fishes: from ecological relevance to physiological effects, *Environ. Rev.*, *15*, 1-14.

Rueda, F. J. (2001), A three-dimensional hydrodynamic and transport model for lake environments, Ph.D. Dissertation thesis, University of California, Davis.

Rueda, F. J., and S. G. Schladow (2002a), Quantitative comparison of models for barotropic response of homogenous basins, *J. Hydraul. Engr.*, *128*(2), 201-213.

Rueda, F. J., and S. G. Schladow (2002b), Quantitative comparison of models for barotropic response of homogeneous basins, *Journal of Hydraulic Engineering*, *128*(2), 201-213.

Rueda, F. J., and S. G. Schladow (2003), Dynamics of large polymictic lake. II: Numerical simulations, *J. Hydraul. Engr.*, *129*(2), 92-101.

Rueda, F. J., et al. (2003), Dynamics of large polymictic lake. I: Field observations, *J. Hydraul. Engr.*, *129*(2), 82-91.

Rueda, F. J., and E. A. Cowen (2005), Exchange between a freshwater embayment and a large lake through a long, shallow channel, *Limnol. Oceanogr.*, *50*(1), 169-183.

Schladow, S. G. (1992), Bubble plume dynamics in a stratified medium and the implications for water quality amelioration in lakes, *Water Resour. Res.*, *28*, 313-321.

Schladow, S. G. (1993), Lake destratification by bubble-plume systems: Design methodology, *J. Hydraul. Engr.*, *119*(3), 350-368.

Singleton, V. L., and J. C. Little (2006), Designing hypolimnetic aeration and oxygenation systems - A review, *Environ. Sci. Technol.*, *40*, 7512-7520.

Singleton, V. L., et al. (2007), Linear bubble plume model for hypolimnetic oxygenation – Full-scale validation and sensitivity analysis, *Water Resour. Res.*, *43*, W02405.

Smith, P. E. (1997), A three-dimensional, finite-difference model for estuarine circulation, Ph.D. Dissertation thesis, University of California, Davis.

Wells, S. A. (2000), CE-QUAL-W2 Version 3: Hydrodynamic and water quality river basin modelling, paper presented at HydroInformatics 2000, IAHR.

Wüest, A., et al. (1992), Bubble plume modeling for lake restoration, *Water Resour. Res.*, *28*, 3235-3250.

Zic, K., and H. G. Stefan (1994), Destratification Induced by Bubble Plumes, 39 pp, U.S. Army Corps of Engineers, Waterways Experiment Station.

Table 12. Conditions for coupled linear bubble plume/reservoir model applications for rectangular basin simulation and full-scale diffuser test in Spring Hollow Reservoir (SHR), VA, U.S.A. during September 28–October 13, 1998.

Parameter	Rectangular Basin	SHR
Oxygen in gas supply (%)	21	21
Operational diffuser length (m)	60, 360	360
Gas flow rate (Nm^3/hr)[a]	43	43
Average diffuser depth (m)	51	48
Reservoir maximum depth (m)	52	64
Reservoir surface area (10^6 m^2)	0.018	0.53
Reservoir total volume (10^6 m^3)	0.94	12
W2 cell size (m)	length = 10 (60 m diffuser), 60 (360 m diffuser) width = 50 height = 1	length = 60–100 width = varies by elevation height = 1.5
Si3D cell size (m)	length = 10 width = 10 height = 1	length = 15 width = 15 height = 1
W2 timestep (s)	autostepping, 1 s minimum	autostepping, 1 s minimum
Si3D timestep (s)	5	10

[a]1 Nm^3 denotes 1 m^3 of gas at 1 bar and 0 °C.

Table 13. Effect of plume update period and diffuser length on oxygen input to rectangular basin predicted by CE-QUAL-W2 (W2) and Si3D coupled models.

Model	Diffuser length (m)	Plume update period (hr)	Predicted Oxygen Input (kg)	Deviation from Theoretical Oxygen Input[a]
W2	60	6	1104	-48%
W2	60	1	1859	-13%
W2	360	6	655	-69%
W2	360	1	1364	-36%
Si3D	60	6	1446	-32%
Si3D	60	3	1796	-16%
Si3D	60	1	2098	-2%
Si3D	60	0.5	2180	+2%
Si3D	60	0.083	2249	+5%
Si3D	360	6	671	-69%
Si3D	360	3	1264	-41%
Si3D	360	1	1897	-11%
Si3D	360	0.5	2078	-3%
Si3D	360	0.083	2248	+5%

[a]Theoretical oxygen mass input = 2135 kg total for 7-day operating period with air, assuming 100% oxygen transfer efficiency.

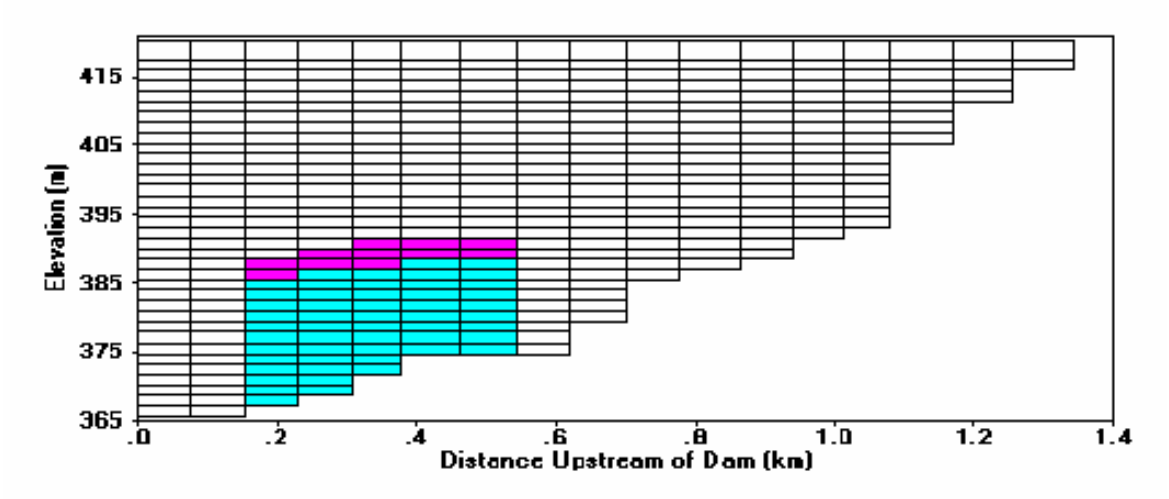

Figure 19. Two-dimensional grid of Spring Hollow Reservoir, Virginia, U.S.A. in CE-QUAL-W2. Columns with grey cells indicate location of linear diffuser along bottom of reservoir. Light and dark grey cells represent plume entrainment and detrainment zones, respectively.

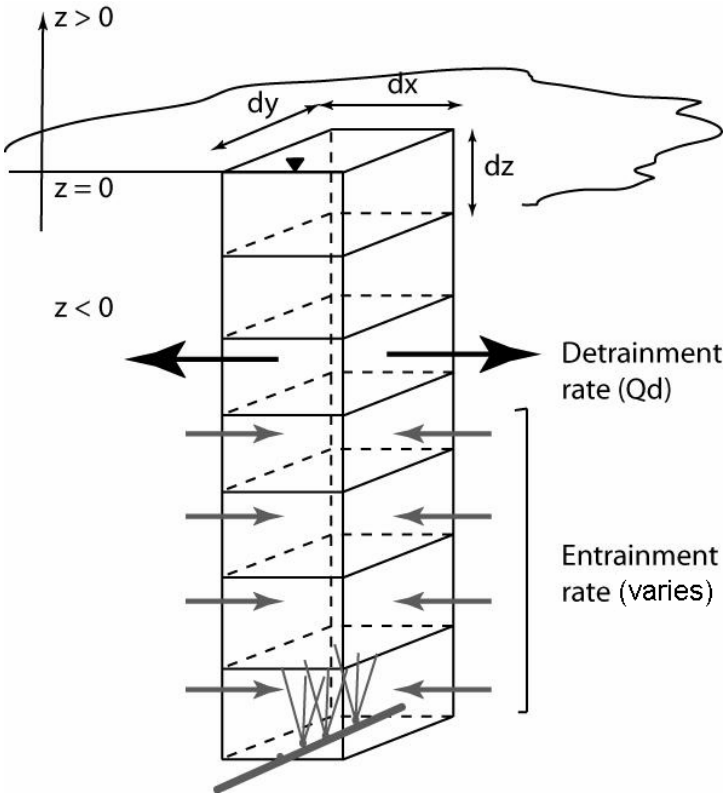

Figure 20. Schematic of coupling of linear bubble plume model with Si3D, showing entrainment and detrainment cells.

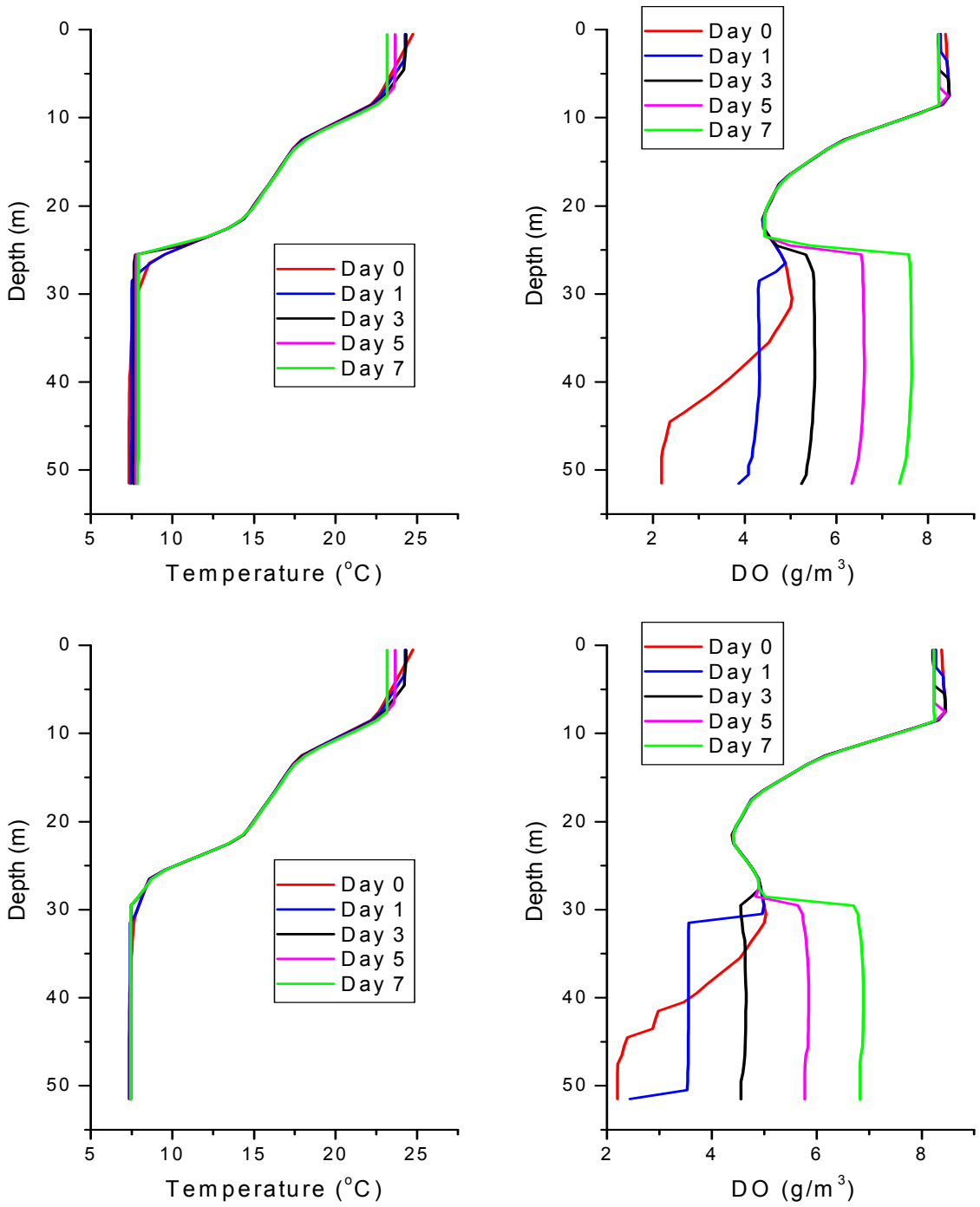

Figure 21. Temperature and DO profiles predicted by coupled bubble plume/W2 model for rectangular basin simulation with 60 m (top) and 360 m (bottom) diffuser and 1 hour plume update period. Profiles are from center of basin.

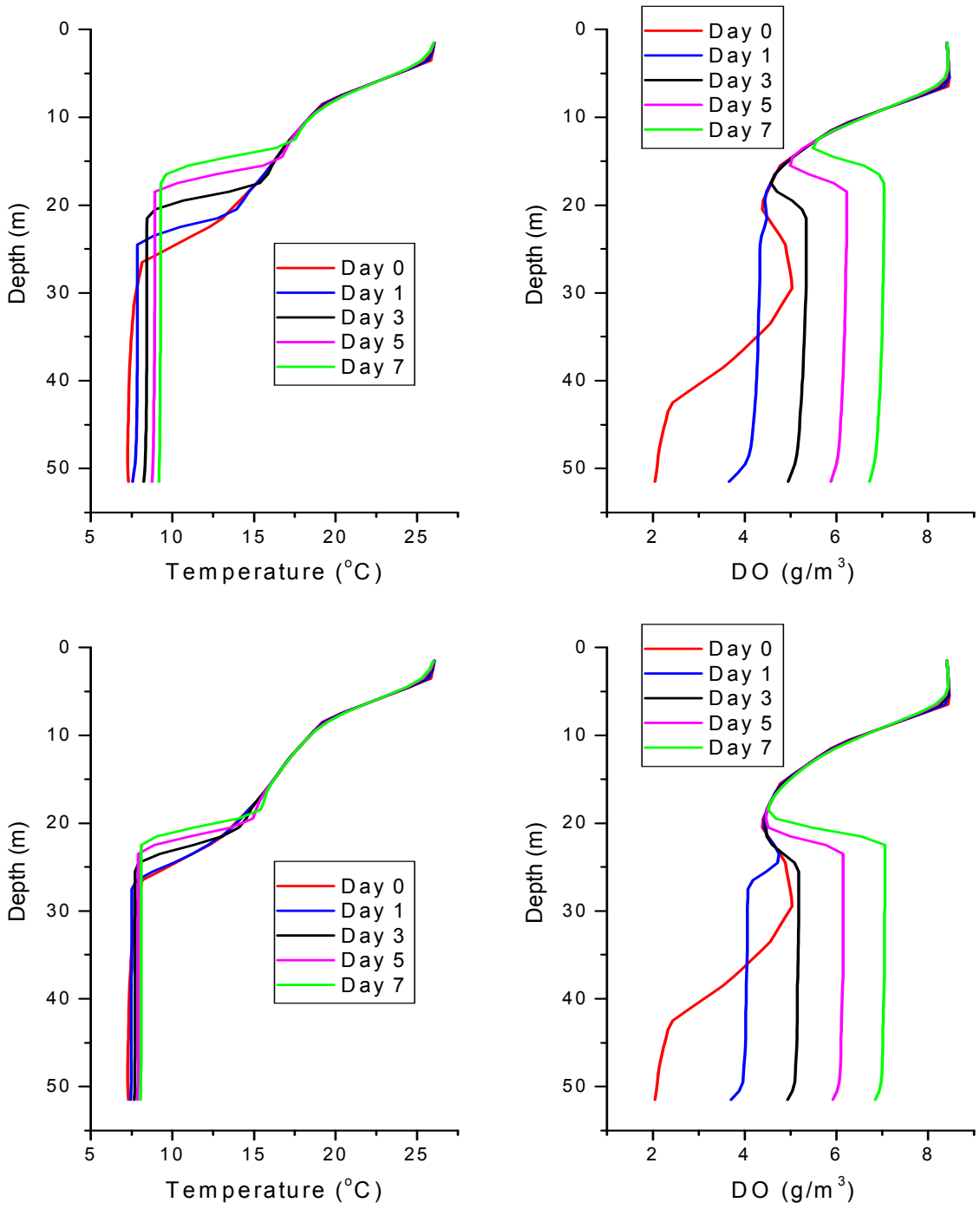

Figure 22. Temperature and DO profiles predicted by coupled bubble plume/Si3D model for rectangular basin simulation with 60 m (top) and 360 m (bottom) diffuser and 1 hour plume update period. Profiles are from center of basin.

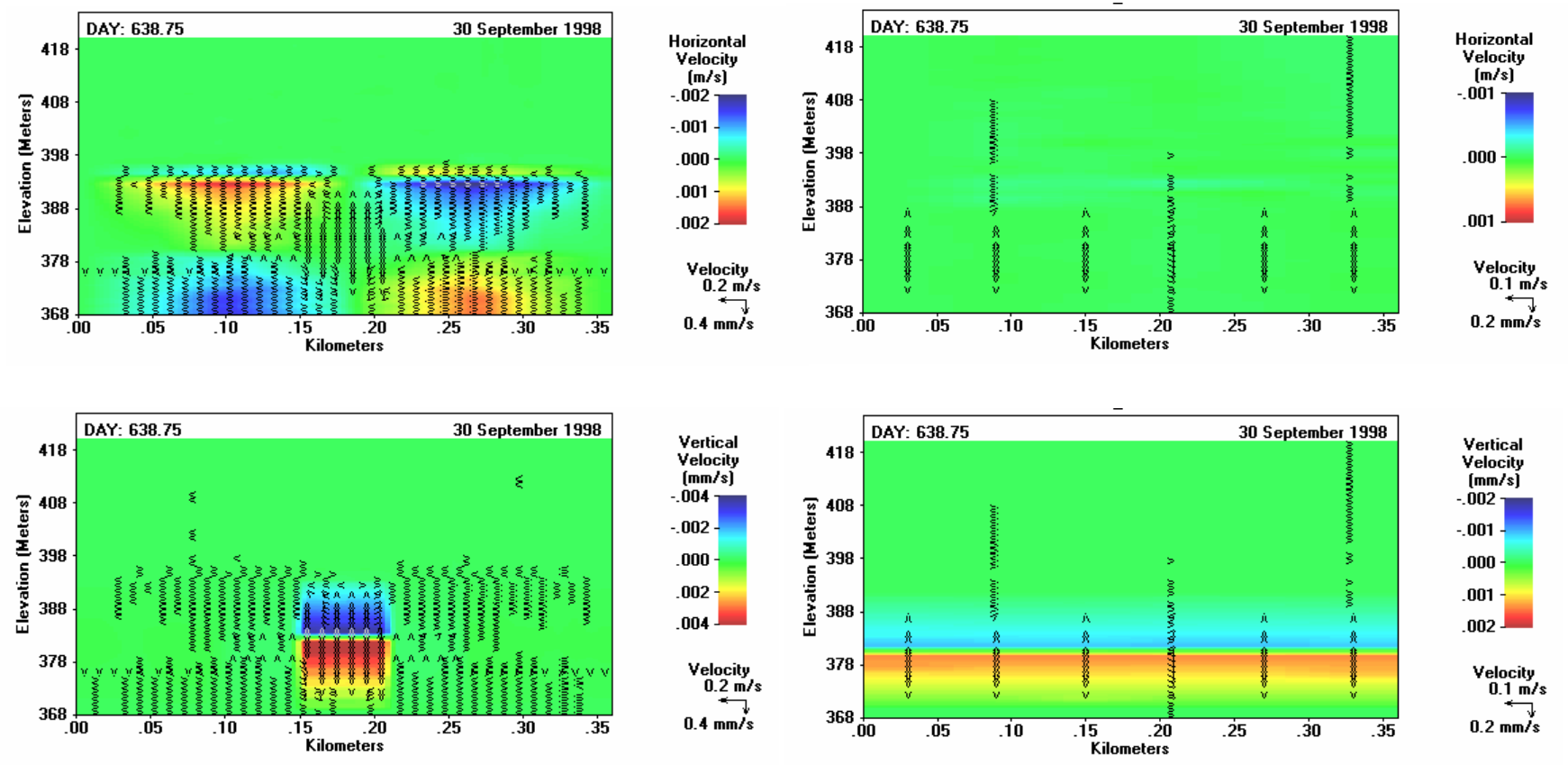

Figure 23. Longitudinal view of horizontal (top row) and vertical (bottom row) velocity induced by linear bubble plume operation in rectangular basin simulation, as predicted by coupled bubble plume/W2 model. Graphs on right and left correspond to 60 and 360 m diffuser, respectively, and are from Day 2.25. The velocity contours and vectors for the 360 m diffuser are shown at half the scale as for the 60 m diffuser.

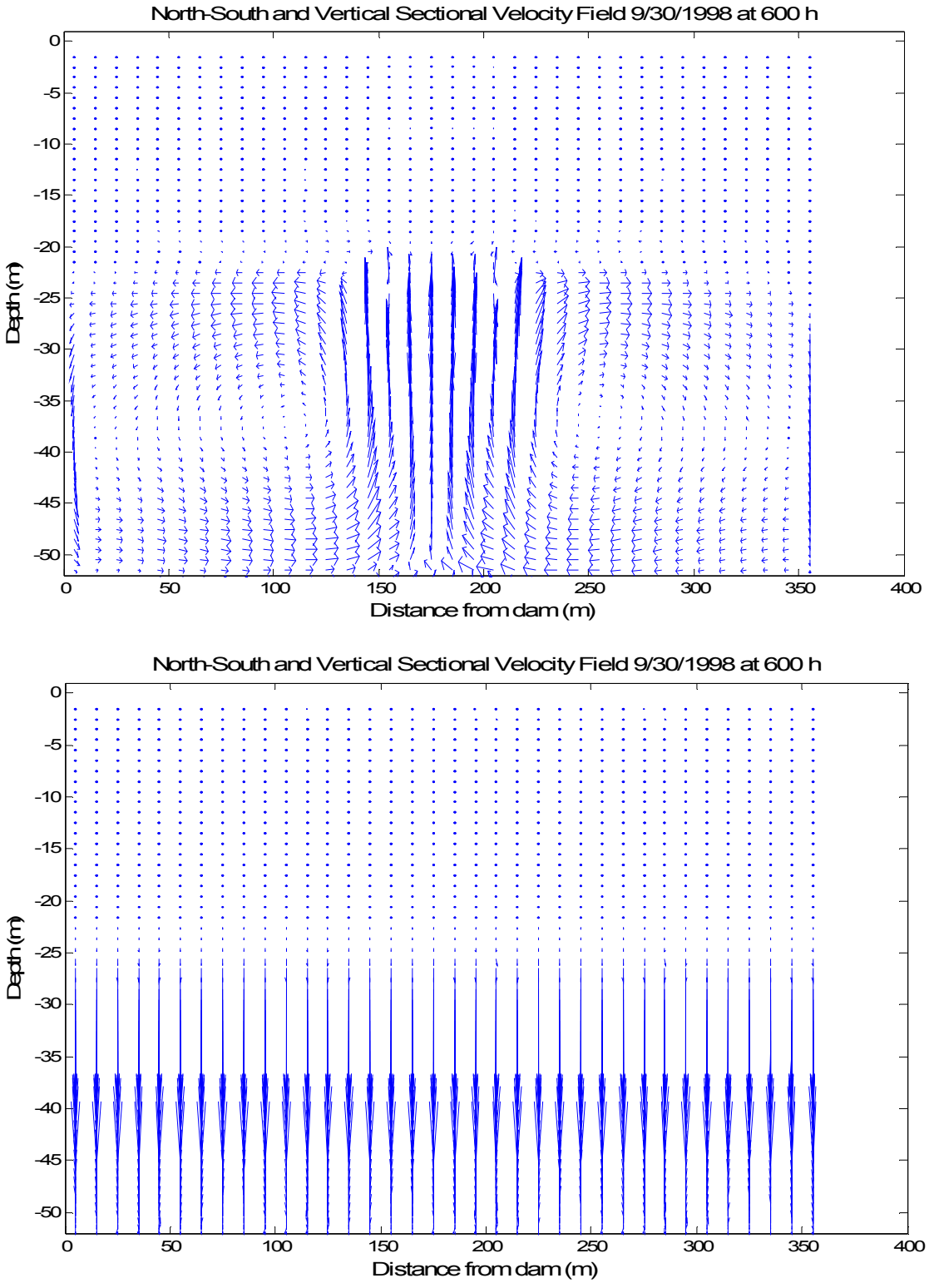

Figure 24. Sectional view of longitudinal and vertical velocity induced by linear bubble plume operation in rectangular basin simulation, as predicted by coupled bubble plume/Si3D model for 60 m (top) and 360 m (bottom) diffuser for Day 2.25.

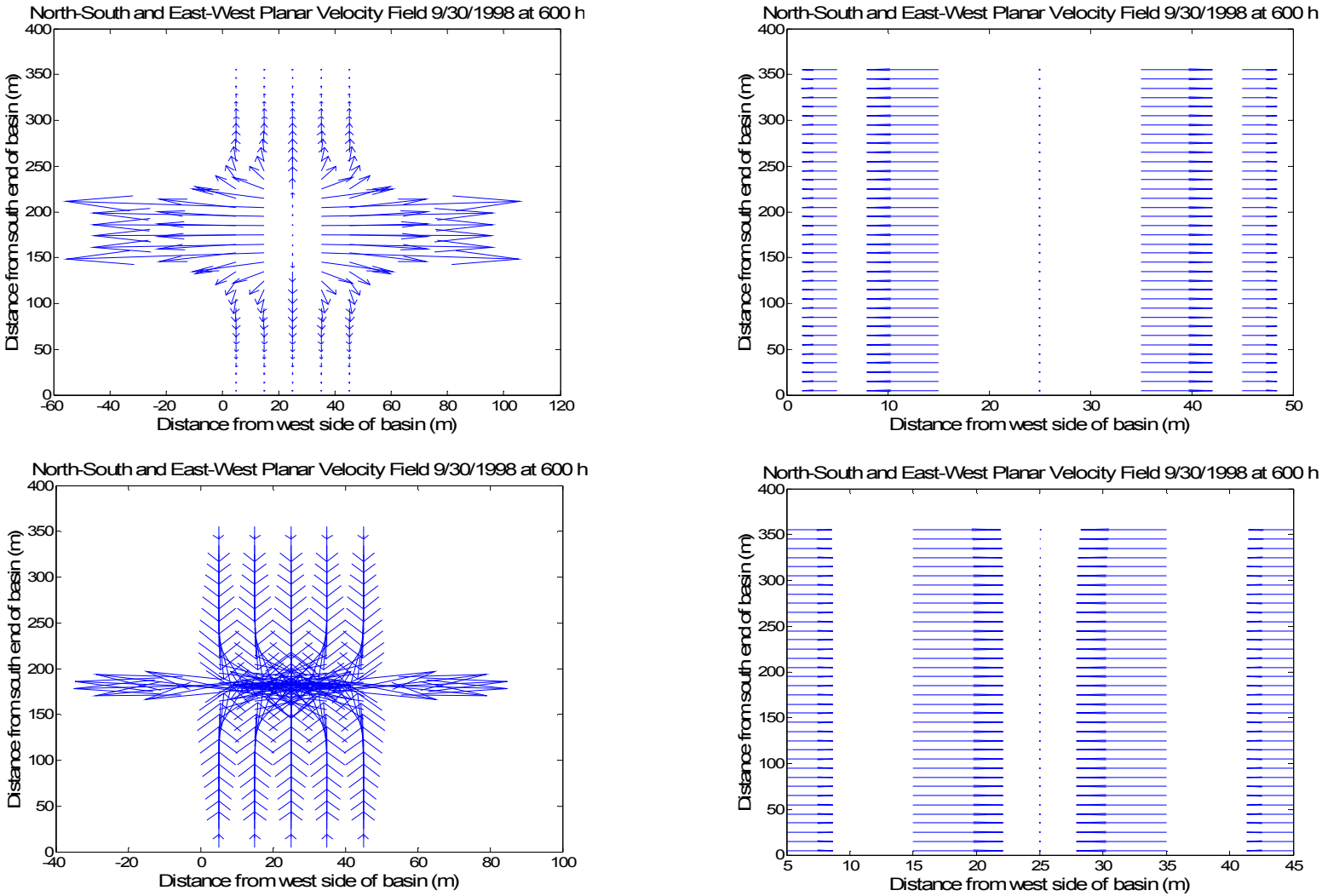

Figure 25. Planar view of longitudinal and lateral velocity induced by linear bubble plume operation in rectangular basin simulation, as predicted by coupled bubble plume/Si3D model for 60 m (left) and 360 m (right) diffuser for Day 2.25. Graphs represent 23 m (top) and 45 m (bottom) depths for 60 m diffuser and 28 m (top) and 45 m (bottom) depths for 360 m diffuser. For all plots, the diffuser is oriented vertically along the north-south axis of the basin.

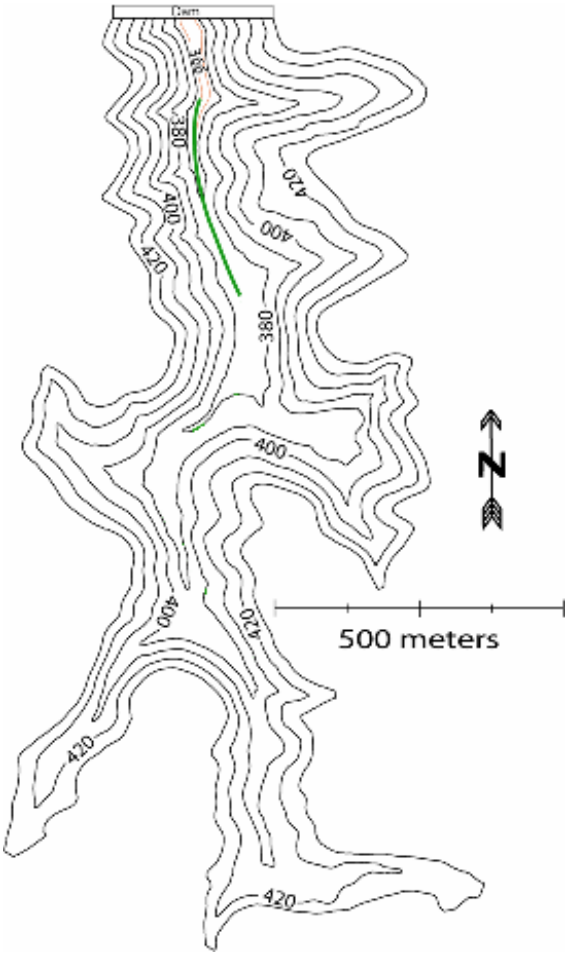

Figure 26. Bathymetric map of Spring Hollow Reservoir, VA, U.S.A. showing location of linear bubble plume diffuser in 1998.

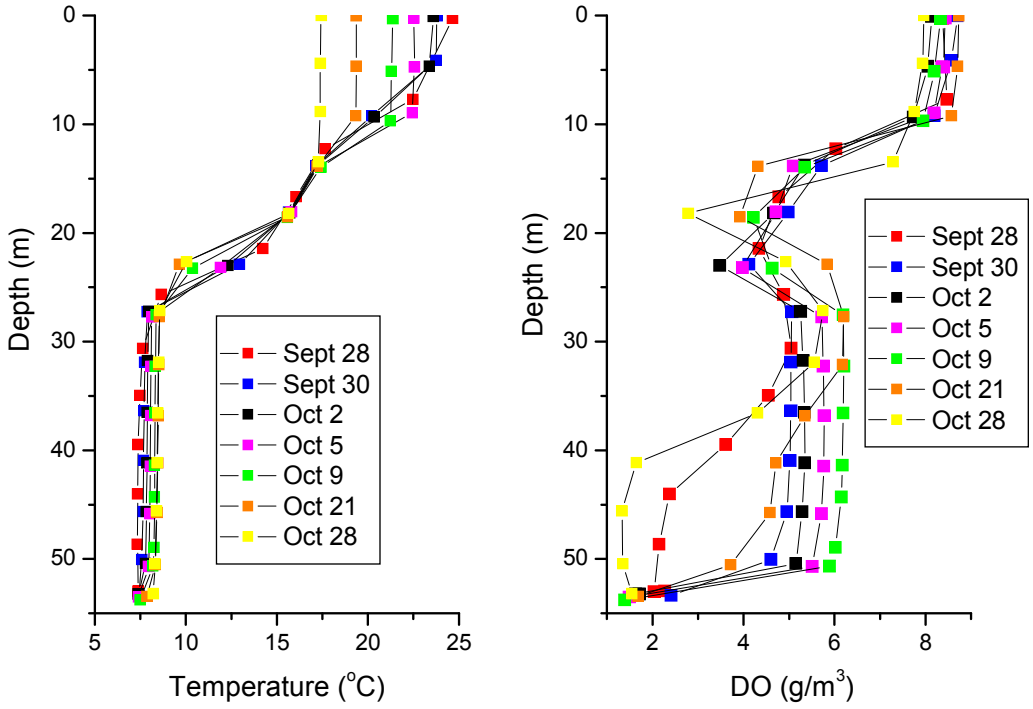

Figure 27. Observed temperature and DO profiles in Spring Hollow Reservoir, Virginia, U.S.A. in Fall 1998. Profiles from September 28 were used as initial boundary conditions for the coupled models.

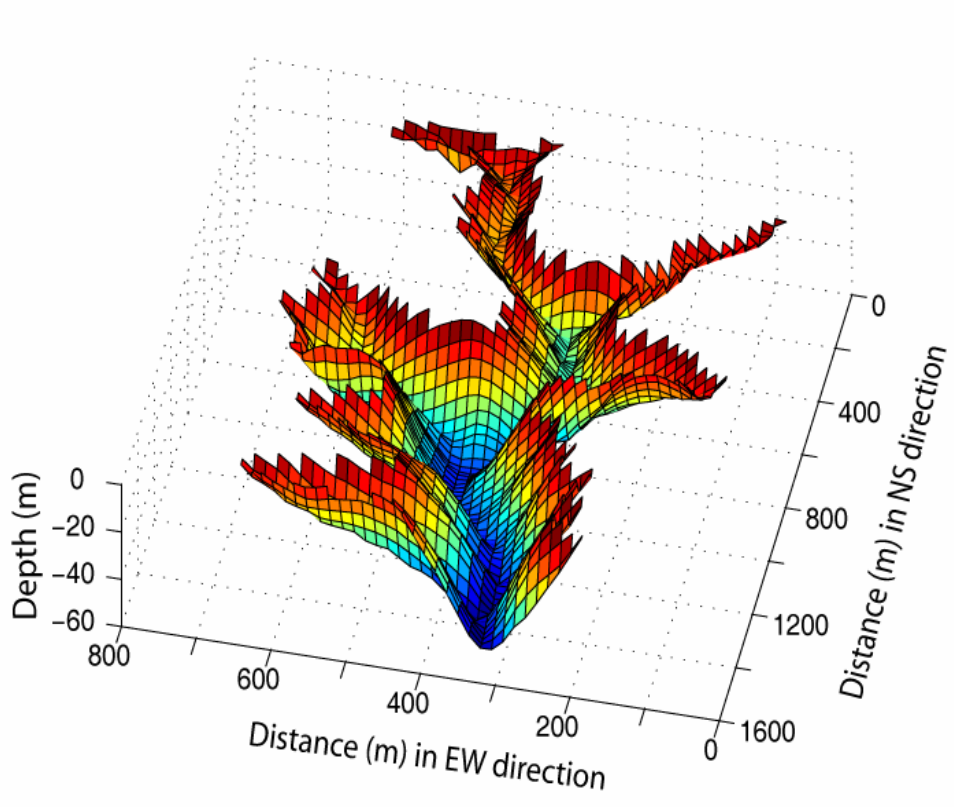

Figure 28. Three-dimensional grid of Spring Hollow Reservoir, Virginia, U.S.A in Si3D.

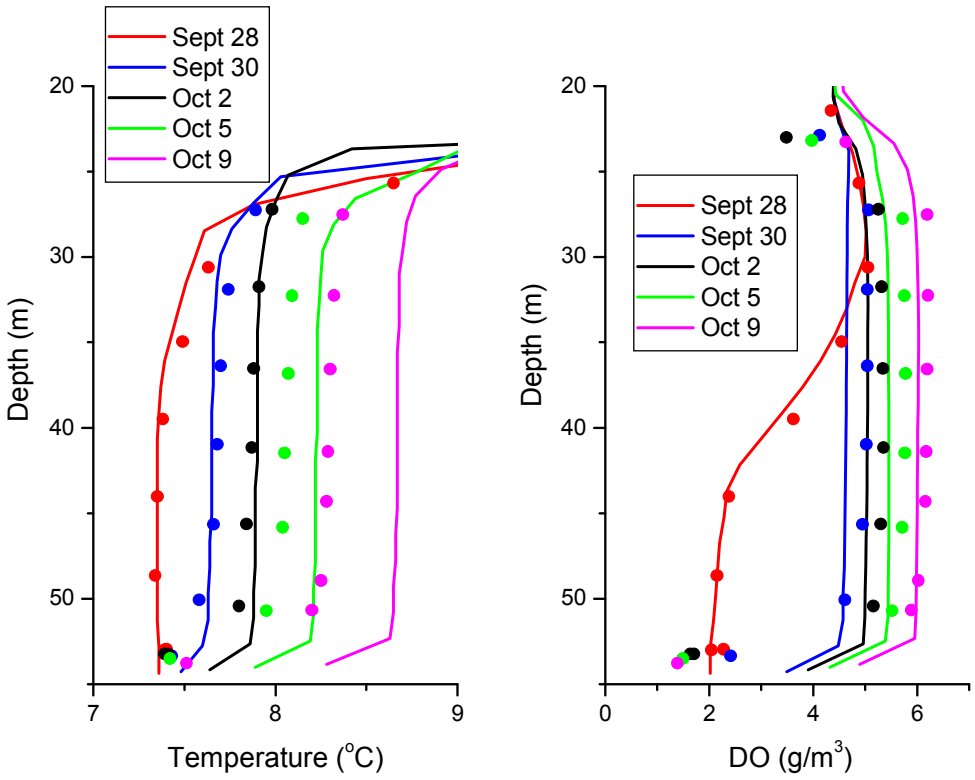

Figure 29. Hypolimnetic profiles predicted by coupled bubble plume/W2 model, represented as solid lines. Input data collected from Spring Hollow Reservoir, VA, U.S.A. during diffuser operation in 1998. Observed temperature and DO represented as symbols.

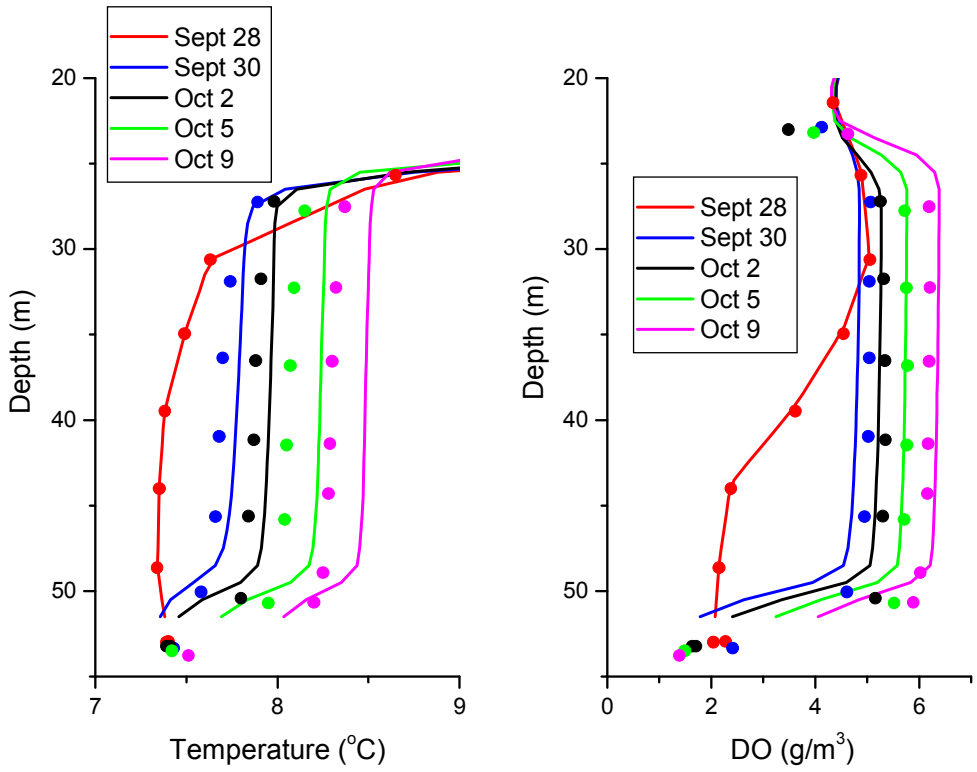

Figure 30. Hypolimnetic profiles predicted by coupled bubble plume/Si3D model, represented as solid lines. Input data collected from Spring Hollow Reservoir, VA, U.S.A. during diffuser operation in 1998. Observed temperature and DO represented as symbols.

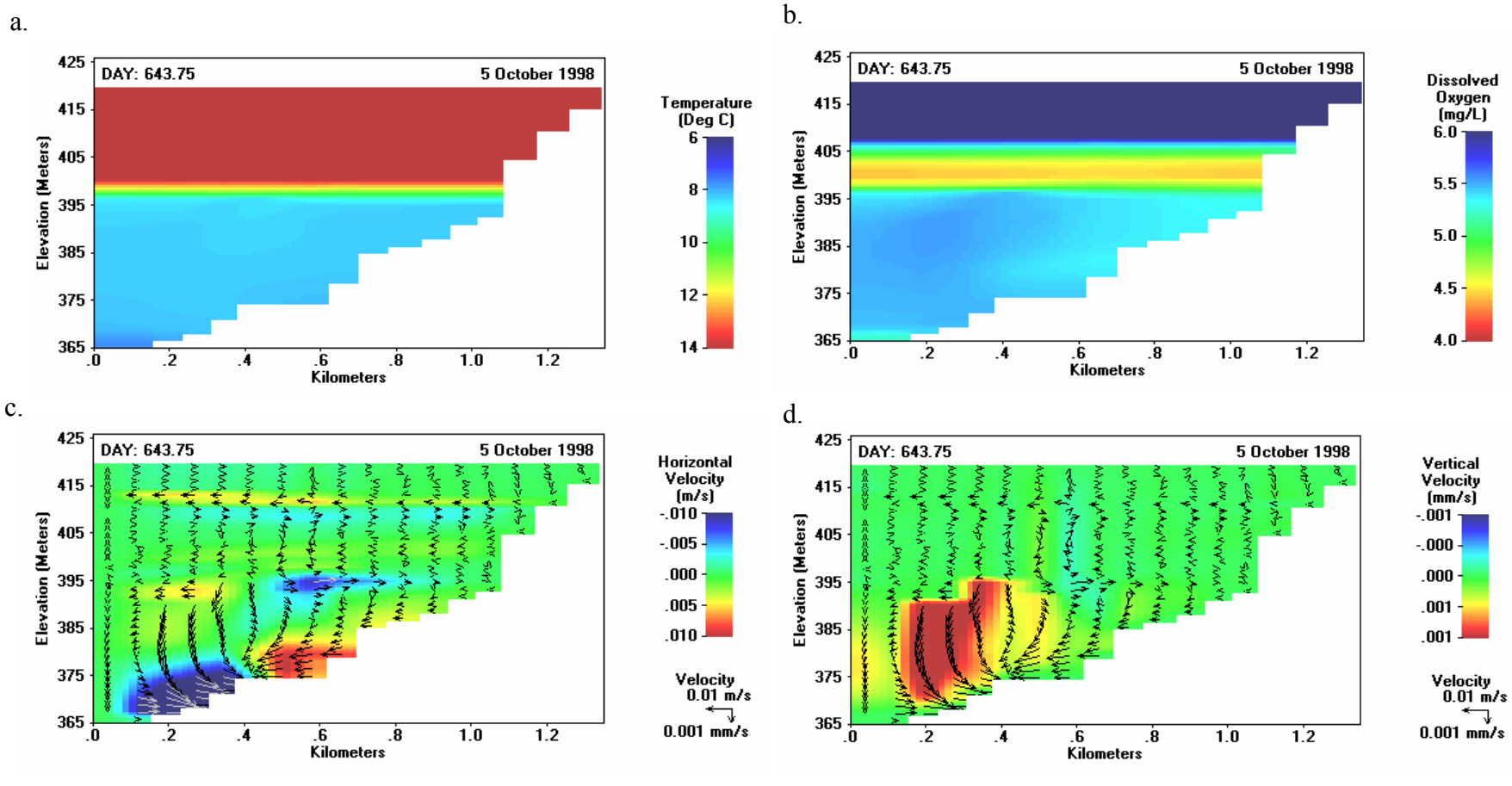

Figure 31. Longitudinal view of (a) temperature, (b) DO, (c) horizontal velocity, and (d) vertical velocity predicted by coupled bubble plume/W2 model for Spring Hollow Reservoir, VA, U.S.A. during diffuser operation on October 5, 1998. Temperature and DO scaled to show gradients caused by plume operation.

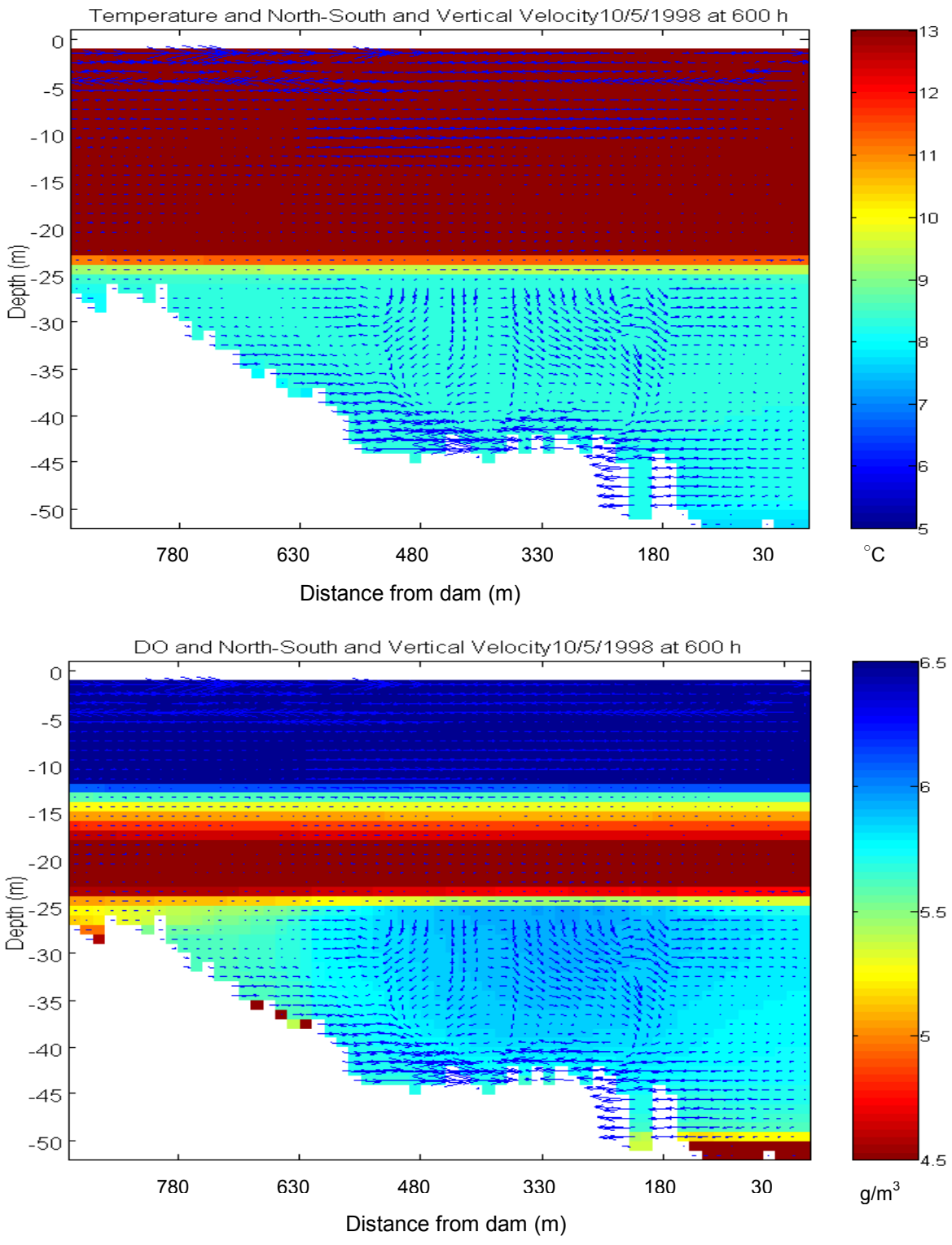

Figure 32. Two-dimensional view of longitudinal and vertical velocity field with temperature (top) and DO (bottom) contours predicted by coupled bubble plume/Si3D model for Spring Hollow Reservoir, VA, U.S.A. during diffuser operation on October 5, 1998. Temperature and DO scaled to show gradients caused by plume operation.

CHAPTER 5. DISSERTATION SUMMARY AND CONCLUSIONS

A method commonly employed to ameliorate low dissolved oxygen conditions within the hypolimnions of stratified lakes and reservoirs is hypolimnetic oxygenation/aeration, which consists of adding oxygen to bottom waters while maintaining density stratification. The three primary oxygenation and aeration devices are bubble plume diffusers, airlift aerators, and Speece Cones. Bubble plume diffusers may be either circular or linear in geometry. Despite the large number of oxygenation installations and the increasing use of this lake and reservoir management technique, relatively few studies have been conducted on designing hypolimnetic oxygenation devices. Early design models for bubble plumes did not account for gas transfer and stratification, and early design methods for airlift aerators were primarily empirically based. No early design work was found for the Speece Cone. A significant unifying advance in modeling oxygen transfer from hypolimnetic oxygenation devices was development of the discrete bubble approach by *Wüest et al.* [1992]. Because of its fundamental nature, the discrete bubble model has been successfully applied to an airlift aerator [*Burris et al.*, 2002], a Speece Cone [*McGinnis and Little*, 1998], a circular bubble plume diffuser [*McGinnis et al.*, 2004; *Wüest et al.*, 1992], and a linear bubble plume diffuser [*McGinnis et al.*, 2001; *Singleton and Little*, 2005; *Singleton et al.*, 2007].

As part of this research, the existing linear bubble plume model of *McGinnis et al.* [2001] was improved and validated with data from a full-scale diffuser system and a sensitivity analysis was performed [*Singleton et al.*, 2007]. Predicted plume rise height, spreading, and constituent profiles compared well to experimental observations. Also, plume rise height, water flow rate, and oxygen transfer efficiency were found to be primarily dependent on gas flow rate and initial bubble radius.

To model the complex interaction between the plume and the ambient water body, the validated linear bubble plume model was coupled with two different reservoir models, W2 and Si3D. Simulations were run using a rectangular basin, and predicted oxygen addition was found to be directly proportional to the frequency of plume model updates. The coupled models were then applied to a simplified test of a full-scale linear diffuser in a water-supply reservoir. Both models reproduced the rate of DO addition by the plume well but over-estimated warming within the hypolimnion. Using this simplified data set, coupling of the linear bubble-plume model with both W2 and Si3D has produced encouraging results. Therefore, the coupled models will be

more extensively evaluated by the same research team using additional diffuser data collected over a range of operating conditions. Coupling of the plume model with either W2 or Si3D is promising as an engineering tool for design and evaluation of linear diffusers. A natural extension of this is work to couple either W2 or Si3D with the discrete-bubble models for the airlift aerator, Speece Cone, and circular diffuser to predict the performance of a range of hypolimnetic oxygenation methods. This comprehensive coupled model could be then used to compare the effects of different oxygenation scenarios in order to implement the most suitable one.

References

Burris, V. L., et al. (2002), Predicting oxygen transfer and water flow rate in airlift aerators, *Water Res.*, *36*(18), 4605-4615.

McGinnis, D. F., and J. C. Little (1998), Bubble dynamics and oxygen transfer in a Speece Cone, *Water Sci. Technol.*, *37*, 285-292.

McGinnis, D. F., et al. (2001), Hypolimnetic oxygenation: Coupling bubble-plume and reservoir models, paper presented at Asian Waterqual 2001: First IWA Asia-Pacific Regional Conference, Intl. Wat. Assoc., Fukuoka, Japan, 12-15 Sept.

McGinnis, D. F., et al. (2004), Interaction between a bubble plume and the near-field in a stratified lake, *Water Resour. Res.*, *40*(10, W10206).

Singleton, V. L., and J. C. Little (2005), Linear bubble plume model for hypolimnetic oxygenation: Full-scale evaluation and sensitivity analysis, paper presented at 9th Workshop on Physical Processes in Natural Waters, Lancaster Univ., Lancaster, England, 4-6 Sept.

Singleton, V. L., et al. (2007), Linear bubble plume model for hypolimnetic oxygenation – Full-scale validation and sensitivity analysis, *Water Resour. Res.*, *43*, W02405.

Wüest, A., et al. (1992), Bubble plume modeling for lake restoration, *Water Resour. Res.*, *28*, 3235-3250.